Technical University of Crete
School of Mineral Resources Engineering

Interaction of *Penicillium purpurogenum* fungus with bentonite and kaolin clays

Athanasakis Nikolaos, Mineral Resources Engineer

This thesis is submitted for the completion of the postgraduate program “Geotechnology & Environment” of the School of Mineral Resources Engineering, Technical University of Crete

Greece, Chania, 2021-2022

To my family

Acknowledgements

My sincere gratitude goes first and foremost to **Prof. Dr. Christidis Georgios** who assisted, guided and taught me during my undergraduate and graduate studies. Also, I wish to express my gratitude to:

Prof. Dr. Anastasiadis Spiros for accepting me in the Institute of Electronic Structure & Laser (IESL) of the Foundation for Research & Technology - Hellas (FORTH), in order to complete the electrokinetic measurements of my samples

Dr. Charles Knapp, Reader of Strathclyde University, Glasgow and Assoc. Prof. Dr. Venieri Danai of School of Chemical and Environmental Engineering for participating in the master thesis examination committee

Prof. Dr. Chryssikos George, Director of Research of the Center for Research and Technology, Hellas, for the ATR/FT-IR measurements

Dr. Chrissopoulou Kiriaki for providing me with clearance to work in the laboratories of Institute of Electronic Structure & Laser (IESL) of the Foundation for Research & Technology - Hellas (FORTH) during the electrokinetic characterization of my samples

Ms. Gounaki Iosifina for her patience and help during the microbial experimental procedures

Mr. Karnis Ioannis, M.Sc. for assisting me with the titration measurements

Dr. Makri Pagona for her assistance in processing the data from the XRD patterns

Ms. Rotonto Pavlina, M.Sc. for assisting me with the ED XRF measurements

Dr. Stylianakis Minas for his valuable help and advice about the electrokinetic mobility tests

Dr. Stratakis Antonios for performing the XRD measurements

My appreciation goes to the Pancretan Endowment Fund, established by Pancretan Association of America, for providing me with a generous scholarship to carry out this thesis.

Abstract

The present Thesis investigates the impact of the surface properties and specifically the isoelectric point (IEP) of clay minerals, on the production of antimicrobial, extracellular metabolites by the fungus *Penicillium purpurogenum*. The tested materials were KGa-2 kaolinite and SWy-2 Na-smectite reference samples (CMS Source Clay Project) and a white Ca-smectite (B3) derived from the Greek island of Kimolos. The materials underwent chemical and mineralogical characterization. Also, their electrokinetic properties were investigated, by determining the IEP of each material with acid titration. The results were confirmed by measuring the zeta potential, electrophoretic mobility and particle size. The resulted IEPs for KGa-2, SWy-2 and B3 samples were 2.81 ± 0.03, 6.71 ± 0.01 and 6.40 ± 0.02 respectively. The fungus was cultivated in potato dextrose for 14 days, in presence of each of the aforementioned clay minerals. The pH was regulated at the IEP of each sample. For reference purposes, the culture was repeated in different pH, above and below the IEP of each material to observe possible variations in the antimicrobial performance of the leachates. The antimicrobial performance of the extracellular metabolites was determined by the Minimum Inhibitory Concentration (MIC) test. According to MIC, the extracellular leachates were introduced into bacterial colonies of *Staphylococcus aureus* to obtain the minimum concentration of leachates capable of reducing 60% of the initial bacterial population. The results proved that the isoelectric point of clay minerals is not a stimulation factor for the fungus, since the former produced antimicrobial, extracellular metabolites under the influence of Na-smectite (SWy-2) regardless of the pH. Furthermore, Ca-smectite stimulated the fungus at pH=7.5, which is above the observed IEP. Kaolinite did not affect the microorganism in any way, since the antibacterial activity of the leachates was absent in lower concentrations.

CONTENTS

FIGURES

TABLES

EQUATIONS

Introduction

Procaryots and microfungi make up 75% of the biomass on Earth, a great portion of which live in contact with minerals (Cuadros, 2017). This relationship has contributed to the evolution of more complex organisms and geological/geochemical cycles, especially in the late Precambrian, when the concentration of atmospheric oxygen increased sharply (Kennedy et al., 2006). The unique properties of clay minerals, such as their ability to adsorb inorganic ions is derived from their surface charge, which occurs, because of the isomorphic substitution of the silicon and aluminum atoms by lower-valenced ions in the crystal lattice. This phenomenon is described by the term "cation exchange capacity" or CEC and is responsible for supplying flora and fauna with necessary nutrients. Furthermore, they act as DNA preservatives, due to their ability to adsorb ions and molecules, mainly in their interlayer spaces, which was an important factor of early life evolution (Gui et al., 2019). The symbiotic relationship of clay minerals and microbes was discovered by ancient civilizations, such as the Greeks and Egyptians. Many unearthed texts of Theophrastus *(Theophrastus on Stones)*, Dioscurides *(De Materia Medica Book V)* (Photos-Jones et al., 2018) and other ancient historians mention a wide variety of applications, which included the use of specific types of soils (mainly consisting of clay minerals), which contained secondary metabolites (Venieri et al., 2020). However, they were not able to comprehend the origins of the organic products. The most important among them were the medicinal clays, such as the ritual related *Lemnian Earth, Samian Earth* and *miltos of Kea Island* (Photos-Jones et al., 2017; Photos-Jones et al., 2018). The explanation behind their properties lies between the minerals themselves and the microbial derived antibiotic metabolites. The target of this thesis is to examine the interaction between fungi and clay minerals and their ability to yield end products with antibacterial properties, under specific pH conditions, related with the isoelectric point (IEP) of the clays. The IEP is an important parameter of clay minerals because it affects their surface properties.

Chapter 1: Smectite and kaolin group of minerals: Structure, characteristics and applications

1.1 Structural characteristics of clay minerals

Clay minerals belong to the family of phyllosilicates, due to their sheet-structured crystal lattices. They occur as a weathering/erosion product of igneous rocks and usually co-exist with other fine-sized non-clay minerals, such as quartz, pyrite, opal CT, etc. Their crystal size is smaller than 0.002 mm and the dimension of the [001] plane belongs to the nanometric scale, from which their characterization as "natural nanomaterials" is derived. The terms "clay minerals" (hydrous, aluminosilicate minerals) and "clays" (mix of clay minerals with other fine-grained minerals) must not be confused. Their basic structure units are the tetrahedron SiO_4^{-4} and the gibbsite type octahedron $Al(OH)_6$. They are classified mainly by the number and arrangement of their sheets and the number of cations in the octahedral sheet.

The tetrahedral sheet is formed, when numerous tetrahedral units consisting of a silicon (Si) atom (or an aluminum atom, due to isomorphic substitution) surrounded by four oxygen atoms are linked together. The linkage occurs, when three basal oxygens are shared between two tetrahedra, with the fourth being apical oxygen. This repeated arrangement of tetrahedra forms a hexagonal network, which expands horizontally in two dimensions (Weaver & Pollard, 1973).

The second type of sheet that contributes to the formation of clay minerals is the octahedral sheet. The atomic structure of the octahedral sheet consists of oxygens or hydroxyl groups linked together with aluminum, magnesium and iron atoms. The octahedral sheet is also classified by the valence of the cation, which is linked together with the surrounding anions. Specifically, if the cation has a valence (3+), such as Al^{3+} or Fe^{3+}, only 2/3 of the available positions are occupied, since the total charge of the unit cell cannot exceed the valence of +6. Hence, the mineral is classified as *dioctahedral*. On the other hand, if all three positions are occupied by magnesium, ferrous iron or other cation with a valence of +2, then the mineral is classified as *trioctahedral.*

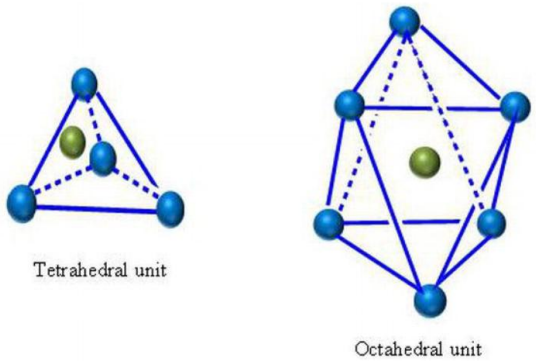

Figure 1.1: Tetrahedral and octahedral unit cells (Kumari & Mohan, 2021)

The dioctahedral clay minerals are classified into trans-vacant and cis-vacant sub-groups depending on the position of the hydroxyl group of the vacant position in the octahedron. If the vacant position is between the hydroxyl groups, then the mineral is characterized as "trans-vacant". "Cis-vacant" clay minerals occur when the hydroxyl groups in the vacant octahedra occur at the same side of the vacancy. The main difference is located at different dehydroxylation temperatures, with the cis-vacant minerals showing higher values (~700^{o}C) than their trans-vacant counterparts (< 600^{o}C) (Kahr & Emmerich, 2001; Christidis, 2013).

The combination of the fundamental structural units of phyllosilicate minerals yields three main types of layer arrangements:

1:1 phyllosilicates are formed when a tetrahedral sheet (T) is linked to an octahedral sheet (O). The linkage occurs between the apical oxygen ions of the tetrahedral sheet and the oxygen ions of the octahedral sheet. The layers are strongly connected together by hydrogen bonds. As a result, there is restricted displacement (such as expansion) between the layers and the reactive area of external surfaces is also limited. Representative minerals of this category are the kaolin and serpentinite groups of minerals (Meunier, 2005).

2:1 phyllosilicates occur when two tetrahedral sheets enclose one octahedral sheet in between. The tetrahedral sheets are linked with the octahedral sheet by sharing the apical oxygen of the fourth corner of the tetrahedra, which points towards the center of the octahedra. This shared oxygen atom forms part of an adjacent octahedral sheet, in which octahedra are linked by sharing edges (Meunier, 2005; Murray, 2007). The junction plane between the tetrahedral and octahedral sheets consists of the shared apical oxygen atoms of the tetrahedra and the unshared hydroxyls of the octahedra. The three-sheet crystals have an approximate thickness of 1 nm and

they are held together either by strong electrostatic bonds between the interlayer cations and the clay surface or by van der Waals forces resulting from the hydrated, interlayer cations. The most common hydrated cations are Na^{+}, $Ca^{2+}$and Mg^{2+}. Monovalent hydrated cations with small atomic weight and ionic radii apply weaker attractive forces between the layers and thus the swelling ability of the crystals is enhanced. The 2:1 structures may occur as the following polytypes: 1M (one-layer monoclinic), 2M (two-layer monoclinic), 1 Md (disordered one-layer monoclinic) and 3T (three-layer trigonal) (Weaver & Pollard, 1973). The 2:1 phyllosilicates are divided into three subgroups; mica, smectite and vermiculite groups. The structural formula of micas is similar to that of talc and includes dioctahedral (muscovite type) and trioctahedral (biotite type) subgroups, Micas do not swell because interlayer cations are not hydrated.

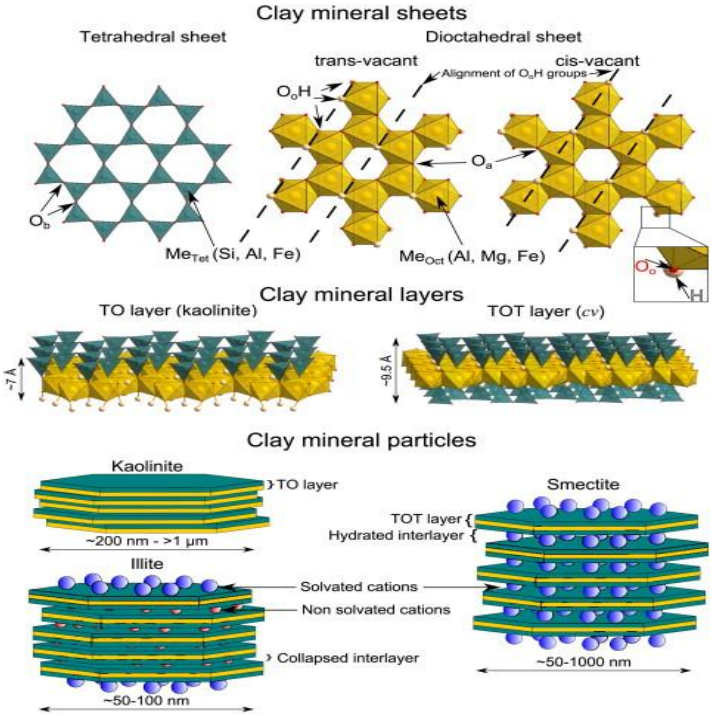

Figure 1.2: Basic clay mineral units and structures (Tournassat et al., 2015)

2:1:1 or chlorite type structure is a common variation of 2:1 structure. The crystal lattice of this type includes a talc-structured 2:1 layer, linked to a brucite layer underneath (Bailey, 1975). Isomorphic substitutions give talc a net negative charge of -1. The brucite layer is connected to the talc layer with coulombic forces. As a result, the charge deficit is neutralized, the entrance of exchangeable cations is blocked and swelling phenomena is prohibited.

1.2 Smectites

In this section, the characteristics and properties of smectites are presented. Smectites belong to the family of 2:1 phyllosilicates. They possess a layer charge of 0.2-0.6 electrons per half unit cell (p.h.u.c. - Christidis, 2013). As mentioned above, a 2:1 layer consists of an octahedral sheet between two tetrahedral sheets. In the interlayer space can enter hydrated, exchangeable cations or other polar molecules. Minerals of the smectite group (mainly montmorillonite) are the main phases that constitute the clays known as bentonites. Ross & Shannon (1926) gave an early definition to the term "bentonite" as an exclusively volcanic, glassy material, which turned to cryptocrystallic minerals, such as smectites, zeolites and opal CT. Also, other rock-forming minerals with larger grain sizes may co-exist in this material. The most complete definition of the term "bentonite" was given by R.E. Grim in 1972, at the international clay conference held in Madrid. According to R.E. Grim, bentonites include clays, which consist mainly of smectite group minerals, regardless their formation mechanism.

1.2.1 Classification of smectites

The classification of smectites and generally clay minerals has been under study for almost 80 years. Ross & Hendricks (1945) were the first scientists who tried to create a classification protocol for clay minerals. In their turn, Brown (1955), Warshaw & Roy (1961), Güven (1988), Drits et al. (1998) and last but not least Christidis & Eberl (2003) continued this project. Major classification factors are their structure type, layer charge, formation mechanisms and swelling capabilities.

- **Structure type classification**

Clay minerals belong to either the 1:1 or the 2:1 phyllosilicate groups, except for the chlorite group of minerals, the interlayer space of which is occupied by a brucite layer. Smectites belong to the 2:1 group of minerals and they can be divided further into dioctahedral and trioctahedral depending on the number of occupied positions in the octahedral sheet. The dioctahedral ones are also subdivided into cis-vacant and trans-vacant, depending on the position of the hydroxyl groups of the empty octahedral position (section 1.1).

Table 1.1: The most important dioctahedral and trioctahedral smectites

Dioctahedral smectites	Trioctahedral smectites
Montmorillonite	Hectorite
Beidellite	Saponite
Nontronite	Stevensite

- **Layer charge classification**

The charge magnitude of the unit cell is a major classification parameter of smectites. Also, the charge localization (tetrahedral or octahedral) and the amount of ferric iron in the octahedral sheet are also considered. Formally, there is no accepted classification protocol based on the layer charge and until now they are divided into high-charge and low-charge smectites. A classification process for dioctahedral smectites, which utilizes XRD data of K-saturated ethylene glycol-solvated smectites, was proposed by Christidis et al. (2006). According to this proposal, low charge smectites possess layer charge values <0.425 h.u.c, medium charge smectites have values between 0.425 and 0.475 h.u.c and high charge smectites acquire values >0.475 h.u.c.

The electric charge of the unit cell does not coincide with the net surface charge. Because of the small grain size and the net negative charge of these materials, adsorption of atoms and molecules can easily occur. This phenomenon changes dramatically the net surface charge of the material and thus traditional unit cell charge determination methods, such as the alkylammonium, methylene blue or structural formula methods (Christidis, 2016) are not precise. Instead, electrokinetic mobility and zeta potential measurements must be applied. More information about the surface charge of clay minerals is given in Chapter 2.

- **Genesis mechanism classification**

A classification characteristic of smectites is their formation mechanism. Usually, dioctahedral smectites occur in volcanic environments as a product of diagenetic or hydrothermal alteration of volcanic glass. Also, they can be formed in sediments of alkaline lakes and *sabkha* environments, being the dissolution products of clastic materials, whose origin is not volcanic. In such environments, trioctahedral smectites (mainly saponite and stevensite) are formed, along with sepiolite and palygorskite (Christidis & Huff, 2009).

- **Swelling ability classification**

The swelling capability of smectites is highly dependent on their exchangeable cations. Harben & Kužvart (1997) categorized smectites, based on their swelling capability in aqueous environments. As "swelling smectites" are characterized the materials, the interlayer space of which is dominated by hydrated Na^+ cations. These smectites can form gels, due to delamination of their aggregates.

On the other hand, the group of non-swelling bentonites includes Ca-and Mg-smectites. These materials usually aggregate and precipitate fast. Consequently, they are not appropriate for rheological modifiers opposite to their Na- counterparts.

1.2.3 Properties and applications of smectites

The smectite group of minerals acquires some unique properties, which make them useful in many industrial applications, being at the same time environmentally friendly and low-cost materials.

The largest quantity of the annually produced bentonite is consumed as animal litter. Bentonite is the main competitor of palygorskite and diatomite. It is able to adsorb fluids and odors. At the same time, it forms uniformly sized aggregates and does not produce dust as the sand based materials used in the past (Eisenhour & Brown, 2009).

Drilling fluids lubricate and cool the drilling bits of the drilling machine, while transporting the fragmented material outside the boring hole. Another important function of these suspensions is the filter cake formation, which stabilizes and reduces the permeability of the walls (Mckeen & Geehan, 1989). Bentonites are ideal additives in drilling fluids, because they form viscous suspensions when dispersed in a fluid phase. Na-smectite shows exceptional rheological characteristics, since it can be completely delaminated in the water and is preferred to its Ca-smectite counterpart. The latter is more commonly found in nature and it undergoes cation exchange with soda ash to obtain Na^+ cations in the interlayer space. Excellent rheological properties have been presented also by hectorite (Athanasakis, 2019).

Foundry sands contain bentonite in concentrations between 5-10% w/w. Its adhensive properties contribute to the bonding and plasticity of foundry sands, which must not be susceptible to deformations, after the molten metal is poured inside the mould. Na-bentonites perform better than Ca-bentonites, due to higher wet tensile and dry compression strength

(Christidis, 2013). Because of the great amounts of heat transferred instantly to the mould from the melt (usually greater than 1000^{o}C), smectite loses its binding ability and is susceptible to structure deformations. To avoid quality issues, metallurgical industry takes into consideration the dehydroxylation temperature of smectites. "Normal" or "ideal" montmorillonites are considered the materials with dehydroxylation temperatures at 700^{o}C, while "abnormal" smectites undergo dehydroxylation at 500-550^{o}C. Dehydroxylation can occur in one or two stages (550 and 700 ^{o}C). Consequently, the most appropriate choice is the cis-vacant smectites, because the dehydroxylation takes place above the desirable limit of 700^{o}C and they can be recycled (Paluszkiewicz et al., 2008: Holtzer et al., 2011: Żymankowska et al., 2011).

Thei increased swelling ability of Na-smectites results to low permeability. For this reason, they are used as geosynthetic materials in sanitary burial of urban wastes (Browning, 1998). Their high CEC, low hydraulic conductivity and permeability make them a subject of extensive research in backfill applications to contain radioactive wastes (Bucher & Müller-Vonmoos, 1989).

Smectites possess unique characteristics, which enable them to participate in many industrial applications, without undergoing any modifications. In this way, the cost is reduced. Their properties can be modified, in order to be used in more refined applications. Their natural properties are presented below:

- **Layer charge**

Smectites possess two types of electric charges. The first type is a permanent, negative charge due to isomorphic substitution in the tetrahedral and octahedral sheets. In the tetrahedral sheet, Al^{3+} cations commonly substitute for Si^{4+} cations. Similar substitutions occur in the octahedral sheet, mainly by Mg^{2+} and Fe^{2+} for Al^{3+} cations. This charge is balanced by monovalent and bivalent. In addition, charged may also be physically adsorbed in the interlayer space of the particles.

Some clay minerals, including smectites, develop a variable electric charge at the fractured edges of their particles, due to uptake and release of H^{+} from exposed functional groups, such as aluminols and silanols (Christidis, 2011). This charge can be positive or negative depending on the pH of the aqueous environment. The point at which the surface is net uncharged (positive charge equilibrates negative charge) is defined as "the point of zero charge"

(PZC). This type of charge affects mainly the kaolin group of minerals, in which the isomorphic substitutions are minimal.

- **Hydration properties**

Hydration of smectite particles causes swelling and eventually delamination of their aggregates. The swelling mechanism of clay particles is divided into two main categories: the crystalline and the osmotic or double-layer swelling,

During crystalline swelling the *d(001)* dimension of the crystals varies from 10 to 20 Angstroms. There can be 1 to 4 distinct water layers in the interlayer space (although the fourth layer has not been formally recognized). When dehydration occurs, the structure collapses. This phenomenon is reversible and as such, after some hydration-dehydration cycles, it is not expected to hydrate again to the same degree. This type of swelling is connected to the formation of quasicrystals.

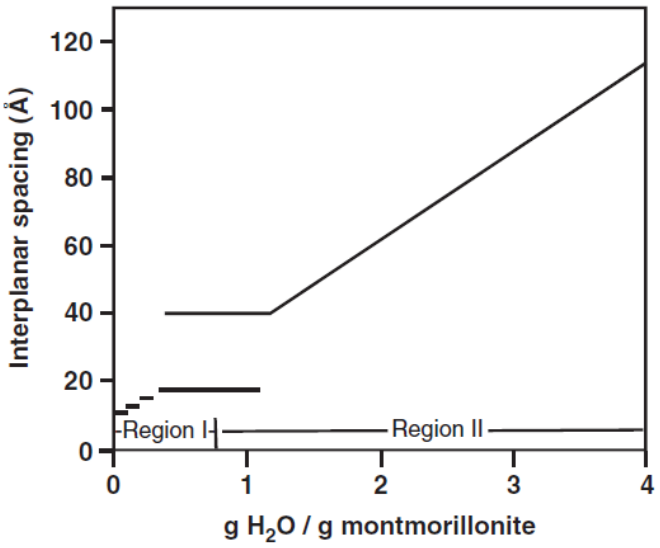

Figure 1.3: Diagrammatic illustration of crystalline and osmotic swelling (Christidis, 2011)

If the hydration process continues, the aggregates tend to delaminate (provided that the interlayer space is saturated with Na^+ or Li^+ atoms). When the interlayer space varies from 20-40 Angstroms, tactoids are formed. Above 40 Angstroms, the second swelling mechanism occurs, called osmotic swelling. The particles are totally delaminated and they interact via repulsive and attractive forces from hydration and Coulomb electrostatic forces respectively (Christidis, 2011; Laird, 1999; Laird, 2006).

- **Cation Exchange Capacity (C.E.C)**

Cation exchange is a stoichiometric reaction, which belongs to the adsorption processes. It is stoichiometric, because each adsorbed cation replaces an adsorbed one. On the other hand, in the common adsorption, a chemical species can be connected to a surface, until the latter is saturated. CEC is measured in *meq./100 g of dry clay*.

Cation exchange capacity occurs in smectites and other clay minerals, due to the isomorphic substitution of cations in the tetrahedral and octahedral sheets. Extensive substitution means increased layer charge and thus increased CEC. Consequently, CEC determination is an indirect way to measure the layer charge of clay particles.

- **Grain size, shape and specific surface area**

Smectites consist of small-sized particles, usually <0.5 μm and form lath, subhedral and euhedral lamellae-shaped aggregates (Grim & Guven, 1978). Because of their shape variability, small grain size and internal pore structures, they acquire increased specific surface area, which ranges between 10 and 800 m^2/g. The pore structures are slit-like or they can form channels among the clay aggregates.

1.3 Kaolin group of minerals

Kaolinite and its polymorphs (halloysite, dickite, nacrite) are 1:1 phyllosilicates. In brief, the crystalline structure of this group consists of a tetrahedral sheet connected to an octahedral sheet, without any interlayer space. Kaolins are important raw materials for the industry and are included in many everyday applications. Kaolinitic clays acquire different names, derived from their application purpose and their geological environment, such as “ball clays” and “fire clays”.

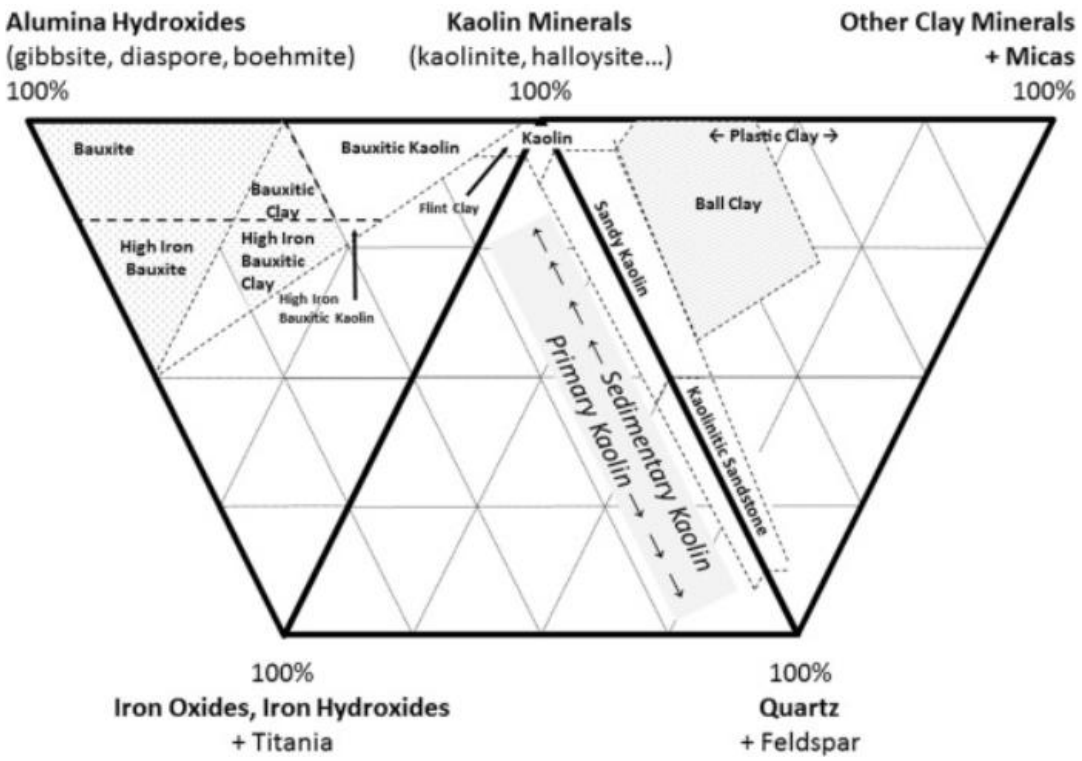

Figure 1.4: Ternary diagrams showing the classification of kaolinite-rich industrial clays (Pruett, 2016)

The term "China clays" refers to kaolinite-rich clays with well-crystallized kaolinite. The name originates from England. As "Tonsteins" are known the kaolinitic materials originated by in situ alteration of airborne volcanic ash. They are also an index for coal deposits. "Soft clays" are coarsed-grain, well-crystallized materials with high Hincley index values. On the contrary, "hard clays" acquire low Hincley index values, due to disordered structure (Christidis, 2011).

1.3.1 Kaolinite polymorphs and kaolinitic clays

- **Dickite, nacrite and alloysite**

Kaolinite is a 1:1 phyllosilicate, dioctahedral mineral. Its particles have hexagonal shape when formed by acidic solutions and fibrous shape when the formation environment includes alkaline solutions (Fialips et al., 2000). Kaolinite crystallizes to the triclinic system. The lath-shaped structures form in case of foreign cation adsorption on the external surface of the crystals, which causes their elongation. In tropical soils, the pH of which is more acidic, such as laterites, the possibility of disordered structure is higher, due to partial dissolution of the crystal lattice. Also, Fe^{3+} cations may substitute for Al^{3+} cations in the octahedral sheet, which also induces disorder. The lateritic soils may contain iron-bearing kaolinite, which is formed by the mixture of

the aluminous and ferric end members (Meunier, 2005). In diagenetic environments, the kaolinite crystals are intact and form booklet-like structures, several microns thick. Its structure follows 1M symmetry, in which each sheet is shifted on the *α* crystallographic axis by *a/3*, while the empty octahedral site remains at the same position.

Halloysite is chemically identical to kaolinite. The main difference is in the crystalline water molecules adsorbed in its interlayer space, which form hydrogen bonds with the octahedral sheet. Halloysite is formed in fluid-rich, high-anionic-strength environments. The crystallization takes place rapidly, causing defects in the crystalline structure and facilitating the entrance of crystalline water (Giese, 1988). The hydration causes an increase of the d-spacing (from 7.2 to 10 Angstroms), which is the identification factor between kaolinite and halloysite. Dehydration of halloysite is irreversible, causing identification problems. Kaolinite may convert to halloysite, due to hydration and rolling up of its layers (Meunier, 2005). This cylindrical structures form, because the octahedral sheet is smaller than the tetrahedral sheet and thus the alignment of two sheets is not perfect. The external surface of the cylinder consists of the tetrahedral sheet.

Dickite and nacrite are kaolinite polytype. Dickite forms monoclinic, rhombohedral crystals with irregular stacking sequence, which becomes more symmetrical in the later stages of crystallization. The crystals of both minerals follow the 2M1 symmetry, in which the empty octahedral site of each layer rotates 120^{o}. Also, each layer shifts by b/3 (nacrite) and a/3 (dickite) in each crystallographic axis respectively. They derive from hydrothermal alteration, with minor occurrences in sedimentary and residual deposits (Murray, 2007; Meunier, 2005).

- **Kaolinitic clays**

Ball clays

They are sedimentary kaolinitic materials originated from fresh water basins and rivers. They are mined as cubic-shaped bodies, which are transformed into ball-shaped masses in time, due to their plasticity. They are connected to lignite deposits (Hosterman, 1984; Burst & Hughes, 1994).

Fire clays

They are refractory kaolins and are closely related to sub-vituminous coal deposits. They were widely used during the industrial revolution in NW England. Nowadays, they are not used in refractory applications.

Flint clays

Flint clays are recognized by their increased hardness and smooth texture, a result of extensive diagenetic phenomena. They are the only kind of kaolinitic materials used in refractory applications nowadays. Flint clays are the transitional stage between bauxites and kaolinitic clays, due to the increased concentration of Al-hydroxides and the intense diagenetic phenomena undergone.

Grog, chammote, molochite

These terms refer to calcined, kaolinitic clays used as framework structures in brick manufacturing. Molochite is exclusively calcined "China clays".

1.3.3 Applications of kaolinite

Kaolinite is a widely used industrial mineral, because of its physical and chemical properties. Depending on its quality and processing, it is included in high added value applications such as paper, ceramic, plastic and paint manufacturing. Other lower value applications include the production of alumina and refractories.

Paper

Kaolinite is used in paper industry as fillers and coatings. Coarse-grained material (≤5 μm) is mixed up with cellulose fibers (wood pulp) in specific proportions (2-30% w/w, depending on the paper), which are designed to achieve equilibrium between strength and opacity. The fibrous cellulose strengthens the paper, but it increases transparency. On the other hand, excessive amount of kaolinite enhances opacity, but undermines the structural integrity of the paper.

Fine-grained kaolinite (≤0.5μm) is mixed up with adhensives and other additives, to form coatings onto the surface of the paper. Coated paper acquires smoother surface and good optical properties (opacity, brightness, gloss), while its printability is enhanced (Phipps, 2014).

Paints

Paints need to be resistant to scrubbing, staining and water, with good opacity to cover dark surfaces. Many decorative paints contain pigment, binding substance and calcined, delaminated kaolinitic fillers, in specific proportions. Kaolinite helps in pigment extension. An enhanced extension lowers the concentration of pigment required and consequently the overall cost. At the same time, it regulates the viscosity and dispersion of paints. Fine-grained kaolinite (98% of the material should be <2 μm) is added in proportion up to 50%, in semi-gloss and high-gloss paints (Bundy, 1993).

Plastic products

Kaolinitic fillers aid the mechanical properties of plastic products, such as impact resistance, flexular and compressive strength, while preventing the material from cracking and shrinking during processing. Kaolinite particles form platelets, which contribute to the stability, surface smoothness and insulation of the final product. By increasing the concentration of well-dispersed, kaolinitic fillers, the mechanical properties of the final product continue to augment, until the compaction limit is reached (Tawfik et al., 2018).

Ceramics

The quality of ceramics depend on certain, representative properties such as plasticity, refractoriness, strength under mechanical tension (green and dry), shrinkage, water absorption, color and degree of difficulty during casting. In order to comply with all the above criteria, the use of kaolinite is recommended, because of its physical and chemical properties.

Kaolin based suspensions acquire appropriate viscosity for ceramic manufacturing by using the “casting slip” method. The rheological properties of the suspension and the demand for other additives are the main factors contributing to the successful production of ceramics with refined shapes (Jepson, 1984; Murray, 2007).

Chapter 2: Surface charge properties

In this chapter, the surface charge properties of the smectite and kaolin groups of minerals are investigated. The electric charges of the particle surfaces interact in various ways,

contributing to the unique properties of clay minerals. This thesis relies on the comprehension of these interparticle phenomena that develop among clay minerals and is possible to influence microorganisms, resulting in the production of antimicrobial, chemical substances.

2.1 Surface charge distribution of smectites and kaolinite

Smectites

Smectites possess two different types of electric charges. Major influence in the overall particle charge has the permanent negative charge, which derives from isomorphic substitutions in the tetrahedral and octahedral sheets. This results in charge deficit, due to the lower valence of the substituting cations. The tetrahedral substitutions cause more localized charge distribution than the octahedral ones, which yield a diffuse, negative charge (Johnston & Tombacz, 2002). The charge imbalance is neutralized by exchangeable, hydrated cations in the interlayer space (Van Olphen, 1963). The permanent charge participates up to 95% in the net surface charge (Grim, 1962).

The other 20% derives from imperfections, distortions and shattering of the crystal lattices of clay minerals. As a consequence, the incompletely formed particles have exposed, broken edges, which are chemically active, polar, anionic centers and thus are able to adsorb and desorb H^+ and other cations. These groups include silanols and aluminols.

Tombacz & Szekeres (2004) highlighted the mutual influence of the potential-regulating OH^- and H^+ ions and other indifferent electrolytes in the electrokinetic and colloidal properties of clay minerals. Moreover, they separated the charge neutralization mechanisms, which are derived from indifferent ions, from the influence of H^+ ions, which are produced by the ionization of water molecules. The adsorption/desorption rate is a function of pH of the polar liquid, in which these materials are immersed and the ionic strength of the dissolved electrolytes. Thus, the charge is called “non-permanent” or “pH-dependent”.

As reference point is the point of zero charge (and its relevant variations), which signifies the electrical neutrality of the surface, due to the equilibrium of positive and negative charges. Below the PZC, the surface becomes positively charged, because of the increased intake of H^+ cations and the opposite.

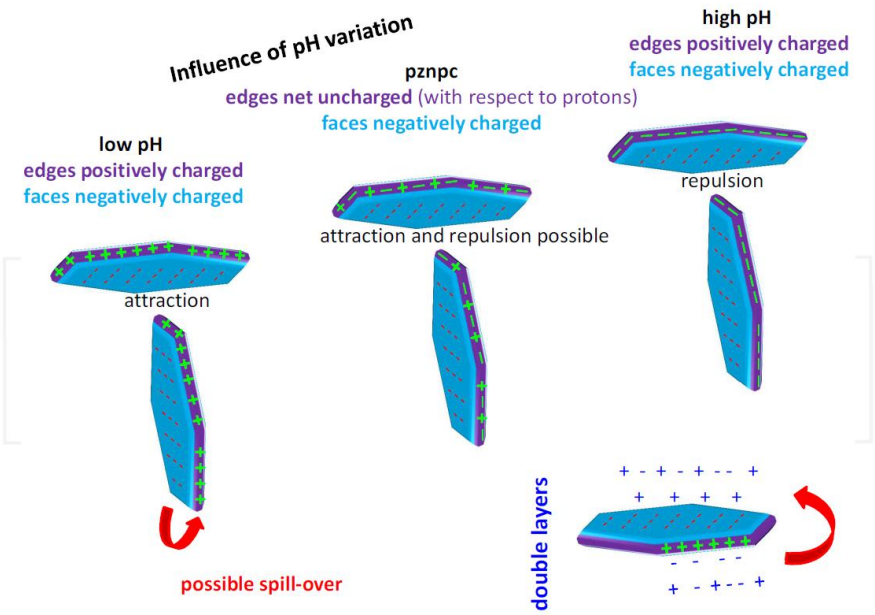

Figure 2.1: The anisotropic charging behavior of ideal clay lamellae (Preocanin et al., 2016)

The overall surface charge of clay minerals does not coincide to the unit cell charge, because of the co-existence of permanent charges from isomorphic substitutions in the crystal lattice and variable edge charges. Consequently, the measurement of the net charge is more complicated than that of pure metal oxides (James & Parks, 1982). The value of surface charge density (σ_{in}) is the sum of the net permanent structural charge density (σ_0), and the net proton surface charge density ($\sigma_{0,H}$).

$$\sigma_{in} \equiv \sigma_0 + \sigma_{0,H} \quad \textbf{(Eq. 2.1)}$$

Kaolinite

Kaolinite is a 1:1 phyllosilicate mineral, which does not possess a permanent negative charge similar to the smectite group of minerals, due to the lack of substitutions in the tetrahedral and octahedral sheets. Minor substitutions of Al^{+3} by Fe^{+2} in the octahedral sheet are possible in residual deposits, in which the concentration of ferric iron is increased.

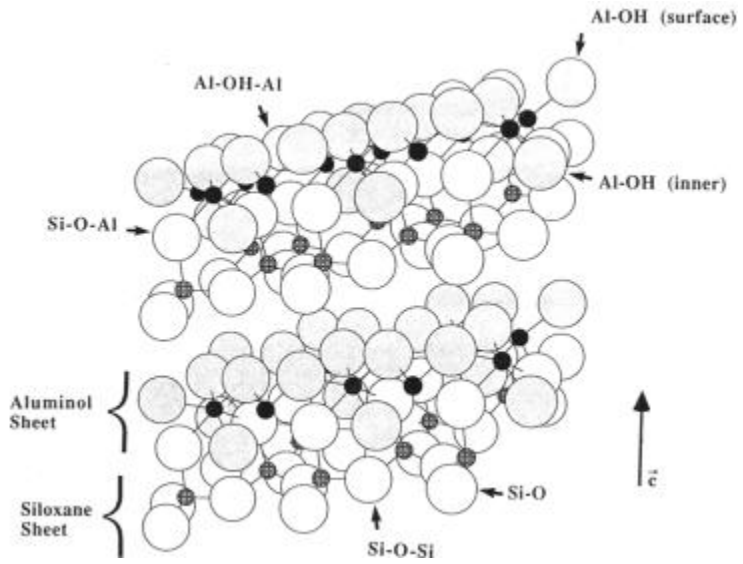

Figure 2.2: Illustration of chemically active sites in a kaolinite crystal (O'Day et al., 1994)

The development of surface charge is the result of one or more factors described below:

1. As mentioned above, a small permanent charge may occur, owing to substitutions of cations in the layers. Al^{3+} cation is usually replaced in kaolinite, while Si^{4+} is the most common cation to be replaced in beidellite, which belongs to the smectite group of minerals (Schofield & Samson, 1954).
2. The particle edges of kaolinite are chemically active and react in various ways and in different pH values. Firstly, the incomplete crystal formation or shattering, results in unoccupied hydroxyl group at the edges. These groups are connected to Al^{3+} or Si^{4+} cations, forming aluminols and silanols respectively. These compounds act as proton donors and acceptors. Specifically, the adsorption of water onto aluminol groups forms Lewis acid sites (Sposito, 1984). Because of the different PZC of alumina and silanol, there is simultaneous development of positive and negative charges in the crystal lattices. At pH values below 8.7, aluminol sites possess positive charge, whereas silanol groups possess negative charge until pH=3. In strongly alkaline environments, all active sites repel the H^{+} cations and the overall surface charge becomes negative (Brady & Walther, 1989).

3. Apart from the hydroxyl groups at the edges, there is ionization of the occupied hydroxyls in the octahedral sheet. Individual hydroxyl groups also exist in the tetrahedral sheet (Zhou & Gunter, 1992). However, it has been assumed that the hydroxyls inside the crystal lattices do not contribute to the total surface charge as much as previously thought, contrary to the exposed edges (Brady et al., 1996).
4. During the natural formation of kaolinite, the existence of defects in the structure or even the simultaneous formation of smectite layers are possible. The interlayer cations of the smectites are able to be exchanged for protons, causing the surface charge to differentiate. This phenomenon is relevant to the kaolinite formation and it has not been entirely comprehended yet (Brady et al., 1996).

2.2 Zeta Potential and electric double layer

The electric double layer model (EDL) describes the behavior of electrically charged particles, when immersed in a polar liquid phase, such as water. This mechanism plays a key role in the stabilization of colloid systems. The EDL is responsible for the development of repulsive, electrostatic forces among the particles, maintaining them suspended. The EDL is electrically neutral, but it can be polarized or distorted. In this way, electrorheological phenomena are manifested (Hao, 2005). In case of an increase of the ionic strength in the solution, the EDL is compressed and aggregation occurs.

The Poisson-Boltzmann equation (2.4) is considered the most accurate mathematical expression of the diffuse double layer model. There is not an exact solution for this equation, but different approaches have been proposed, which are applicable in some occasions. The most popular are the Gouy-Chapman and Debye-Huckel approaches. However, the DDL model has some inaccuracies, which are summarized below:

- The size of ions is inaccurate
- The structure and electrical properties of the water are not taken into consideration
- The charge is considered equally distributed on the surface, which is not representative for most particles (especially clays)
- The hydration of the solid surface is not taken into consideration
- Boltzmann distribution overestimates the concentration of the adsorbed ions on the surface

$$\frac{\partial^2 \Psi}{\partial \chi^2} = \frac{1}{\varepsilon_0 \varepsilon_r} \sum_i v_i e n_{i(\infty)} \exp\left(\frac{-v_i e \Psi_\chi}{kT} \right) \quad \textbf{(Eq. 2.2)}$$

The concept of the EDL and zeta potential are described in this paragraph. Clay particles acquire a net negative charge in the water, as a result of the negative charges of their layers and other chemically active groups, such as exposed edges. The negative-charged surfaces attract opposite-charged ions (counter-ions), which form a stable layer around the particle known as "Stern layer" (Park & Seo, 2011). The particle surface and Stern layer are enveloped by a diffuse layer, which consists mainly of opposite-charged particles. The Stern and diffuse layer compose the structure of the electric double layer or diffused double layer. When a particle is moving in the suspension, it is surrounded by the Stern layer and a part of the diffuse layer. The electric potential that develops at the shear plane of the diffused layer is known as "zeta potential" (ZP, Furukawa et al., 2009). The diffuse layer interacts with the solid surface by long-range forces but it is not an inseparable part of the Stern layer-solid surface system. Electrochemically active groups attract opposite-charged ions, which form hidden EDLs. The face-derived EDL is fused together with the secondary EDLs. The former spills over in low ionic strength solutions, provided that the particle is smaller than the Debye length (Tombacz & Szekeres, 2004).

The ZP acquires positive or negative values and it controls the stability of the colloid. The higher the absolute value of the ZP, the more stable the suspension is. The range of values, at which the suspension is considered prone to precipitation, is from -30 mV to +30 mV. The possibility of aggregation increases at the IEP (ZP=0 mV). Zeta potential is mainly influenced by pH, ionic strength of the solution and valence of the dissolved ions. Also, it is important to identify possible impurities, which are capable of distorting the EDL.

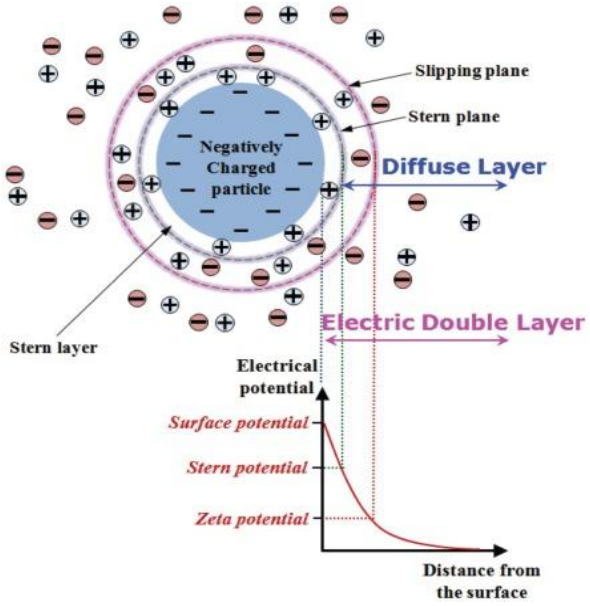

Figure 2.3: Illustration of the Diffused Double Layer model (Park & Seo, 2011)

It must be clarified that zeta potential and surface charge refer to different characteristics. Surface charge is strictly limited to the electrochemical interactions that take place on the particle surface, which result to electric charge development. Zeta potential refers to the potential of the solid-solution interface, during particle motion. In many cases, it is convenient to equate the two terms, because zeta potential can give representative results about the electrokinetic mobility of the solids and can be experimentally determined, unlike the surface charge (Furukawa et al., 2011). This is the case for materials of high electrokinetic complexity, such as clays. Since the origin of the clay particles charge varies, the ZP expresses average potential values, without knowing the contribution of each parameter to the net charge.

In conclusion, the evolving phenomena in a colloidal system are complex and introduce concepts, which are not fully understandable yet. A good approximation is to comprehend the developing interparticle forces. For this reason the DLVO theory has been proposed. According to DLVO theory, the forces that develop among particles include the Brownian motion, double layer diffusion/repulsion, van der Waals and Bohr repulsion forces. On the other hand, the non-DLVO forces are not expressed by the DLVO theory. In this group belong the repulsive forces that are developed among hymens, double-layer attractive forces and repulsive forces caused by entropy and hydration interactions. Park & Seo (2011) support that DLVO theory is applicable in colloidal systems with low concentration in solids, without overlap of the electric potentials. It is considered that the only existing forces are the repulsive electrostatic interaction and attractive

van der Waals forces. Also, the shape of the particles should not be complex. As far as counter-ions are concerned, they must be uniformly affected by the developed electrostatic forces, entropy derived repulsion and Brownian motion.

2.3 Point of zero charge (PZC) and isoelectric point (IEP)

As "point of zero charge" (PZC) is the pH, at which the positive and negative charges of particle surface are equal. Consequently, the net surface charge is zero for amphoteric oxides. Minor pH adjustments above and below this point have a big impact on the electrostatic interactions between the ions and surface. The protonation and deprotonation of the surface can be described by the chemical equation below (Parks & Bruyn, 1962):

$$[MOH_2^+] \rightleftharpoons [MO^-] \quad \textbf{(Eq. 2.1)}$$

If the difference between the concentration of H^+ and OH^- ions adsorbed in the mineral surface is zero, at a specific pH value, it is called the "Point Zero Net Proton Charge" (PZNPC). The quantification of this parameter can be obtained by Acid/Base Titration, Mass Titration and Powder Addition (Mullet et al., 1997; Mustafa et al., 2002; Stumm, 1992; Noh & Schwarz, 1989).

The isoelectric point (IEP) and PZNPC are identical, provided that no adsorption of indifferent ions other than H^+ and OH^- occurs. Generally, adsorption of cations results in decrease of the PZNPC and to an increase of the IEP. The opposite is true for anions. If the incoming ions do not affect the surface charge, such as perchlorates, the IEP and PZNPC will obtain diametrically opposed values to each other (Stumm & Morgan, 1981). The point of zero net proton charge (PZNPC) for $\sigma_{0,H}=0$ is representative for the anisotropic charges of smectite surfaces (Cristiano et al., 2011). However, protons show specific correlation to the permanent charges (Tombácz et al., 1990). Therefore, the use of the $pH_{PZC,edge}$, parameter is recommended.

One more variation of PZC is the "Point of Zero Salt Effect" (PZSE). This term is used in mass titration technique, in which different concentrations of electrolyte are added. The common intersection point of the curves is the PZSE. Nevertheless, this parameter mostly appears when the surface charges are not balanced. The values of PZC and PZSE do not match, unless the mineral is free of impurities and the PZC is not influenced by the ionic strength of the electrolyte (Cristiano et al., 2011).

Sposito, (1992) introduced a zero charge term, specifically for the charge neutralization of the outer sphere complexes and diffuse layer ($\sigma_{os}+\sigma_d=0$). It is called "point of zero net charge" (PZNC).

Generally, the terminology of points of zero charges varies among the researchers. The PZC parameter is accurate for the variable charge of amphoteric oxides, but it is not representative for clay minerals, which develop permanent and pH-dependent charges (Tombacz & Szekeres, 2004). By introducing the above zero charge definitions, a more accurate interpretation of the unfolding phenomena is ensured. Regardless of the investigated material, the five charge parameters, which are summarized below, must have a sum of zero.

$$\boldsymbol{\sigma_0+\sigma_H+\sigma_{is}+\sigma_{os}+\sigma_d=0 \text{ (Eq. 2.2)}}$$

- σ_0: structural charge from isomorphic substitution
- σ_H: net proton charge
- σ_{is}: inner sphere complex charge
- σ_{os}: outer sphere complex charge
- σ_d: diffuse layer charge

An electrically-charged particle, suspended in a polar liquid medium will be mobilized under the influence of an electric field (electrophoresis). Depending on the sign of the developed surface charge, the particle will be directed towards the anode or cathode at a proportional speed to the magnitude of the charge. Given that pH influences the non-permanent charge of the surface, particles acquire positive charge in acidic environments and the opposite, always having PZC as a reference. Immobilization under electric stimulation occurs at a specific pH value, different for each material. At this value, the zeta potential is eliminated and is called isoelectric point (IEP). The IEP and PZC are determined from zeta potential vs pH diagrams. The IEP and PZC are identical, provided that ions other than H^+ and OH^- are absent and the mineral is pure. Otherwise, zeta potential measurements are influenced by possible adsorbed species on the particle surface, counter ions in the EDL and solvent substances bonded to the surface ions (Cristiano et al., 2011). For example, if cations, such as Ca^{2+} are present, which hold two charges, then the zeta potential declines at a high rate (becomes more positive). As a consequence, coagulation of the particles is promoted, due to shrinkage of their double layer. However, the surface potential is not subject to any changes.

Other potential-determining, chemical substances, apart from OH^- and H^+, include ions that surround the mineral and can be transported to the aqueous phase and specifically-adsorbing ions, mainly collectors, capable of forming complexes with ions of the mineral surface. Furthermore, they are able to react with precipitates originated from the deposition of ions at the solid/solution interface. Provided that one or more of the above cases are applied, the x-axis should indicate "activity" instead of "pH".

2.4 PZC determination methods

PZC can be determined by a series of different laboratory tests. These include potentiometric titration, mass titration and powder addition.

Potentiometric titration

In potentiometric titration, the minerals are considered as weak acids or bases. As a result, they can be dispersed in distilled water, in low concentrations and titrated by using small amounts of a strong acid or base. Also, a background electrolyte is added in the suspension to reduce the electrostatic repulsion forces at the water/surface interface (Lützenkirchen et al., 2012). A minimum of three suspensions must be prepared, each one with different ionic strength. A blank suspension is also titrated. The produced curves are plotted and the common intersection point (CIP) corresponds to the PZSE. The blank curve must be subtracted. Titration tests must be performed under inert atmosphere (Ar or He) to avoid carbon dioxide interaction.

In naturally formed clay minerals, the concentration of carbonate impurities, such as calcite and dolomite is increased, which undermines the outcome of the experiment. Other secondary reactions include (Preocanin, 2016):

- Reactions of functional groups located on the surface of basal planes, at the edges and ion-exchange sites
- Dissolution, hydrolysis and complex formation
- Re-precipitation and adsorption of chemical species, which were formed via dissolution

The surface activity complicates the interpretation of the results. Taking into consideration all the above chemical phenomena, even a pure oxide sample would need further analysis, to determine the influence of reaction on pH, surface charge and by extension to PZC. As a result, it is recommended to carry out the test as quickly as possible to minimize the side effects of each active group.

Mass titration

An alternative technique that is used for the determination of PZC is called "Mass Titration" and presents many similarities to Potentiometric Titration (Noh & Schwarz, 1989; Preocanin & Kallay, 1998). The experimental procedure includes the addition of precise amounts of sample to a suspension of known composition. The sample should be a pure oxide, which is considered uncharged before its insertion in the water. The increasing concentration of solid affects pH until it becomes constant. At this point, the surface reactions buffer the suspension and the PZNPC can be detected. The function that correlates the final pH value to the final sample concentration can be expressed by Eq. 2.5 (Cristiano et al., 2011):

$$N_t = \frac{(C_{OH} - C_H) \cdot ([MOH] + [MOH_2^+] + [MO^-])}{[MOH_2^+] - [MO^-]}$$

(Eq. 2.5)

where

- N_t: Total number of ionizable sites on the solid phase
- (C_{OH}-C_H): Difference between the concentrations of hydroxyl anions and protons in the suspension
- [MOH^+_2]: Concentration of positive sites
- [MOH]: Concentration of neutral sites
- [$MO^=$]: Concentration of negative sites

As for clays, their naturally-charged surfaces interact in a unique way with the electrolytes and thus the measurements would be strongly modified. In particular, the cation-exchange, which is stoichiometric, may involve uptake and release cations of different valence in the buffer solution, modifying the initial electrostatic interactions.

The results are plotted as *pH vs mass content* diagrams. It is important that no addition of acid or base to the system is required. In addition, the use of distilled water as a liquid phase hinters the adsorption of background electrolytes. A main drawback of this method is the precondition of the insolubility of the immersed mineral. Furthermore, the ratio of oxide to water

should not exceed 20% w/w. at higher ratios, the concentration of the suspension is too high for a representative pH measurement (Cristiano et al., 2011).

Powder addition

This technique does not relate to any type of the aforementioned titration techniques. It is performed by preparing solutions with identical ionic strength and variable acidity. Subsequently, fixed amounts of mineral are immersed to the solution. The added solid phase affects the pH of the suspension by adsorbing or releasing protons in the solution, depending on the PZC of the material. If the initial pH (pH_i) is lower than the PZC of the material, then protons are adsorbed, resulting into a pH increase, On the other hand, if the initial pH is higher than the PZC, then hydroxyl molecules are adsorbed, resulting into a pH decrease. The process is lengthy until equilibrium is achieved. For this reason, it is recommended to leave the suspension overnight, before the final measurement is taken. The data are plotted in a pH_i *vs* pH_f diagram. The PZC is determined when $\Delta pH=0$ (Mullet et al., 1997; Jirhatova, 1981).

2.5 IEP determination methods

At the IEP, the zeta potential of the mineral particles equals zero. The zeta potential-determining methods include electrophoretic and electroacoustic techniques. Secondary techniques use the electro-osmosis and streaming potential to determine the surface zeta potential (SZP).

Electro-phoretic method

The electro-phoretic procedures mobilize the suspended, electrically-charged, solid particles via an electric field. When the zeta potential becomes equal to zero, the particles are immobilized and the IEP is reached. The particle shape and adsorbed chemical species on the material determine the validity of the measurements. As a consequence, clay particles are quite difficult to be accurately examined. For instance, the electrokinetic behavior of smectite particles is mainly affected by the permanent layer charge that derives from cation substitutions in the layers. This type of charge does not vary with changing pH. The opposite is true for the edge charges. Hence, a reliable IEP measurement of smectite particles is obtained when the permanent charge is neutralized (Pecini & Avena, 2013).

Electro-acoustic method

Another type of electrokinetic technique uses acoustic waves produced by an alternating electrical current, which pulses the suspension to mobilize particles. The term that describes this phenomenon is called “Electrokinetic Sonic Amplitude” (ESA) and it is a method of determination of the charge and shape of the particles. The common frequency range varies from 0.3 to 11.5 MHz. Particles larger than 10 μm acquire a velocity below the detection limit of the method. On the other hand, particles below 0.1 μm become inertia dependent at frequencies >11.5 MHz (O’Brien et al., 1995; Appel et al., 2003).

2.6 Aggregation mechanisms

As "aggregate" is described a set of particles and/or colloids that are orderly or randomly stacked. For practical reasons, the term “aggregate” may be synonymous to “agglomerates”, “fecal pellets”, and “flocs”. These structures are formed under the influence of mechanical or physicochemical mechanisms (Furukawa et al., 2009).

The suspension of fine particles (usually <1 μm), such as clays, is primarily affected by the electrical double layer that envelopes the minerals and is responsible for the developing repulsive forces among them. The gravitational forces do not influence their suspension behavior to a great extent, due to their little mass of particles.

The term “colloid” refers to the suspended particles, as well as to the liquid phase. To destabilize a colloid, the electrostatic forces should be eliminated (zeta potential equals to zero) or the EDL should be overcome by closing the distance among the particles. In this manner, the energy barrier is transcended and the attractive van der Waals forces prevail. Also, the electrically neutral particles should be mobilized. The absence of repulsive forces and random movement may lead to coagulation. Coagulation is the first step, followed by flocculation. The former term usually includes both phenomena, as well as the use of flocculants. The most important factors that influence the precipitation of colloids are the following (Johnson et al., 2019):

- EDL compression, due to high anionic strength and valence of dissolved ions in the suspension
- Adsorption of opposite-charged species on the mineral surface
- Sweep precipitation

- Interparticle bridging
- Brownian motion (It is caused by the increased heat transferred τo the suspension. This phenomenon is called "perikinetic flocculation")
- Differential motion of parts of the suspension ("orthokinetic flocculation")
- Differential precipitation caused by gravitational forces

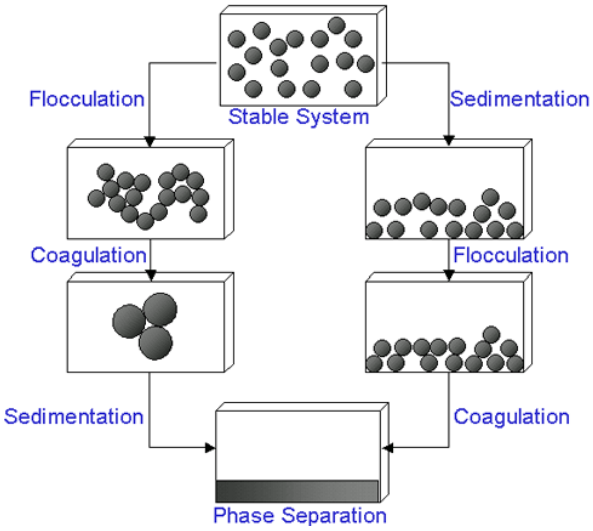

Figure 2.4: Destabilization processes of a colloid (Malvern Instruments Limited, 2015)

Smectite particles hydrate and delaminate more efficiently, when the interlayer space is occupied by Na^+ cations. Depending on the hydration degree, the particles are held together by van der Waals forces caused by the interparticle water molecules (crystalline swelling), forming quasicrystals. Smaller quasicrystals may form by agitation of the suspension. On the other hand, the continuous hydration causes the formation of tactoids, which remain suspended by the long range interactions of their EDLs (osmotic swelling) (Christidis, 2011). Destabilization of the colloids takes place, when EDLs overlap each other and Van der Waals forces prevail. In clay minerals, the formation of quasicrystals is considered as "flocculation", which is a type of coagulation, but involves face-to-face particle stacking. This structure reduces the pore formation, resulting to a lower permeability. On the other hand, an edge-to-face stratification produces scaffolds. Thus, the pore size and permeability are increased. A combination of quasicrystals and scaffolds is possible. Finally, edge-to-edge association may occur, forming chain-like structures. Usually, edge-to-edge morphology is connected to an increasing ionic strength of the suspension and is the transitional layout before the face-to-face aggregation. The edge-to-face and edge-to-edge morphologies are preserved at pH=4-8.5 (Wilkinson et al., 2018).

Kaolinite particles are not as easily dispersed as smectite particles. The only source of electric charge comes from the broken edges of their crystal lattices. Also, this charge is pH-dependent. Gupta et al. (2011) proved that the two composing sheets (silica and alumina faces) define the aggregation mechanism in acidic environment. At pH values 5-5.5, the edge-to-face (silica edge and face, alumina edge and face) and face-to-face (silica face–alumina face) interactions are facilitated. In more alkaline conditions, these sequences are not promoted, due to the increasing surface charge density of the tetrahedral sheet and its exposed edges. At the same time, the surface charge density of octahedral sheet decreases. In strongly alkaline conditions, the overall charge is negative, stabilizing the colloid and the edge-to-edge interaction. In case of precipitation of the suspended kaolinite, the initial edge-to-face and face-to-face orientation is exclusively face-to-face, while settling.

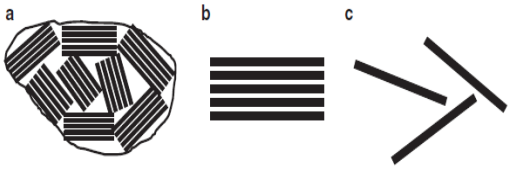

Figure 2.5: Schematic presentation of particle (a), quasicrystal (b), fundamental particle (c) (Christidis, 2011)

Chapter 3: The biogeochemical cycle and its ancient and modern applications

In this chapter, the interaction mechanisms between clay minerals and microbes are under discussion. Minerals and microorganisms depend on each other, since the evolution of the earliest life forms. Nowadays, the available technology and understanding of the biogeochemical cycle are able to adjust these natural mechanisms to improve the quality of life and environment.

3.1 The biogeochemical cycle

Clay minerals possess surface charge and consist of fine mineral particles with various shapes. Their nanometric size and shape diversity lead to increased surface area, which results to augmented adsorption capability. Adsorption is a property of major importance, which transforms clays into nutrient sinks and organic matter storages (Cuadros, 2017). The adsorption of metabolites on the mineral surfaces creates accumulation environments of organic matter,

which was a catalytic factor for the evolution of primary life forms. Representative example of great importance is the ocean bottom (Kennedy et al., 2006). It consists of fine sediments, which accumulate organic matter produced by the decomposition of marine organisms. To comprehend the order of magnitude of the nutrient accumulation, Weiss, (1969) confirmed via laboratory experimentation that a ton of montmorillonite is able to adsorb 550 kg of proteins, 150 kg of fat acids and 220 kg of carbohydrates. The material is held on the solid surfaces by hydrogen, covalent and ionic bonds or Van der Waals attractive forces.

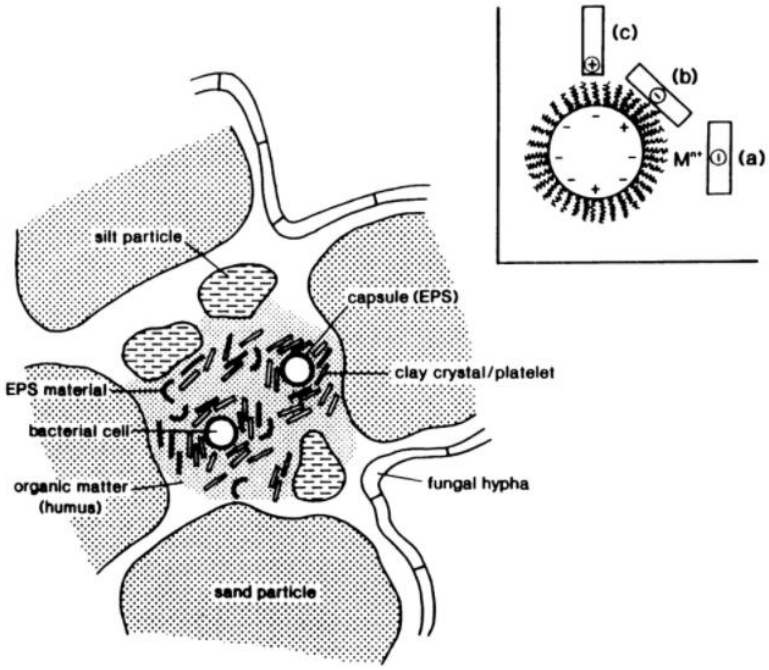

Figure 3.1: Illustration of the symbiotic relationship of microbes and soil minerals (Huang, 2004)

Clay minerals provide shelter and nutrients to microorganisms. The most abundant metal cations provided from minerals include K, Na, Mg, Ca, Fe, Mn, Co, Zn, Cu and Mo, which function as catalysts for vital metabolic reactions of the microorganisms (Fomina & Skorochod, 2020). The stored humic acids among clay particles provide a carbon source for their energy demands, as well as necessary metal cations. The distribution of chemical species is achieved by cation exchange. At the same time, essential DNA, polysaccharides and antibiotic substances are protected from natural phenomena and decomposition from the microbes themselves. These compounds contribute to the evolution and codification of high antibiotic resistance genomes (Ehrlich, 1998).

On the other hand, microorganisms are essential for the disintegration and formation of clay minerals. The disintegration of minerals is a result of two different processes. The first includes biochemical processes, which destroy the crystal lattice of minerals by chemical reactions. The second mechanism is relevant to biomechanical processes originating from the development of microbial colonies (mainly fungi) on clay particles (Burford, 2003). Fungi are directed towards cracks and pores by thigmotropism that is the ability of directed development of fungi hyphae, as a reaction to mechanical stimulation (direct mechanism) (Money, 2004). The indirect mechanical weathering is closely related to the extracellular polymeric substances (EPS), which lubricate the discontinuities of the mineral particles to facilitate the penetration of microbes inside (Chen et al., 2000).

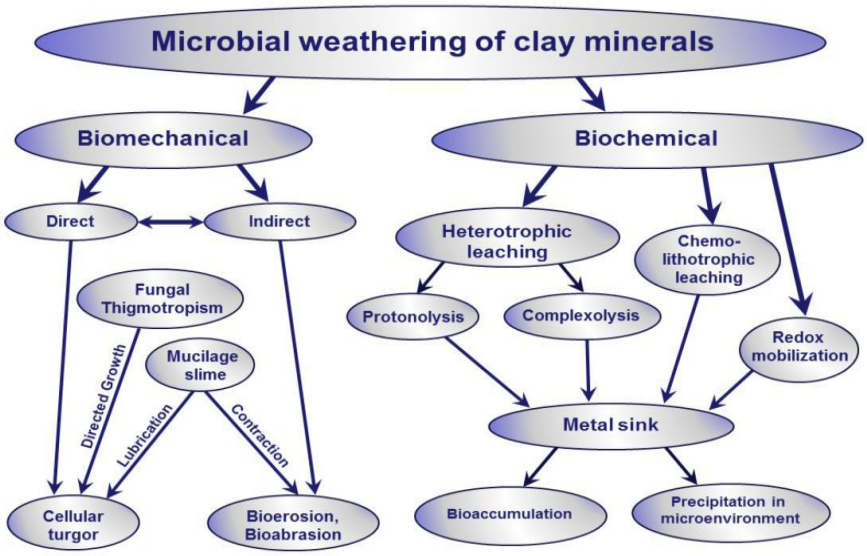

Figure 3.2: Steps of microbial weathering processes (Fomina & Skorochod, 2020)

The biological formation of minerals is known with the term *"*bio-mineralization*"*. The building blocks of minerals are mainly metallic and other non-metallic cations, such as silicon, aluminum and oxygen. These compounds can be received by microbes directly from the crystal lattice of a mineral or they can be utilized as dissolved cations from the water. The biogenic mineral formation occurs in different stages. Firstly, the raw materials are immobilized by bio-sorption and bio-accumulation in organometallic compounds. The next step includes precipitation of metallic compounds as products of metabolic reactions in the microenvironment. For initiation of a crystal formation, a chemically active core is necessary. Such a position is

provided by the surface of microorganisms. The last stage is the formation of new minerals. On a geological time scale, bio-mineralization is able to form mineral deposits.

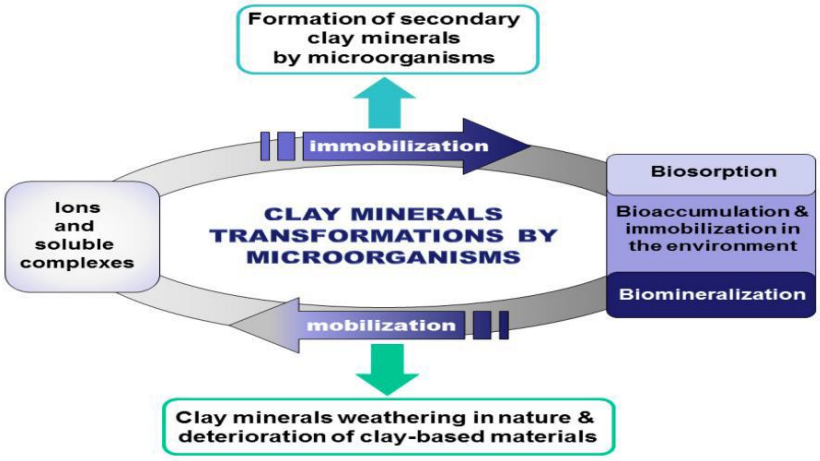

Figure 3.3: The bio-mineralization cycle (Fomina &Skorochod, 2020)

3.2 Ancient and modern applications of the mutual relationship between clays and microbes

The interaction of clay minerals with microorganisms was discovered from the ancient times and continues to be useful in more refined applications, according to modern needs of humanity.

One of the most recognized materials is the *"*Lemnian earth*"*. This material occurs in the Greek island of Lemnos and was compressed in tablets. The tablets produced during a religious event dedicated to the ancient Greek goddess Artemis, in which a priestess mixed wheat and water along with this soil and produced the tablets. These materials were effective against diseases such as dysentery, poisons and bleeding. The material contains 45% smectite, 35% kaolinite, 5% hematite and 10% alum (Hall & Photos-Jones, 2008). Materials with antimicrobial properties were the "Samian earth" and the "miltos of Kea island". The antibacterial properties of these materials have been attributed to mineralogical and chemical composition.

Figure 3.4: Lemnian earth tablet (Macgregor, 2013)

Over the years humanity has evolved, due to the continuous technological breakthroughs. However, the environmental impact of technology and industrial processes has lead to degradation of the quality of the environment. One way to reduce the environmental footprint of the industry is to modify the natural cleaning mechanisms to suit the modern needs.

A representative example is the degradation of toxic organic compounds, such as PAHs, VOCs and H/Cs, by microbial colonies on clay minerals. Clay minerals are able to adsorb the compounds, owing to their increased specific surface area and layer charge (Churchman et al., 2013), while microorganisms use the adsorbed molecules as a carbon source. In this way, the toxic organic molecules are converted to harmless chemical species. Suitable microorganisms for lower molecular weight hydrocarbons are Pseudomonas spp*., Sphingomonas spp., Flavobacterium spp., Burkholderia spp.,Rhodococcus spp., Mycobacterium spp and Bacillus spp.

Chaerun et al., (2004) investigated the degradation capability of heavy oil (Nakhodka oil slick) by cultivating the bacterium P. Aeruginosa, in presence of smectite and kaolinite. The mineral particles worked as support bases for the colonies, making the degradation more efficient and protecting the microbes from the toxic environment. Also, clays obtain buffer properties, which stabilize the pH of the environment. In this way, the microbial colony thrives. Eventually, heavy oil formed aggregates with the clay particles and the microorganisms disintegrated the heavy organic compounds.

Chapter 4: Materials and methods

This chapter describes the origin and characterization techniques of the clay minerals samples used in the dissertation, as well as the culture and antimicrobial test methods used for the fungus and their produced metabolites respectively.

4.1 Clay minerals

The materials used in this research include two reference samples; the SWy-2 smectite and KGa-2 kaolinite. The third sample was a Ca-smectite originated from the Kimolos island (B3).

SWy-2 consists mainly of Na-smectite and it comes from the Newcastle bentonite formation of Cretaceous age, located in County of Crook, State of Wyoming, USA. The bentonite deposit formed from weathering of airborne, volcanic ash deposited in fresh water. The

bentonite is intercalated with sandstones, sandy and carbonaceous shales, siltstones and lignite. It has maximum thickness of 18 m, becoming thinner to the east (Moll, 2001).

KGa-2 kaolinite obtains extensive crystal defects. It originates from County of Warren, State of Georgia, USA. Its stratigraphic sequence is uncertain and it is dated from the lower Tertiary period (Moll, 2001).

B3 sample comes from the Prassa area of kimolos, Greece and is a white Ca-bentonite. Kimolos belongs to the SW part of the south volcanic arc of the Aegean Sea and is known, along with the neighboring Melos, for its bentonite mining activity. Two volcanic phases have evolved in Kimolos. The first took place 3.5-2.0 Ma ago, yielding the ignimbrite of Kastro. The second phase (2.0-0.9 Ma) created the Prassa ignimbrite, acidic pyroclastic sediments and lava domes in the SE of Kimolos and pyroclastic sediments and lava domes at Geronicola. These pyroclastic sediments have andesitic composition (Fyticas & Vougioukalakis, 1992; Christidis & Scott, 1997).

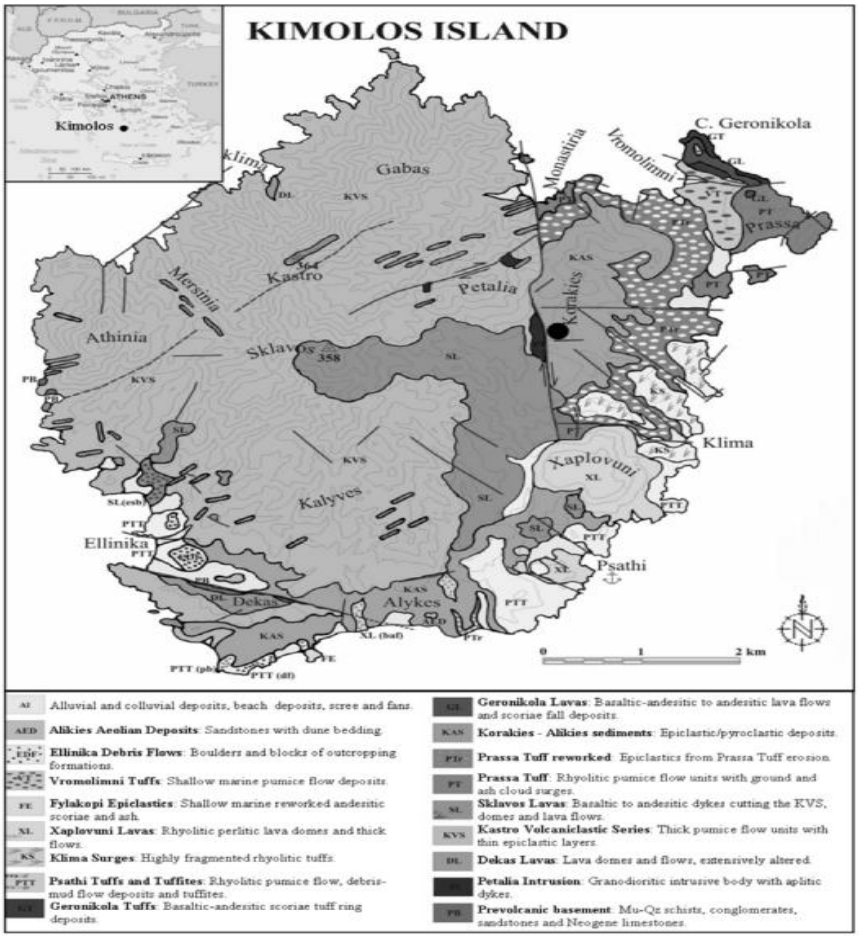

Figure 4.1: Geological map of Kimolos island (Fyticas & Vougioukalakis, 1992)

4.2 Microorganisms

The clay mineral samples were added to the culture of *Penicillium purpurogenum* fungus. *Penicillium purpurogenum* contributes to a variety of everyday products essential to humans, such as blue cheese, salamis, red pigments, penicillin and other extracellular products. According to Houbraken et al., (2014), most *Penicillium* species, which do not contribute to biotechnological applications, are enlisted in the homonymous *Penicillium* genus. This is not the case with the *Penicillium purpurogenum*, which is now enlisted in the genus *Tallaromyces*, since its contribution to applied biotechnological research is important.

Similar to clay minerals, the microbial cells, including fungi, possess a negative electric charge on their cell membranes and walls at normal pH, due to the existence of proteins, phosphates and hydroxyl groups. However, the active groups of the cell wall are able to intake or expel protons in different pH conditions. The surface charge of microbes is essential for their survival, since they contribute to nutrient intake and metabolic wastes expulsion. Also, it provides identification information about the cell composition, IEP and metabolite production (La Quita-Mai, 2005).

For the purposes of this thesis, *Penicillium purpurogenum* was cultured in potato dextrose broth for 14 days. The corresponding clay mineral sample was added to each culture at a concentration of 50 mg/mL. For reference purposes, a "control" was prepared, which contained only the fungus and the nutrient. After 14 days, the cultures were centrifuged at 10.000 g, at 4^{o}C, for 20 minutes. The precipitated material contained the intracellular metabolites, which was dissolved in sterilized water and stored for further investigation. The solution was heated to 98^{o}C for 5 minutes and was filtered through a 0.45 μm cellulose filter. The supernatant contained the extracellular metabolites, which were tested for their antimicrobial properties against the bacterium *Staphylococcus aureus*.

Staphylococcus aureus is a common intracellular pathogen, which is able to survive and reproduce in a wide variety of cells (Watkins & Unnikrishnan, 2020). Usually, it causes skin or soft tissue related infections, but it can infest vital organs with fatal results (Bose & Bayles, 2013). Furthermore, this bacterium produces enterotoxins, which are responsible for food poisoning (Staphylococcal Food Poisoning) via ingestion (Liu, 2015). The microbial populations form biofilms and thus they thrive on a wide variety of surfaces and materials. A common

antibiotic treatment includes penicillin administration or cephalosporins such as (i.e. cefazolin and daptomycin).

The antimicrobial potential of the extracellular metabolites was determined by the *Minimum Inhibitory Concentration* (MIC) process. The MIC is the minimum concentration of a chemical substance, which inhibits visible growth of a bacterium or bacteria by at least 60%. The process was initiated with the culture of the bacterium *S. aureus* in nutrient agar. The culture was dispersed in nutrient broth and the light absorption was measured by a spectrophotometer, until the value of 0.1 H was reached. This value corresponds to 10^8 CFUs/mL. The suspension underwent decimal dilutions until a value of 10^6 CFUs/mL was reached. Subsequently, 100 μL of the suspension were placed into each cell of the microtitration plate by a multichannel pipette. From columns 1 to 9, a volume of extracellular metabolites of 100 μL was added. The suspensions in each cell were under continuous stirring with the micropipette. The next step included the transportation of 100 μL of the suspensions from the cells of column 1 to the cells of column 2. This process continued until column 8. In this way, each column contained half the concentration of the previous one. In order for the cells to uniformly occupy 100 μL of suspension, containing both bacteria and metabolites, a volume of 100 μL was removed by the micropipette. Next, 5 μL of the original suspension (10^6 CFUs/mL) was transported to all cells to equilibrate the concentration of bacteria. The cells of column 9 contained only the extracellular metabolites in different concentrations, while columns 10 and 11 contained the nutrient broth. Lastly, column 12 contained only the original suspensions, without any extracellular sample. The plate was placed in an incubation chamber for 24 hours, at 37°C. To observe the reduction of the bacterial population, a microplate reader device was utilized. The instrument was set at 600 nm to obtain measurements of the bacterial concentration for each concentration of metabolites. The reduction was calculated by the equation below:

$$\textbf{Reduction} = (C_0 - C)/C_0 * 100 \quad \textbf{(Eq. 4.1)}$$

where:

C_0: The initial bacterial concentration in the nutrient broth suspension

C: The measured bacterial concentration by the microplate reader

4.3 Characterization of clay minerals

This section presents the characterization methods used to determine the chemical and mineralogical characteristics of clay mineral samples, as well as to verify the existence of organic molecules.

4.3.1 Bulk and oriented XRD samples analysis

The mineralogical composition of bulk samples was examined by powder X-ray diffraction (XRD) at the Laboratory of Applied Mineralogy of the School of Mineral Resources Engineering, Technical University of Crete. The clay mineral powders were ground in agate mortar and loaded in Al-holders to avoid particle orientation. The diffractometer was a Bruker D8 Advance, on which a LynxEye silicon strip detector was attached. The diffractometer used Ni-filtered Cu-Ka radiation (40 kV, 40 mA), a divergence slit of 0.298° and anti-scatter slits. The step size was 0.019°/2θ and the counting time was 1 sec/strip step. The qualitative and quantitative analysis of the diffraction patterns was accomplished by the EVA® and AutoQuan® softwares respectively.

The oriented samples were prepared to verify the existence of adsorbed nutrient and metabolites in the interlayer space and on the surface of clay minerals. The samples were prepared by smearing the clay pastes onto glass sample holders. The pastes were air-dried overnight before the measurement.

4.3.2 ED XRF analysis

The chemical characterization of clay minerals samples was accomplished by a Bruker S2 Ranger ED XRF spectrometer. Firstly, the samples were placed in ceramic crucibles and dried at 105^{o}C to remove adsorbed water. Afterwards, the dried samples were fired at 1050^{o}C for 2 hours. The loss on ignition of the samples was calculated as follows:

$$\textbf{L.O.I.} = \frac{(\boldsymbol{sample\ weight})\mathbf{105} - (\boldsymbol{sample\ weight})\mathbf{1050}}{(\boldsymbol{sample\ weight})\mathbf{105}} * \mathbf{100} \quad \textbf{(Eq. 4.2)}$$

The preparation process of the glassbeads included homogenization in agate mortar of 7.5 g of 50:50 Li-tetraborate:Li-metaborate flux, along with 1.5 g of the fired sample and ~0.4 mL of LiBr solution, which acts as binder. The mixture was transferred in a platinum crucible (claisse Fluxer M4) and underwent melting for 25 minutes. After the melt cooled down, the glassbeads were formed and stored in a desiccator.

4.3.3 FT-IR/ATR analysis

The purpose of this test was to verify the existence of organic compounds in the interlayer space or on the external surfaces of the clay mineral samples.

FT-IR/ATR analysis was applied only on KGa-2 and SWy-2 samples. The spectra were collected on neat powder samples in the MIR range (400-4000 cm^{-1}), with an Equinox 55 FTIR/ATR spectrometer (Bruker Optics) equipped with a single-reflection diamond ATR accessory, at the Institute of Theoretical and Physical Chemistry, National Hellenic Research Foundation.

4.4 Isoelectric point (IEP) determination

This section describes in detail the procedures that led to the determination of the isoelectric point (IEP) of each sample.

4.4.1 Acid titration

The IEP of the examined clays was determined by a combination of acid titration and electrokinetic measurements. Because of the complex chemical behavior of clay minerals in aqueous environments, no background electrolytes were used to avoid secondary reactions, which may alter the results (see page 40). Also, the presence of electrolytes compresses the EDL and leads to aggregation and precipitation of the suspended particles, which would be destructive for the measurements. Furthermore, clay particles are able to conduct the electric current on their own. Thus, a background electrolyte is not necessary.

At the first trials, suspensions were based on distilled water, but it was proven that its purity was not at the desirable levels. Therefore, Nanopure® water based suspensions complied with the needs of the experiments. The concentration of solid was 1 mg/mL.

The suspensions were placed in an Elmasonic® S 100 H ultrasonic bath for 10 minutes, to delaminate clay aggregates and disperse the particles. The KGa-2-based suspension was prone to aggregation, due to the low surface charge of kaolinite. Consequently, it was impossible to receive valid results, due to polydispersion indications. The problem was partially solved by filtering the suspension with a 200 μm micro-sieve to separate the larger aggregates.

Subsequently, the IEP of each mineral was determined by titrating the suspension three times with 1M HCl solution, by using a Crison GLP 21 pH meter. The pH meter was calibrated by using two reference buffer solutions with pH values of 4 and 7. The selected resolution was

10^{-2} pH units. The purpose of the second and third titration was to replicate the results. The titration curves were plotted in OriginPro® 9.0 software.

Clay minerals possess exposed active groups at their crystal edges and thus are able to act as amphoteric substances, since they can accept or release H^+, much like proteins, polymers and other substances with active surface groups. As a consequence, the mineral acts as neutral salt at the IEP and the pH value should remain constant at a given added volume of titrant. For easier detection of this point, the added volume of HCl solution near the expected IEP decreased.

The plateau of the titration curves at the IEP is explained by Mosher et al., (1986). Specifically, the plateau is a result of the IEF (isoelectric focusing) phenomenon, which is an important tool for molecule separation and is based on the difference of their IEPs. According to Mosher et al., (1986), the IEF is manifested in two phases. The first phase takes place fast and includes the concentration of the buffer in high purity areas. The second phase is slower. During this part, the boundaries of the high purity areas are guided to the electrodes (anode and cathode). This concentration of pH-regulating species into zones creates a mass diffusion, which balances the intense electrokinetic behavior of the buffer zones. The above phenomenon is expressed by a plateau in the titration curve.

The aforementioned results were confirmed by electrokinetic mobility and zeta potential measurements. To continue with these experiments, the titrated suspension was centrifuged for 30 minutes at 4500 rpm to settle the coarser particles and successfully separate the clay fraction.

4.4.2 Particle surface size distribution, electrokinetic mobility and zeta potential measurements

For the electrokinetic measurements, a 1000 μg pipette was used to remove the clay fraction of the suspensions. The pH value of the prepared dispersions was adjusted according to the IEP, anticipated from the acid titration experiments. Additional suspensions were prepared with pH 0.5 pH units above and below the anticipated IEP to compare possible variations of the electrophoretic mobility and zeta potential. For reference purposes, buffer suspensions were prepared and measured for each sample (no HCl solution was added). The clay suspensions were placed in quartz vials for the particle size test. The zeta potential measurements required the specifically designed for the Zetasizer Nano-ZS90 micro-electrophoresis, capillary cells.

The particle surface size (diameter) was obtained using the Dynamic Light Scattering (DLS) effect, while the zeta potential was measured by the Laser Doppler Velocimetry (LDV)

technique. The correlation of the particles velocity to their size distribution requires the application of the Stokes-Einstein equation (4.3). The DLS is related to the thermally-derived Brownian motion by a fundamental principle, which dictates that small particles move quickly, while the larger ones move slower. The particles shape is considered spherical. A He-Ne laser beam was utilized for the experiment which was operating at 633 nm. The scattering angle was set at 90^o, while the temperature was regulated at 25 ± 0.1^oC.

$$\mathbf{D=\frac{K_B*T}{6*\pi*\eta*R_h}} \quad \textbf{(Eq. 4.3)}$$

where:

D: Translational diffusion coefficient (m^2/s)
K_B: Boltzmann constant ($m^2*kg/K*s^2$)
T: Temperature (K)
η: Viscosity (Pa*s)
R_h: Hydrodynamic radius (m)

For zeta potential determination, the device uses electrophoresis measurements in combination with the LDV effect to obtain precise zeta potential values. The LDV effect is a widely used technique for the study of fluid flow and drifted particles. The optical instruments of the device are focused accordingly, to detect the scattered light from the moving particles. The velocity acquired by the particles, under the influence of the electric field, depends on its intensity, viscosity and dielectric constant of the liquid medium and zeta potential of the particles. The software of the Zetasizer Nano-ZS90 uses the Henry equation (4.4) to measure the zeta potential of the suspended particles.

$$\mathbf{U_E=\frac{2*\varepsilon*z*f(ka)}{3*\eta}} \quad \textbf{(Eq. 4.4)}$$

where:

U_E: Electrophoretic mobility
Z: Zeta potential
η: Viscosity
ε: Dielectric constant
f(ka): Henry's function

The suspension is aqueous and the particles size is of the order of hundreds of nanometers. Thus, the Smoluchowski's approximation is used and the Henry's function obtains a value of 1.5.

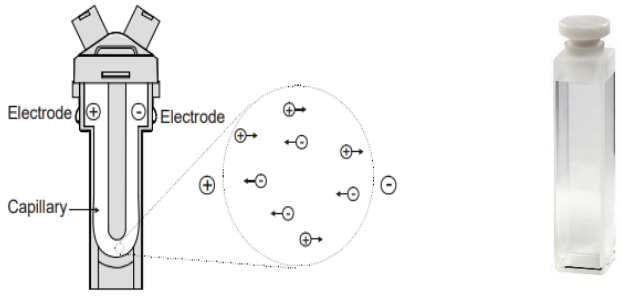

Figure 4.2: Capillary cell for zeta potential measurements (left and quartz cell for size distribution measurements (Malvern Instruments, 2009)

Chapter 5: Results and discussion

This chapter includes a thorough presentation and description of the data obtained from the experimental processes. The characterization of the materials is preceded, followed by the electrokinetic data and antimicrobial performance test results.

5.1 Characterization of clay minerals

In this section the chemical and mineralogical data are presented, which were obtained by ED XRF, ATR-FTIR and XRD methods respectively.

5.1.1 ED XRF analysis

Table 5.1: ED XRF elemental analysis of clay mineral samples

Sample	SiO_2 (%)	TiO_2 (%)	Al_2O_3 (%)	Fe_2O_3 (%)	MnO_2 (%)	MgO (%)	CaO (%)	Na_2O (%)	K_2O (%)	P_2O_5 (%)	L.O.I. (%)	Total
B3	60.59	0.27	17.08	2.61	0.00	3.47	1.18	0.63	0.24	0.00	13,68	99,74
SWy-2	59.87	0.13	17.82	4.51	0.03	2.42	1.80	1.59	0.58	0.04	11,02	99,82
KGa-2	44.46	2.21	38.08	1.15	0.00	0.00	.0.16	0.04	0.03	0.06	13,05	99,21

Table 5.1 presents the chemical composition of the examined samples. The chemical characteristics of smectites present some variations, mainly because of the different exchangeable cation in their interlayer space (sodium concentration is higher in SWy-2 sample) and the high impurity content of SWy-2 sample. Furthermore, the presence of gangue minerals,

such as gypsum, calcite, as well as Ca-smectite increases the calcium content of SWy-2. The iron content of both smectites indicates partial substitution of the octahedral Al^{3+} by Fe^{2+}, which is more intense in SWy-2.

According to XRD patterns, KGa-2 sample contains only kaolinite and anatase and the chemical composition results confirm this suggestion. Also, there is a minor substitution of Al^{3+} by Fe^{2+} in the octahedral layer, which is a common phenomenon, especially if the formation environment is enriched in iron.

5.1.2 FT-IR/ATR analysis

- **KGa-2**

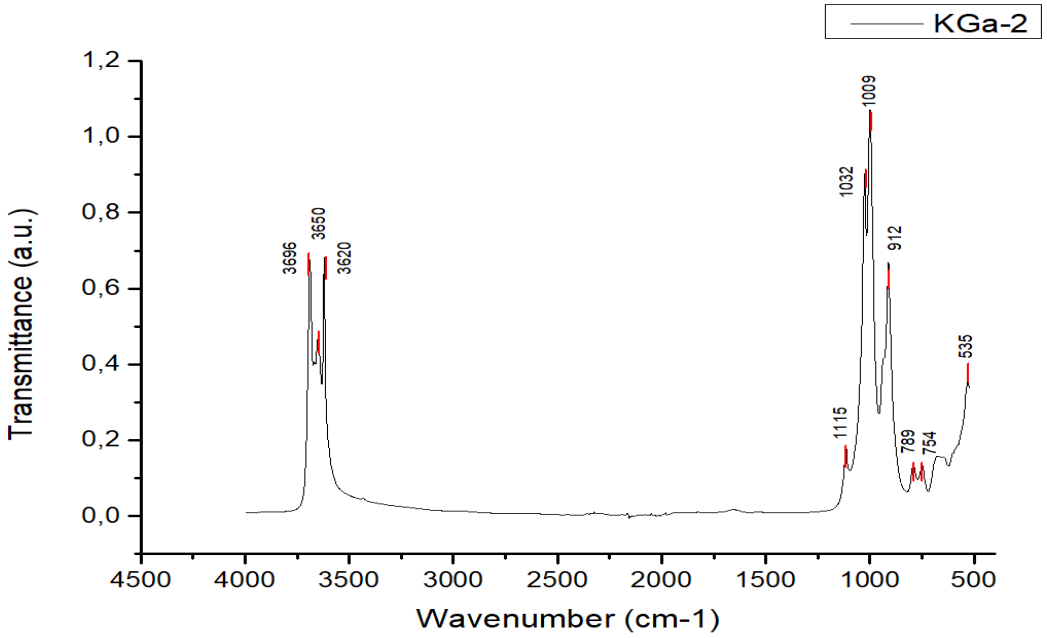

Figure 5.1: ATR/FT-IR spectra of KGa-2 sample

According to ATR/FTIR results of KGa-2 sample (Figure 5.1), kaolinite does not present any bands correlating to organic compounds and especially to proteins. Consequently, the contact of fungus with the kaolin did not produce any organic compounds.

The spectra confirm that KGa-2 is a high defect kaolinite, since the transmittance band at 3670 cm^{-1} is missing (Bich, 2005). The band at 3696 cm^{-1} represents exposed, surface hydroxyl groups, which vibrate vertically to the crystal lattice (Ece et al., 2003). The band at 3650 cm^{-1} occurs due to the sub-parallel vibration of the crystal, while the vibration of the fourth internal

hydroxyl group is represented by the band at 3620 cm^{-1} (Diko et al., 2016). The typical transmittance bands of KGa-2 are summarized in Table 5.2 (Diko et al., 2016; Khang et al., 2016; Tironi et al., 2012).

Table 5.2: Summary of the detected active groups and their respective wavenumber and layout of KGa-2 sample.

Active group	**Wavenumber (cm^{-1})**	**Layout**
Internal surface -OH	3696, 3650, 3620	stretching
-SiO	1115, 1032, 1009	stretching
-OH deformation	912	-
-OH deformation linked to Al^{3+} and Mg^{2+}	789, 754	-
-SiOAl or –FeO / $-Fe_2O_3$	535	stretching

**The possible presence of iron-containig active groups is due to minor substitutions in the octahedral sheet.*

- **SWy-2**

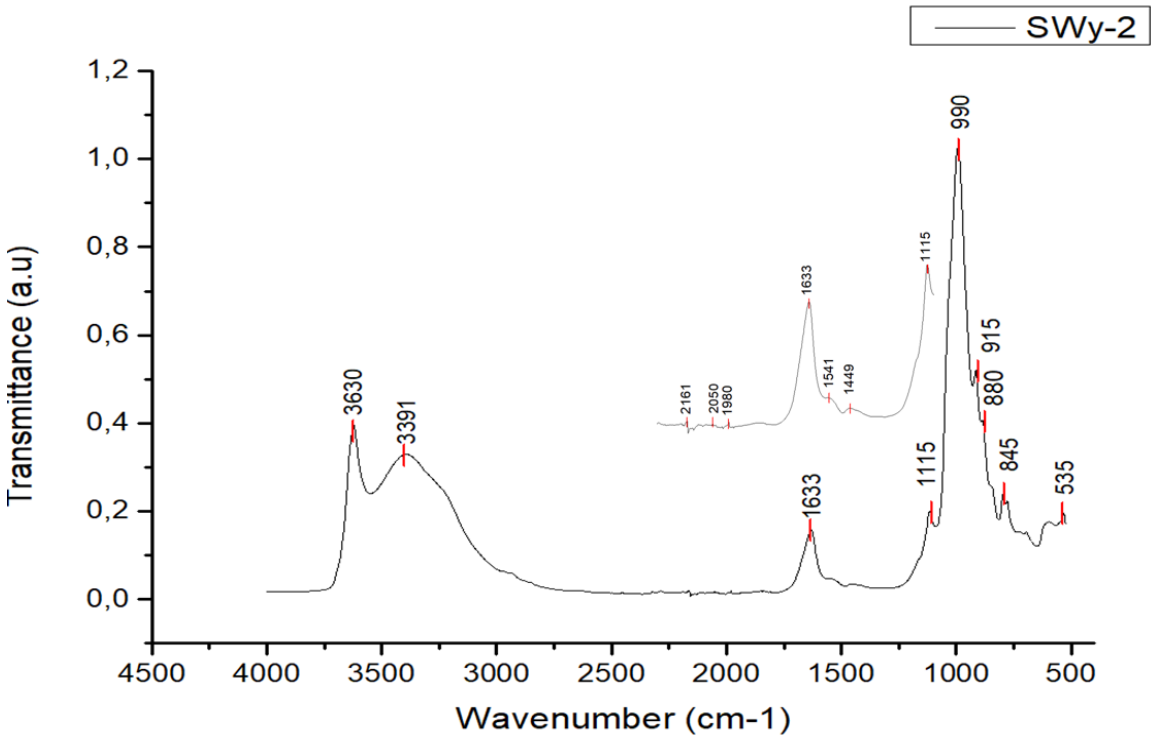

Figure 5.2: ATR/FT-IR spectra of SWy-2 sample (clay mineral and organic active groups)

The spectra from the examination of SWy-2 sample are presented in Figure 5.2. It is important that active groups, which are attributed to organic substances, have been detected.

Some carbon-containing groups may be attributed to the potato dextrose nutrient, which is possible to have been intercalated in the interlayer space. These groups also contain nitrogen. These results are in accordance with the antimicrobial tests, in which SWy-2 has exceptional performance.

Other bands, which are characteristic in terms of mineral structure, include the 3630 and 3391 cm^1 peaks. The former refers to the vibration of octahedral hydroxyl groups, while the latter indicates presence of adsorbed water. Table 5.3 summarizes the transmittance bands of Figure 5.2 (Pironon et al., 2018; Zviagina et al., 2020).

Table 5.3: Summary of the detected active groups and their respective wavenumber and layout of SWy-2 sample.

Active group	**Wavenumber (cm^{-1})**	**Layout**
-OH (octahedral)	3630	stretching
-HOH (water)	3391	stretching
-HOH	1633	bending
-SiO	1115, 990	stretching
-AlAlOH	915	bending
-AlFeOH	880	bending
-AlMgOH	845	bending
-SiOAl	535	bending
-N=N=N	2161	stretching
-N=C=S	2050	stretching
-C=C=C	1980	stretching
-NO	1541	stretching
-CH	1449	bending

5.1.3 Bulk and oriented XRD analysis

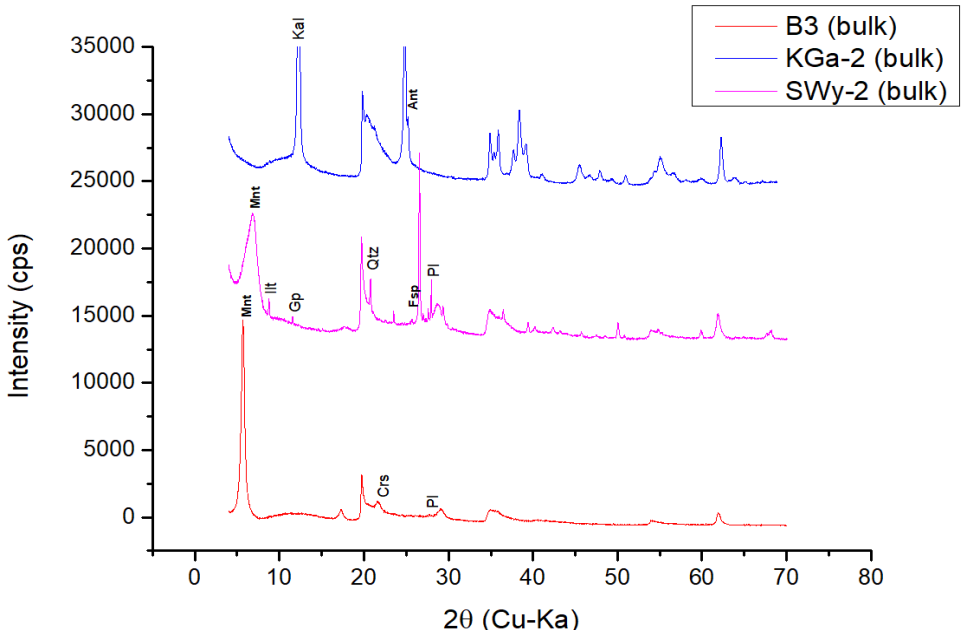

Figure 5.3: Bulk XRD results

Figure 5.3 presents XRD traces of bulk samples. B3 sample from Kimolos consists mainly of pure Ca-montmorillonite, with minor cristobalite. SWy-2 contains more impurities, consisting of Na-montmorillonite, Ca-montmorillonite, illite, gypsum, K-feldspar, plagioclase (albite) and quartz. The bulk mineralogical composition of KGa-2 sample includes kaolinite and anatase. The XRD pattern agrees with the ED XRF results, which show increase concentration of TiO_2. Both mineralogical and chemical analyses agree that KGa-2 is very rich in kaolinite. Table 5.4 summarizes the quantitative mineralogical composition of the bulk samples, determined by AutoQuan® software.

Table 5.4: Quantitative analysis of clay mineral samples

Mineral phase	Percentage (%)
KGa-2	
Kaolinite	98.45
Anatase	1.54
B3	
Ca-smectite	86.3
Cristobalite	4.1
K-feldspar	3.9
Plagioclase	5.1
Quartz	0.6
SWy-2	

Na- smectite	62.1
Ca-smectite	14.4
Illite	4.0
Calcite	1.2
Quartz	11.3
Gypsum	0.9
Orthoclase	4.1
Plagioclase-Albite	2.0

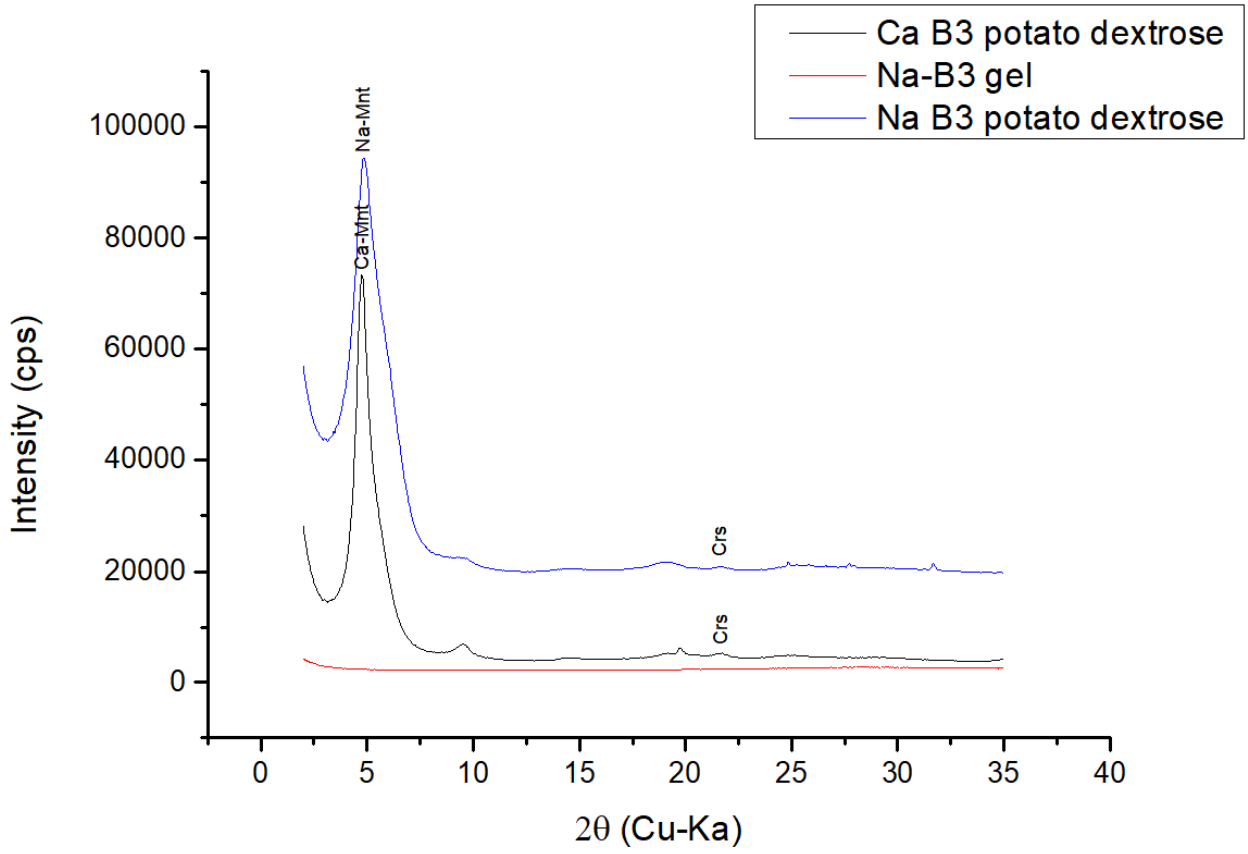

Figure 5.4: XRD patterns of the oriented B3 samples. Na-saturated samples are included

In order to examine the nutrient adsorption capability of smectites, oriented samples were prepared. Each one of these samples are presented in Figures 5.4 (B3 sample) and 5.5 (SWy-2 sample). It appears that the unprocessed B3 smectite has adsorbed carbohydrate molecules, since the d-spacing has increased from 12.5 to ~18.6 nm. However, the layout of the adsorbed molecules in the interlayer space is unknown. A small amount of cristobalite (Crs) has also been detected in the oriented sample.

A series of B3 samples were saturated with 1M NaCl solution. The purpose was to exchange the naturally-existing Ca^{2+} cation in the interlayer space with Na^{+} and observe the

carbohydrate molecules adsorption and gel formation capability. In time, the MIC will be performed in Na-saturated samples, to compare the antimicrobial performance of the unprocessed to modified samples.

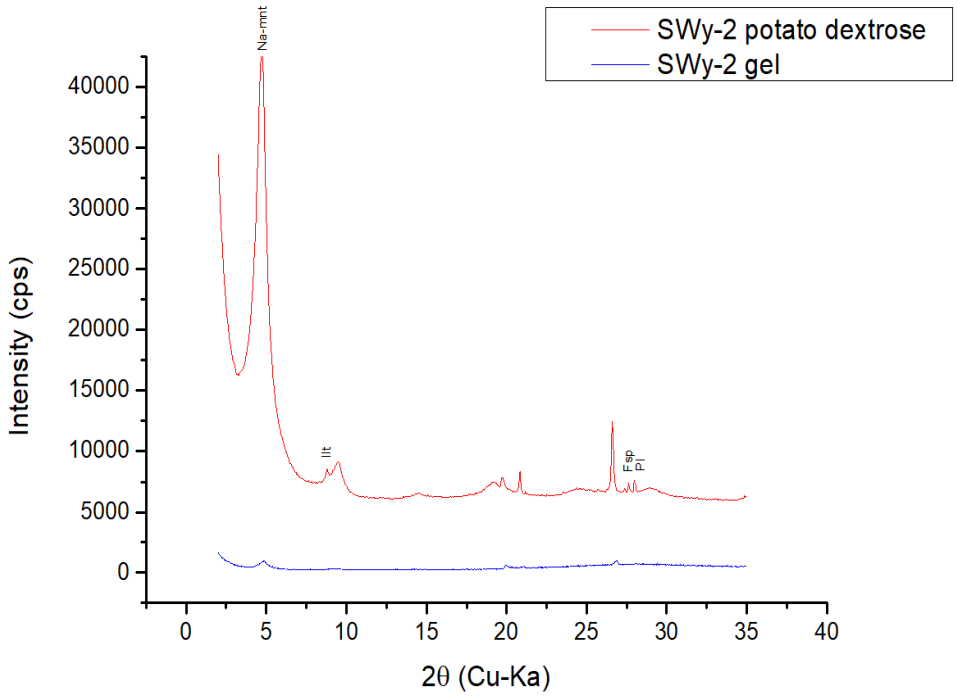

Figure 5.5: XRD pattern of SWy-2 oriented samples

The oriented SWy-2 sample, in presence of the nutrient (Figure 5.5), shows a considerable increase of the *d(001)* dimension. However, a quantity of the dextrose did not enter the interlayer space, since the peak is lower than its B3 counterpart, along with a minor overlap in the first peak, which is attributed to unattached nutrient molecules. Most of the SWy-2 gel sample has been delaminated, although some of the montmorillonite peaks are still obvious.

5.2 Acid titration, electrokinetic mobility and particle surface size analysis

5.2.1 Acid titration

In this section, the results, which lead to the IEP determination, are presented. First of all, the titration curves are attached in Figures 5.6-5.8. Three titration curves were obtained for each

sample, which are attached separately for visual convenience. The titration data are listed in Appendix 2.

- **KGa-2**

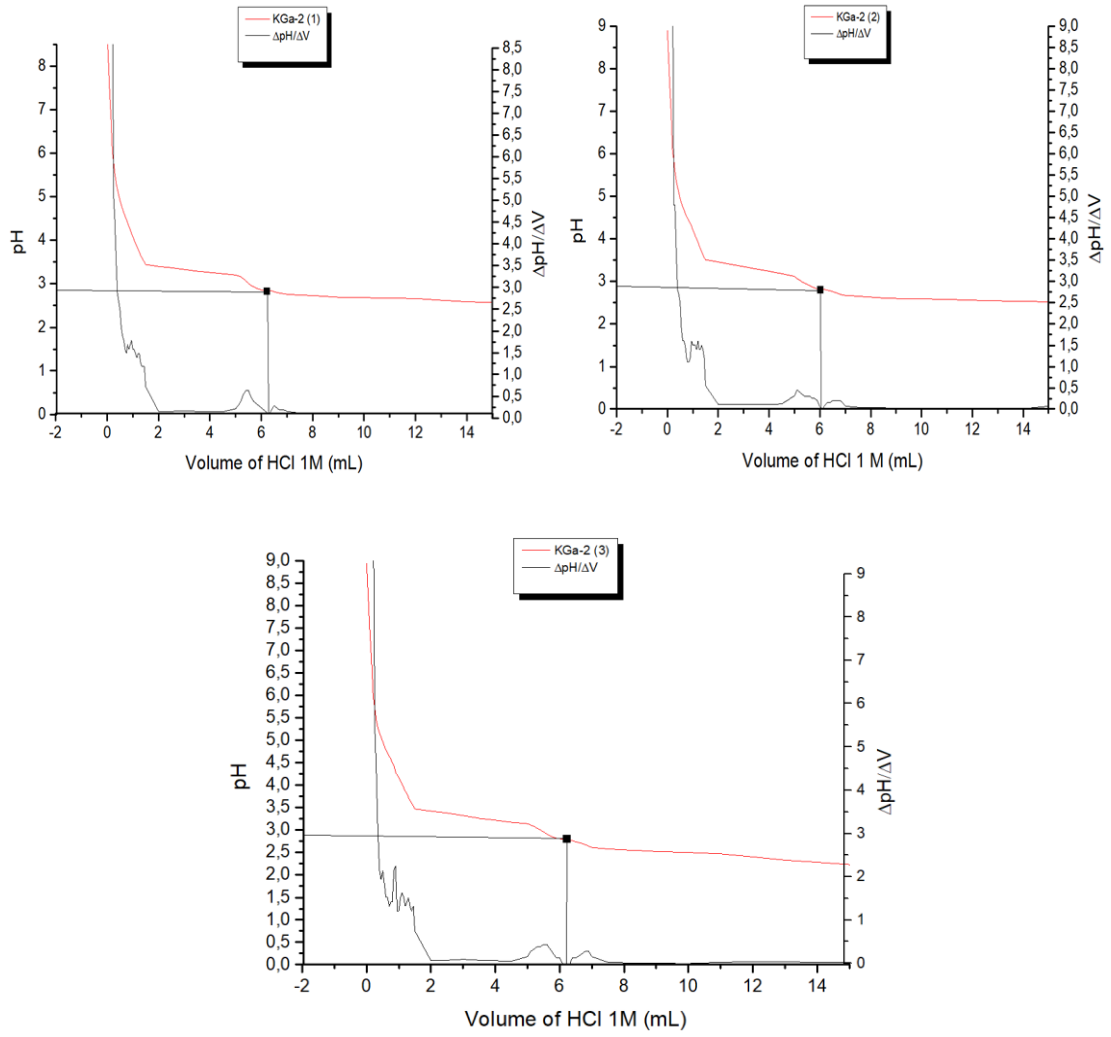

Figure 5.6: The titration curves of the KGa-2 suspension. The red line represents the titration data and the black line represents the first derivative (ΔpH/ΔV)

Figure 5.6 indicates the titration results of KGa-2 sample. Kaolinite does not possess a high surface charge on its crystalline surfaces. The main charging source comes from the broken edges, which develop a pH-dependent charge. For this reason, it was challenging to keep the particles suspended, especially when the dispersion became more acidic and the edges possessed positive charge. In order for the results to be reliable, the particles had to be suspended during the titration. Otherwise the pH was fluctuating by the depth of the suspension. To achieve the above desirable conditions, continuous stirring was applied. Also, kaolinite creates acidic

environment in water. Consequently, 0.5 mL of 1 M NaOH solution was added in each titrated suspension, in order for the titrations to begin from higher pH values (pH~9).

The poorly crystallized KGa-2 sample is susceptible to self-aggregation, because of hydrogen bonds development between neighboring particles. The continuous stirring exposes different crystal planes. This phenomenon influences the repulsive and attractive forces among the particles and promotes or inhibits their aggregation and precipitation (Ndlovu et al., 2014).

An interesting observation was the increased buffering capacity of kaolinite at the anticipated IEP. By observing the titration curves, it can be verified that below the IEP, the added volume of titrant was increased, because the descending ratio of the pH value was decreased. The first, second and third suspension show a plateau at pH values of 2.84, 2.81 and 2.79 respectively (Appendix 2). At these points, the first derivative equals to zero. The IEP of KGa-2 sample (2.81 ± 0.03) is in accordance to the existing bibliography (pH = 2.8-4) (Garcia-Gonzalez et al., 2000; Miu et al., 2013; Ndlovu et al., 2014).

The most appropriate statistical model to determine the standard deviation is the T-Student function, at a confidence interval of 68%, since the number of titration experiments is small. The variability was expressed by SD, according to Barde & Barde (2012), who suggested that is more appropriate to use the standard deviation as a mean of uncertainty determination, in comparison to the standard error of mean (SEM).

- **SWy-2**

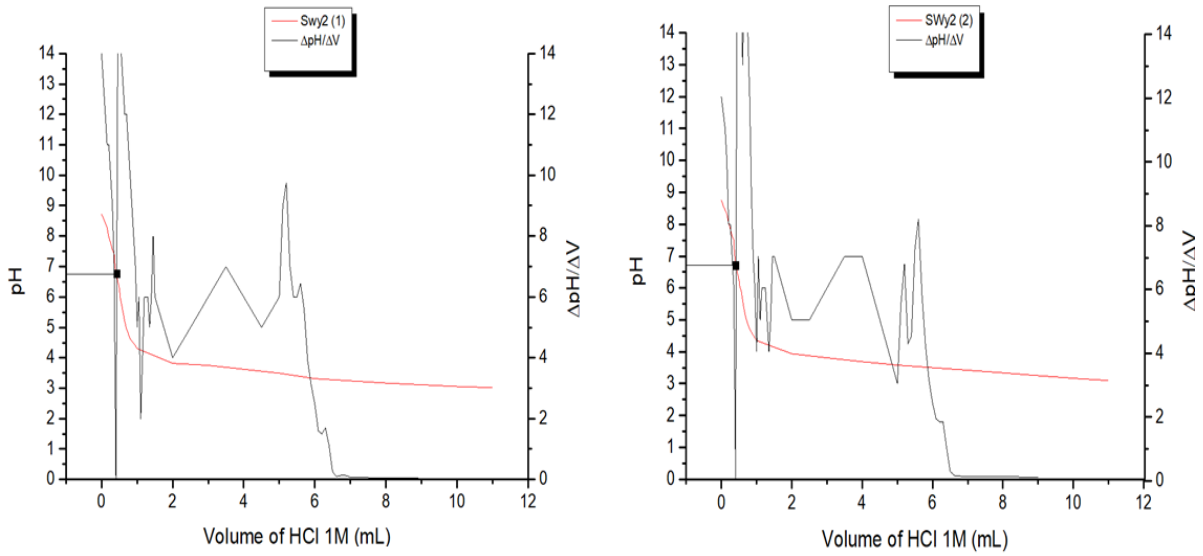

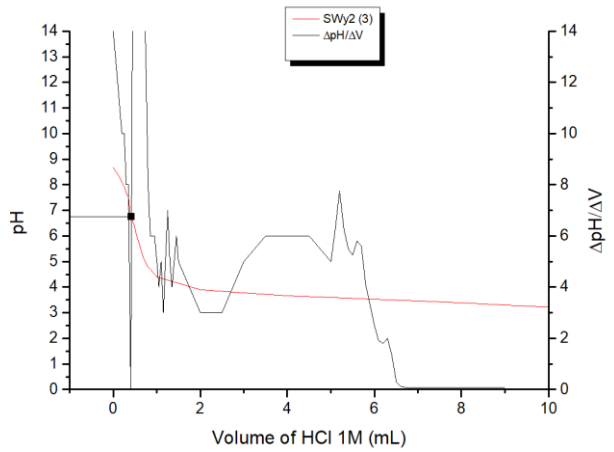

Figure 5.7: The titration curves of the SWy-2 suspension. The red line represents the titration data and the black line represents the first derivative (ΔpH/ΔV)

Figure 5.7 depicts the titration curves of SWy-2. The first experiment detected the IEP at pH=6.72, the second at pH=6.71 and the third at pH=6.70, according to the first derivative charts and the titration data in Appendix 2. Consequently, the mean IEP value of SWy-2 is 6.71 ± 0.01, which is consistent to the reported range for smectites (6.1-7) (Wanner et al., 1994; Duran et al., 2000; Ramos-Tejada et al., 2001; Tombacz & Szekeres, 2004).

SWy-2 sample consists mainly of Na-montmorillonite, which should be easily hydrated and dispersed in water. However, the mineralogical characterization proved the existence of Ca-montmorillonite, the particles of which are not dispersed as efficiently as its counterpart, as well as multiple gangue mineral phases. For this reason, the dispersion was not as spontaneously dispersed as anticipated and the sample needed to remain in the ultrasonic bath for at least 5 more minutes compared to B3 sample.

In acidic conditions (pH<4.5), the buffering capacity of the suspension increased sharply, while it tended to get destabilized, even though no electrolyte was added. In these conditions, the particles are prone to edge to face aggregation. Also, it is possible to have acquired their H-form, which explains the regulatory behavior.

➢ **B3**

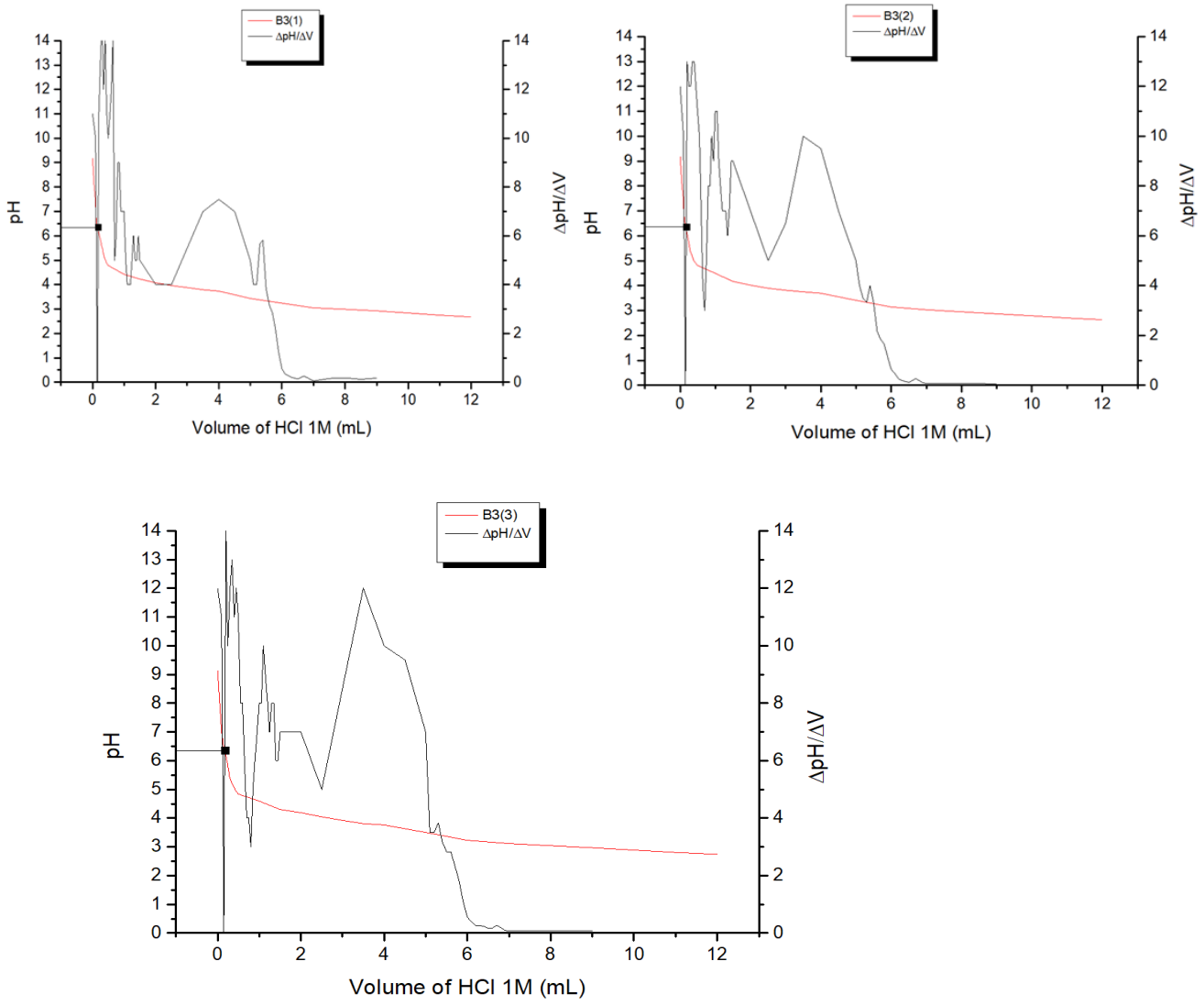

Figure 5.8: The titration curves of the B3 suspension. The red line represents the titration data and the black line represents the first derivative (ΔpH/ΔV)

The titration curves of B3 sample are presented in Figure 5.8. The IEP was determined for the first, second and third titration experiments at the pH values of 6.42, 6.40 and 6.39 respectively. Similar to SWy-2, B3 presents its IEP at pH=6.40±0.02, which falls in the reported range for smectites.

Generally, Ca-smectites possess inferior dispersion properties, because the interlayer Ca^{2+} cations bridge the adjacent smectite particles. However, it appears that the aggregates were disintegrated properly by the ultrasonic bath. At pH=5, the buffering capacity of smectite tends to rise sharply, which is close to that of SWy-2 sample. Also, the dispersion tended to coagulate

below this point, similar to SWy-2 and the pH indications started fluctuating. In more acidic environment (pH ~ 3), the particles precipitated quickly, when the stirring paused.

Below the IEP, the exposed sites obtain positive charges and are attracted by the permanently negative charged planes of adjacent particles. In this way, edge to face coagulation occurs, which leads gradually to aggregate formation (Kuentz & Roethlisberger, 2003).

5.2.2 Particle surface size results

Table 5.5: Particle size and polydispersion index results

Sample	Z-Average (d.nm)	PDI
SWy-2	300.2	0.232
B3	317.6	0.175
KGa-2	214.4	0.476

- **B3**

The particle surface size distribution and polydispersion index of all samples are depicted in Table 5.5. Polydispersion index is a parameter, which expresses the existence of aggregates. Pdi values range between 0 and 1, with the latter indicating severe polydispersion. The mean size (diameter) value of the B3 particles equals to 317.6 nm, with a polydispersion index (pdi) of 0.175. The lack of major impurities produces only one, yet wide curve, which implies size heterogeneity. The lack of secondary curves indicates that uncontrolled aggregation does not exist.

For the measurement purposes, a B3 buffer suspension was prepared, which acquired pH~7.5. Consequently, the exposed edges obtain negative charges and thus there is development of repulsive forces among the particles. The mean diameter size is similar to SWy-2, since Ca-smectite forms quasicrystals, because the exchangeable cation does not permit a complete delamination. Also, the correlation of particle surface size data is acceptable (Appendix 3).

- **SWy-2**

The mean particle surface size of SWy-2 equals to 300.2 nm and the pdi equals to 0.232. The polydispersion index is almost two times higher than B3 sample. The main distribution curve is wide suggesting that the particles are not uniformly sized. Two more minor curves

indicate the existence of fine particles (tens of nanometers) and larger aggregates (4 μm), which are not considered to affect the mean Z-average value. Consequently, the hydration of the interlayer space was not complete. The correlation data are acceptable, although there is a slight diversion during the first measurements at the range of 0.5 to 100 μs (Appendix 3).

- **KGa-2**

The absence of permanent surface charge of KGa-2 leads to coagulation and eventually precipitation of aggregates. The unique source of electric charge originates from the exposed active groups at the edges of the crystals, which explains the difficulty of kaolinite to get properly dispersed. The ultrasonic bath, the micro-sieve (<200 nm) and the dilution of the suspension managed to partially disintegrate and separate the coarser crystal booklets up to a point, since size distribution curve indicates values below 10 μm. However, the existence of kaolinite aggregates of the order of tens and hundreds of nanometers leads to the conclusion that the low-charged particles are difficult to delaminate properly without the addition of anti-coagulants to obtain reliable measurements. However, the anti-coagulants were avoided to ensure the intergrity of the zeta potential measurements.

In conclusion, the average surface size of kaolinite particles is 214.4 nm and pdi value equals to 0.476, which is logically increased compared to smectite samples, due to the inability of particles to delaminate properly. Also, the data correlation is not well expressed.

5.2.3 Zeta potential and electrokinetic mobility results

Table 5.6: ZP and EM results

Sample / pH	Zeta Potential (mV)	Electrokinetic mobility (μm*cm/V*s)
Swy-2 / ~6.7 (IEP)	-14.2	-1.115
B3 / ~6.4 (IEP)	-1.61	-0.126
KGa-2 / ~2.8 (IEP)	-0.015	-0.00118

Swy-2 / ~8.7 (Buffer)	-63.7	-4.995
B3 / ~7.5 (Buffer)	-49.6	-3.890
KGa-2 / ~5.3 (Buffer)	-21.6	-1.693
Swy-2 / ~7.2 (IEP + 0.5)	-37.6	-2.950
B3 / ~7.0 (IEP+0.5)	-38.9	-3.049
KGa-2 / ~3.3 (IEP+0.5)	-0.262	-0.02057
SWy-2 / ~6.2 (IEP-0.5)	-36.4	-2.855
B3 / ~6.0 (IEP-0.5)	-36.6	-2.871
KGa-2 / ~2.4 (IEP-0.5)	2.92	0.2286

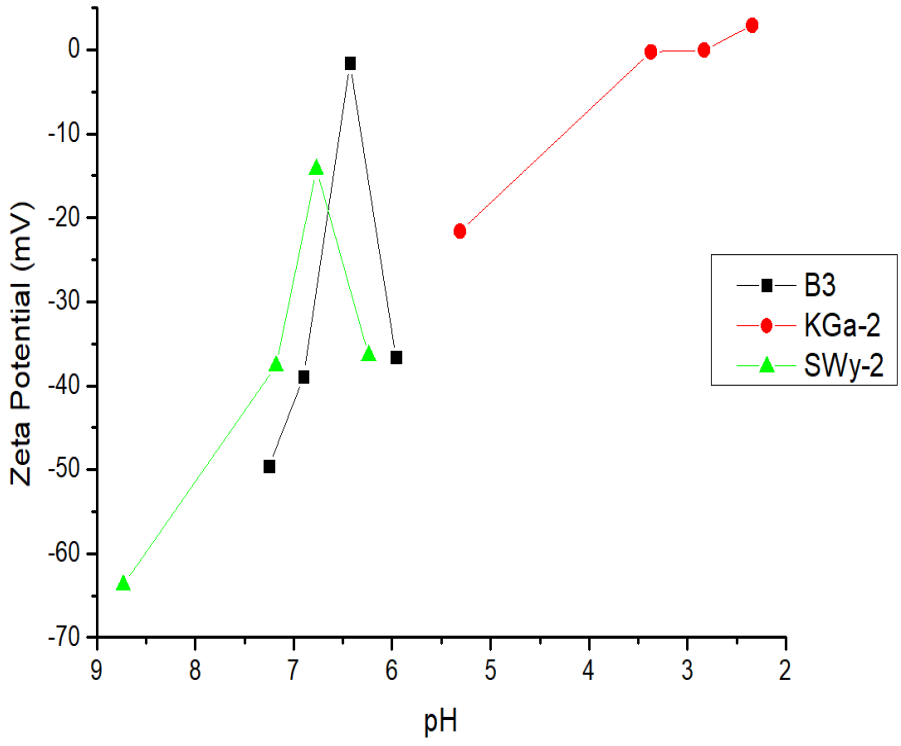

Figure 5.9: Summary diagram indicating the fluctuation of zeta potential as a function of pH

Table 5.6 provides information about the zeta potential and electrophoretic mobility of B3, SWy-2 and KGa-2 samples, regulated at various pH values. Raw data are presented in Appendix 4.

- **B3 (IEP)**

The B3 suspension, regulated at the estimated IEP, had a zeta potential and electokinetic mobility equal to -1.61 mV and -0.126 μm*cm/V*s respectively. It is not possible to neutralize the ZP, because of the permanent basal charge, which primarily affects the overall surface charge. The inferior quality of the measurements is due to destabilization of the suspension. The pH-dependent charge is neutralized and thus the total surface charge is decreased. Hence, the repulsive forces decay, the particles coagulate and precipitate. Malvern instruction manuals suggest that suspensions with zeta potential values between -30 and +30 mV are considered unstable and the measurements may have inferior quality. This is also proven by the high standard deviation value of the ZP and electrophoretic mobility (Appendix 4).

A noticeable observation is the disproportional decrease of the zeta potential, considering the existence of permanent basal charges. Since the basal charge participates to the overall charge in a percentage greater than 95% (Grim, 1962), the EM and ZP should have been higher.

The first thought would be a possible presence of impurities (mostly oxides) in the clay fraction, the IEP of which obtains similar values to montmorillonite. However, this hypothesis is contradicted to the XRD results, which have not detected other gangue minerals than cristobalite, which although is an oxide, its IEP is determined at pH=3.2 (Cuihua et al., 2015), far below in relation to B3 sample.

Another explanation is related to the morphology of the smectite crystals. If the crystals are poorly formed, then there would be many exposed active groups at the edges. As a consequence, the overall charge would be greatly affected by the pH-dependent charges. This hypothesis needs to be verified by TEM to confirm possible crystal disorder. Moreover, it would be useful to measure the layer charge of B3 to determine the intensity of the permanent charge.

- **B3 (Buffer)**

For terms of comparison, a buffer suspension (pH value regulated at ~7.5) was prepared and measured to observe the natural electrokinetic behavior of the material without regulating the pH. The results prove that Ca-smectite is able to form stable colloids, since the ZP and EM values do not suggest destabilized suspensions (ZP=-49.6 mV, EM=-3.890 μm*cm/V*s). B3 sample is almost pure and it can be easily dispersed, even though there is a small concentration of cristobalite in the clay fraction. The standard deviation value is increased (Appendix 4), similar to all measurements, since the instrument is confused by the complicated charging properties of clay minerals and due to the existence of cristobalite.

- **B3 (IEP+0.5)**

The zeta potential and mobility values of this sample is far from the range of instability. The ZP and EM values equal to -38.9 mV and -3.049 μm*cm/V*s respectively. The pH was regulated at ~7.0. The edge site groups are negatively charged, since the pH of the suspension is above their PZC and IEP (~6.5). Since there is not adsorption of electrolytes on the clay surfaces, the PZC and IEP coincide. However, the protonation has initiated and the overall negative charge begins getting neutralized as pH declines. The ZP equals to -38.9 mV, which means that the stability is still sufficient.

- **B3 (IEP-0.5)**

The last set of electrokinetic measurements of B3 Ca-smectite was executed at pH~6. The point was to compare possible changes of the zeta potential in environments with different acidity. The ZP and EM equal to -36.6 mV and -2.871 μm*cm/V*s respectively.

The zeta potential and mobility remain increased below the IEP. A possible explanation for this phenomenon, given by Secor & Radke, (1985) is that the permanent plane charges develop an electric field, which envelops the positive charges of the active groups, making them invisible. This hypothesis is supported by the fact that the zeta potential value is decreased compared to the buffer suspension and the one regulated at pH~7.0. However, its value is still considerably high.

- **SWy-2 (IEP)**

The pH of SWy-2 dispersion was regulated at the anticipated IEP, according to the acid titration data. The zeta potential value is considerably higher than the respective B3 suspension. However, the suspension acquires ZP and EM values equal to -14.2 mV and -1.115 μm*cm/V*s. The zeta potential still lies between -30 and +30 mV, which explains the multiple peaks and increased standard deviation. Ideally, the only source of electric charge on the surface of the particles, at the IEP, originates from the isomorphic substitutions of cations in the crystal lattice. This means that electrokinetic mobility still exists. The weakening of the EDL allows the particles to approach each other until overlapping occurs and Van der Waal attractive forces start developing. Eventually, aggregation and precipitation take place. This phenomenon causes the quality of the measurements to decline.

- **SWy-2 (Buffer)**

The zeta potential of the SWy-2 buffer suspension is the highest of all the suspensions prepared for this study, implying great stability and contradicting to the macroscopic observation mentioned at the acid titration experiments. The difference is that the zeta potential measurements involve exclusively the clay fraction (<2 μm) and not the overall material, which contains many different mineral phases. The clay fraction contains mostly Na-smectite and maybe a small quantity of Ca-smectite. The former indicates excellent dispersivity, due to tactoid formation in low concentrations. Tactoids interact with long range repulsive forces and form

when excessive water enters in the interlayer space of Na-smectites (osmotic swelling) (Güven, 1992). The latter undergoes crystalline swelling and form quasicrystals, since bivalent cations do not permit the complete delamination of the particles. Consequently, the suspension is stable and no aggregation occurs.

- **SWy-2 (IEP+0.5)**

In these conditions, the exposed edge sites are still negative, because the pH of the suspension is above the IEP. The ZP and EM values equal to -37.6 mV and -2.950 μm*cm/V*s. The measurements have good quality as anticipated, since the suspension abstains from the destabilization range.

- **SWy-2 (IEP-0.5)**

The last SWy-2 based suspension acquires ZP and EM values of -36.4 mV and -2.855 μm*cm/V*s respectively. The values are slightly reduced in comparison to the suspension regulated at pH~7.2, since the protonation of the exposed groups is more intense as the pH declines. As a result, the overall negative charge is balanced by the continuous H^+ intake. The more acidic the suspension becomes, the more the zeta potential will be decreased, until its H-form is acquired. At this point, the particles are saturated by H^+ and the buffering capacity is increased (Preocanin et al., 2016).

- **KGa-2 (IEP)**

The KGa-2 based suspension, regulated at its IEP, has ZP and EM values -0.015 mV and -0.00118 μm*cm/V*s respectively. The absence of permanent charges is obvious, since the zeta potential and mobility values are practically zero at pH~2.8. The exposed active groups do not produce an electric field capable of maintaining the kaolinite particles suspended. As a consequence, kaolinite dispersions at the IEP tend to form aggregates and eventually precipitate. This is the reason for the inferior quality of the measurements.

- **KGa-2 (Buffer)**

KGa-2 has ZP and EM values equal to -21.6 mV and -1.693 μm*cm/V*s respectively. Kaolinite regulated the suspension at pH~5.3, which means that the exposed silanols and aluminols have negative and positive charge respectively. The EDLs are still weak and allow the

particles to come close to each other, until attractive forces apply. As a consequence, the stability of the dispersion is undermined, which can be observed by the electrokinetic results. The aggregates structure obtain a edge-to-face layout, which predominates when the active groups are opposite charged, according to Morais et al., (2019). The same layout also occurs when the particles come close to each other and attractive Van der Waals forces start prevailing.

Kaolinite particles tend to aggregate in similar ways to smectites (edge-to-face, face-to-face and edge-to-edge). A major parameter that determines the aggregation mechanisms, apart from the charge distribution among the active groups, is the degree of crystal order. For highly defected particles, such as those of KGa-2 sample, the crystal surfaces are able to self-aggregate, due to the development of hydrogen bonds between the exposed active groups of the planes (Ndlovu et al., 2014).

- **KGa-2 (IEP+0.5)**

Similar behavior to buffer dispersion is displayed by the suspension regulated at pH~3.3. The ZP and EM values equal to -0.262 mV and -0.0206 μm*cm/V*s respectively. The measurements continue to indicate polydispersion phenomena, since the pH is very close to the IEP and zeta potential is almost diminished. Therefore, the suspension is very unstable.

In such conditions, edge to face aggregation occurs, because the positively charged edges are attracted by the mildly negative planes. The final card-like structure occupies large volume and it complicates the rheological behavior of the suspension, which complicates the electrokinetic mobility measurements.

- **KGa-2 (IEP-0.5)**

The last KGa-2 based suspension was regulated at pH~2.4. The ZP and EM values have become positive and equal to 2.92 mV and 0.2286 μm*cm/V*s respectively. However, the aforementioned values are in the unstable range, which is the explanation behind the polydispersed measurements.

According to macroscopic observations, the particles started aggregating and forming dense gel in such acidic environments. In this case, the particles are uniformly positively charged. After some time, the particles were transformed in a gel like mass, probably due to dissolution.

Table 5.7: IEP values for the examined samples

Sample	IEP±SD
SWy-2	6.71±0.01
B3	6.40±0.02
KGa-2	2.81±0.03

5.3 Minimum Inhibitory Concentration test results

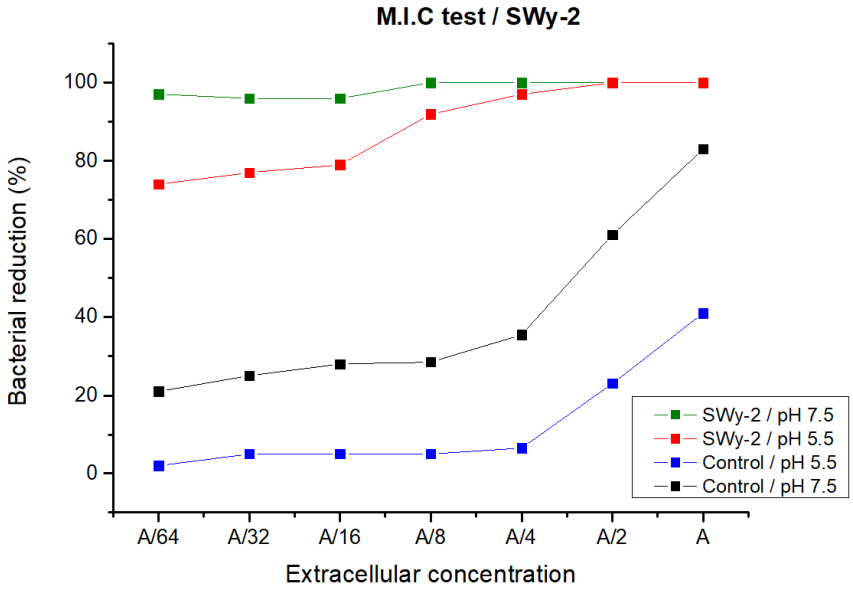

Figure 5.10: MIC results of SWy-2 sample

Figure 5.10 presents the MIC results, in presence of SWy-2 sample and in two different pH values, 7.5 and 5.5. The displayed results include the antimicrobial performance of clay-mineral-free cultures regulated at the same pH, as a reference (Control). It is obvious that the addition of SWy-2 smectite during the culture of *P. purpurogenum* produced leachates with antibacterial properties. Even in low concentrations of the leachates, the bacterial colonies were practically completely inhibited. The minimum inhibitory concentration of leachates is below A/64 and it is not presented in the above figures.

The remarkable resemblance between the reduction rates of the bacterial colonies, in different pH, implies that Na-smectite did not affect the fungus in an unusual way, when the pH was close to the IEP of the former.

Clay minerals and especially montmorillonite act as supportive media for the microbe colonies. In this way, the microbes thrive and form biofilms. The compositition of a biofilm is

based on proteins, polysaccharides and other extracellular polymeric substances. In case of stressful conditions in the microenvironment, fungi might produce molecules, which contribute to the antibacterial behavior, in the case of SWy-2 sample.

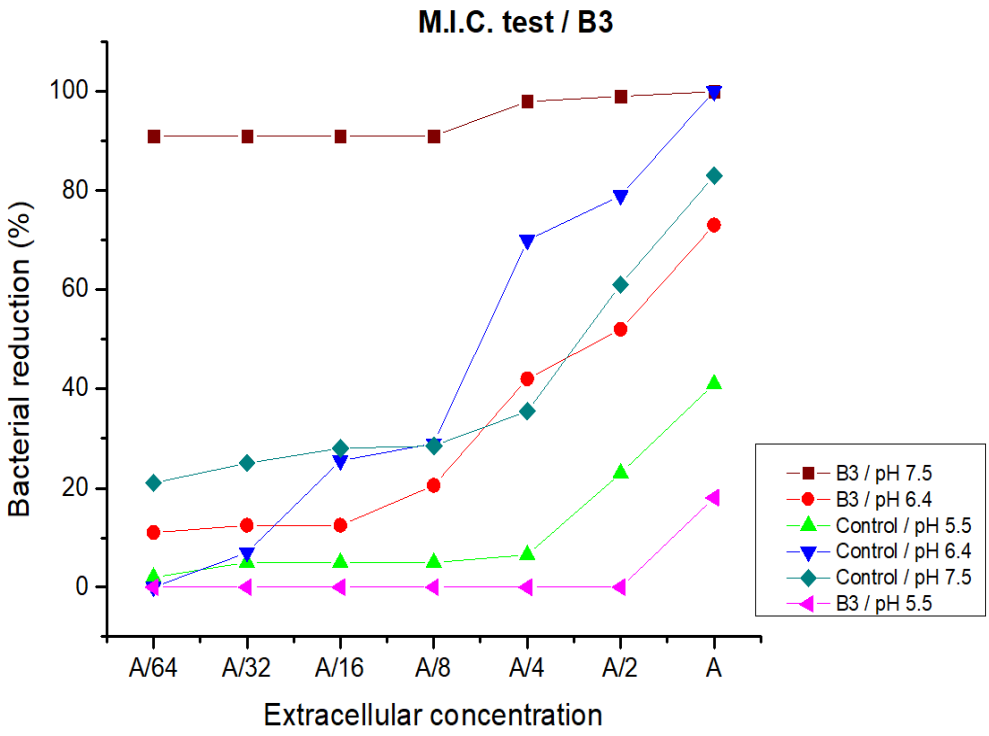

Figure 5.11: MIC results of B3 sample in pH=6.4

Figure 5.11 presents the antimicrobial performance of B3 sample, which consists of Ca-montmorillonite. One can observe great variation of the bacterial population in different pH conditions. Similar to SWy-2 sample, the culture of the fungus at the IEP of the clay mineral does not seem to have major impact on the production of antibiotics, since the MIC is reached at a concentration of ~A/5 (reduction of the bacterial population equals to 60%). When the conditions become more acidic (pH=5.5), the sample does not have antibacterial behavior and the MIC cannot be determined. On the contrary, the whole bacterial activity was inhibited at pH=7.5. The MIC is below the concentration of A/64, similar to SWy-2.

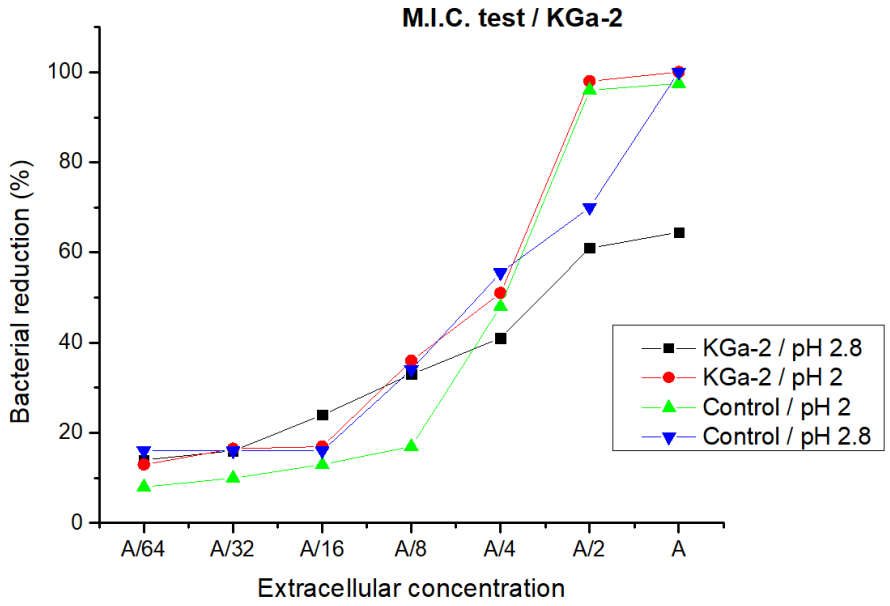

Figure 5.12: MIC results of KGa-2 sample in pH=6.4

The influence of kaolinite in the fungal culture can be observed in Figure 5.12. The fungus *P. purpurogenum* is very resistant at extreme, acidic conditions and it was a chance to examine the influence of kaolinite to the fungal culture at its IEP and below it.

The bacterial reduction at pH=2.8 (IEP of KGa-2) does not exceed 65%, which is not competitive to smectite samples. The MIC is met at a concentration of ~A/4 for the culture at pH=2.0, while the MIC at the IEP is met at ~A/2. At pH=2, any antibacterial activity is due to the Control. In conclusion, the kaolinite does not appear to stimulate or actively influence the fungus development in any way.

Chapter 6: Summary and conclusions

Three samples were characterized and added in *Penicillium purpurogenum* cultures to verify the impact of their surface properties, specifically of their isoelectric points, on the production of antibacterial properties. The isoelectric points of the tested materials were determined by acid titration along with zeta potential and electrokinetic mobility measurements. The IEPs of KGa-2, SWy-2 and B3 samples were detected at pH values of 2.81 ± 0.03, 6.71 ± 0.01 and 6.40 ± 0.02 respectively. In time, these measurements will be repeated by using the original potentiometric and mass titration techniques, under inert atmosphere if possible, to detect variations among the different methods. The ATR/FT-IR results proved the existence of

nitrogen and carbon-containing active groups in SWy-2, which suggest the existence of proteins and maybe potato dextrose.

The ED XRF results show an elevated concentration of iron, while no ferrous minerals were detected by the XRD patterns. Consequently, the iron should exist in the octahedral layers of smectites. According to Wang et al., (2007), the exposed smectite edges are able to form superoxide oxygen radicals. These bioactive chemical groups originate from the oxidation of structural Fe^{+2}. Nonetheless, this fact should not be of major importance, since B3 sample presents increased antimicrobial performance in pH=7.5. The only detected mineral phase with proven antimicrobial activity is the anatase, which is present only in KGa-2 sample and does not affect the fungal development, according to the MIC test results.

Both smectites underwent the MIC test in two specific pH values (5.5 and 7.5) and the results were almost identical and very encouraging, except for Ca-montmorillonite sample at the lower pH. On the other hand, KGa-2 was completely inert.

Gournis et al., (2002) highlight the influence of particle surface size of smectites as a stimulation factor of fungi. This assumption is excluded, because the particle surface size of the two smectite samples is similar, as the respective measurements suggest.

In terms of the Na-saturated B3 sample, the only available information originates from the XRD results, which indicate the existence of nutrient in the interlayer space and gel formation capability. The culture of the *P. purpurogenum* in presence of B3 Na-smectite, as well as the MIC test, will be performed in the future to investigate a possible influence of the interlayer cation. For a more accurate determination of the stimulation mechanism, other stimulating parameters should be investigated, such as the layer charge, hydorphobicity and microtopography of the smectite particles (Lünsdorf et al., 2000; Cheng et al., 2019).

References

Appel, C., Ma, L.Q., Rhue, R.D. & Kennelley, E. (2003) Point of zero charge determination in soils and minerals via traditional methods and detection of electroacoustic mobility. *Geoderma*, **113(1–2)**, 77-93.

Athanasakis, N. (2019) Rheological behavior of magnesium bentonites and sepiolites at high temperature conditions. *Institutional Repository of the Technical University of Crete*, Greece, Chania.

Bailey, S.W. (1975) Chlorites. In: *Soil components* (J.E. Gieseking, editor). Inorganic components, **2**, Springer, Berlin Heidelberg, New York, pp. 191–263.

Barde, P. & Barde, P. (2012) What to use to express the variability of data: Standard deviation or standard error of mean?. *Perspectives in clinical research*, **3**, 113-116.

Bich, C. (2005) Contribution à l'étude de l'activation thermique du kaolin: évolution de la structure cristallographique et activitépouzzolanique. Ph.D. Thesis, Institut National des Sciences Appliqués de Lyon, France.

Brady, P. V., Cygan, R. T. & Nagy, K. L. (1996) Molecular Controls on Kaolinite Surface Charge. *Journal of Colloid and Interface Science*, **183(2)**, 356-364.

Brady, P. V. & Walther, J. V. (1989) Geochim. *Cosmochim*, **53**, 282.

Brown, G. (1955) Report of the clay minerals group subcommittee on the nomenclature of clay minerals. *Clay Minerals Bulletin*, **2**, 294-301.

Browning, G.R.J. (1998) Geosynthetic clay liners: a review and evaluation. *Transactions of the Institute of Mining and Metallurgy (Section B: Applied Earth Science)*, **107**, B120–B129.

Bose, J.L. & Bayles, K.W. (2013) Staphylococcus aureus, In: *Brenner's Encyclopedia of Genetics (Second Edition)* (S. Maloy & K. Hughes, editors). Academic Press, pp. 553-555.

Bucher, F. & Müller-Vonmoos, M. (1989) Bentonite as a containment barrier for the disposal of highly radioactive wastes. *Applied Clay Science*, **4**, 157-177.

Bundy, W.H. (1993) The diverse industrial applications of kaolin. In: *Kaolin Genesis and Utilization* (H.H. Murray, W.M. Bundy & C.C. Harvey, editors). The Clay Minerals Society, Boulder, Colorado, USA, pp. 43–73.

Burford, E.P., Fomina, M. & Gadd, G.M. (2003) Fungal involvement in bioweathering and biotransformation of rocks and minerals. *Mineral. Mag.*, **67**, 1127–1155.

Burst, J.F. & Hughes, R.E. (1994) Clay-based ceramic raw materials. In: *Industrial Minerals and Rocks, 6th edition* (D.D. Carr, editor). Soc. Mining Eng., Denver, CO, pp. 317-324.

Chaerun, S.K., Kazue, T., Ryuzi, A. & Kazuhiro, K. (2004) Interaction between clay minerals and hydrocarbon-utilizing indigenous microorganisms in high concentrations of heavy oil: implications for bioremediation. *Clay minerals*, **40**, 105-114.

Chen, J., Blume, H.P. & Beyer, L. (2000) Weathering of rocks induced by lichen colonization–a review. *CATENA*, **39**, 121–146.

Cheng, Y., Feng, G. & Moraru, C.I. (2019) Micro- and nanotopography sensitive bacterial attachment mechanisms: A review. *Front. Microbiol*., **10**, 1–17.

Cristiano, E., Hu, Y. J., Siegfried, M., Kaplan, D. & Nitsche, H. (2011) A comparison of point of zero charge measurement methodology. *Clays and Clay Minerals*, **59(2)**, 107- 115.

Christidis, G.E. (2011) The concept of layer charge of smectites and its implications for important smectite-water properties. In: *Layered Mineral Structures and Their Application in Advanced Technologies* (M.F. Brigatti & A. Mottana, editors). Mineralogical Society, London, UK, pp. 239–260.

Christidis, G.E. (2013) Assessment of industrial clays. *Developments in Clay Science*, **5**, 425-449.

Christidis, G.E. (2016) Surface charge properties of clays with emphasis on smectites. In: *1st IMEKO TC4 International Workshop on Metrology for Geotechnics*. International Measurement Confederation (IMEKO), pp. 12-15.

Christidis, G.E., Blum, A.E. & Eberl, D.D. (2006) Influence of layer charge and charge distribution of smectites on the flow behaviour and swelling of bentonites. *Applied Clay Science*, **34**, 125-138.

Christidis, G.E. & Eberl, D.D. (2003) Determination of layer charge characteristics of smectites. *Clays and Clay Minerals*, **51**, 644–655.

Christidis, G.E. & Huff, W.D. (2009) Geological Aspects and Genesis of Bentonites. *Elements*, **5**, 93-98.

Christidis, G.E. & Scott, P. (1997) The origin and control of colour of white bentonites from the Aegean islands of Milos and Kimolos. *Mineralium Deposita*, Greece, **32**, 271- 279.

Churchman, G.J., Gates, W.P., Theng, B.K.G. & Yuan, G. (2006) Clays and clay minerals for pollution control. In: *Handbook of Clay Science* (F. Bergaya, B.K.G. Theng & G. Lagaly, editors). Developments in Clay Science, **1**, Elsevier, pp. 625-675.

Cuadros, J. (2017) Clay minerals interaction with microorganisms: A review. *Clay Miner.*, **52**, 235–261.

Cuihua, T., Jianxi, Z., Zhaohui, L., Runliang, Z., Qing, Z., Jingming, W., Hongping, H. & Qi, T. (2015) Surface chemistry and reactivity of SiO2 polymorphs: A comparative study on α-quartz and α-cristobalite, *Applied Surface Science*, **355**, 1161-1167.

Diko, M., Ekosse, G. & Ogola, J. (2006) Fourier transform infrared spectroscopy and thermal analyses of kaolinitic clays from South Africa and Cameroon. *Acta Geodyn. Geomater.*, **13(182)**, 149–158.

Drits, V.A., Lindgreen, H., Salyn, A.L., Ylagan, R. & McCarty, D.K. (1998) Semiquantitative determination of trans-vacant and cis-vacant 2:1 layers in illites and illite-smectites by thermal analysis and X-ray diffraction. *American Mineralogist*, **83**, 1188-1198.

Duran, J.D.G., Ramos-Tejada, M.M., Arroyo, F.J. & Gonzalez-Cabalero, F. (2000) Rheological and electrokinetic properties of sodium montmorillonite suspensions: rheological properties and interparticle energy of interaction. *J. Colloid Interface Sci*., **229**, 107–117.

Ece, O.I., Nakagawa, Z. & Schroed, P. (2003) Alteration of volcanic rocks and genesis of kaolin deposits in the Sile region, Northern Istanbul, Turkey. *Clay Mineralogy, Clays and Clay Minerals*, **51(6)**, 675– 688.

Ehrlich, H.L. (1998) Geomicrobiology: Its significance for geology. *Earth Sci. Rev.*, **45**, 45–60.

Eisenhour, D. & Brown, R. (2009) Bentonite and Its Impact on Modern Life. *Elements*, **5**, 83-88.

Emmerich, K. & Kahr, G. (2001) The cis- and trans-vacant variety of a montmorillonite: an attempt to create a model smectite. *Applied Clay Science*, **20(3)**, 119-127.

Fialips, C.I., Petit, S., Decarreau, A. & Beaufort, D. (2000) Influence of synthesis pH on kaolinite "crystallinity" and surface properties. *Clays Clay Miner*, **48**, 173–184.

Fomina, M. & Skorochod, I. (2020) Microbial Interaction with Clay Minerals and Its Environmental and Biotechnological Implications. *Minerals*, **8**, 230-284.

Furukawa, Y., Watkins, J., Jinwook, K., Curry, K. & Bennett, R. (2009) Aggregation of montmorillonite and organic matter in aqueous media containing artificial seawater. *Geochemical transactions*. **10**.

Fyticas, M. & Vougioukalakis, G. (1992) Volcanic structure and evolution of Kimolos and Polyegos (Milos Island group). *6th Congr. Geol. Soc.*, Greece.

García-González, M.T., Vizcayni, C. & Cortabitarte, J. (2000) Effect of kaolinite and sulfate on the formation of hydroxyl-aluminium compounds. *Clays Clay Miner.,* **48**, 85-94.

Giese, R.F. Jr. (1988) Kaolin minerals: structures and stabilities. In: *Hydrous Phyllosilicates (Exclusive of Micas)* (S.W. Bailey, editor). Reviews in Mineralogy, **19,** Mineralogical Society of America, Washington D.C., pp. 29–66.

Gournis, D., Karakassides, M.A. & Petrides, D. (2002) Formation of hydroxyl radicals catalyzed by clay surfaces. *Phys. Chem. Miner*., **29**, 155–158.

Grim, R.E. (1962) *Applied Clay Mineralogy*. McGraw-Hill, New York.

Grim, R.E. & Guven, N. (1978) Bentonites-geology, mineralogy, properties, and uses. *Elsevier*, NY, **256**.

Gui, L. L., Chun, H. Z., Saverio, F. & Wei, H. Y. (2019) Interactions between microorganisms and clay minerals: New insights and broader applications. *Applied Clay Science*, **177**, 91-113.

Gupta, V., Hampton, M.A., Stokes, J.R., Nguyen, A.V. & Miller, J.D. (2011) Particle interactions in kaolinite suspensions and corresponding aggregate structures. *Journal of Colloid and Interface Science*, **359(1)**, 95-103.

Güven, N. (1988) Smectite. In: *Hydrous Phyllosilicates* (S.W. *Baley, editor).* Reviews in Mineralogy, **19**, Mineralogical Society of America, pp. 497-559.

Güven, N. (1992) Rheological aspects of aqueous smectite suspensions. In: *Clay-Water Interface and its Rheological Implications* (N. Guven & R.M. Pollastro, editors). CMS Workshop Lectures, **4**, The Clay Minerals Society, Aurora, Colorado, USA, pp. 81–125.

Hall, A. J. & Photos-Jones, E. (2008) Accessing Past Beliefs and Practises: The Case of Lemnian Earth. *Archaeometry*, **50**, 1034-1049.

Hao, T. (2005) *Mechanisms of the electrorheological effect*. Studies in Interface Science, Elsevier, **22**, pp. 475-517.

Harben, P.W. & Kužvart, M. (1997) A Global Geology. *Industrial Minerals,* London, **128**.

Holtzer, M., Bobrowski, A. & Żymankowska-Kumon, S. (2011) Temperature influence on structural changes of foundry bentonites. *Journal of Molecular Structure*, **1004(1)**, 102-108.

Hosterman, J. W. (1984) Ball clay and bentonite deposits of the central and western Gulf of Mexico Coastal Plain. *US Government Printing Office*, United States.

Houbraken, J., de Vries, R.P. & Samson, R.A. (2014) Modern Taxonomy of Biotechnologically Important Aspergillus and Penicillium Species. In: *Advances in Applied Microbiology* (S. Sariaslani & G.M. Gadd, editors). Academic Press, **86**, pp. 199-249.

Huang, P.M. (2004) Soil Mineral–Organic Matter--Microorganism Interactions: Fundamentals and Impacts. *Advances in Agronomy*, **82**, 391-472.

James, R.O. & Parks, G.A. (1982) Characterization of aqueous colloids by their electrical double-layer and intrinsic surface chemical properties. *Surface and Colloid Science*, **12**. Plenum, New York, 119–216.

Jepson, W.B. (1984) Kaolins: their properties and uses. *Philosophical Transactions of the Royal Society*, London, **A311**, 411–432.

Jirhatova, K. (1981) Isolectric point of modified alumina. *Appl. Catal*., **1**, 165.

Johnson, I., Abubakar, A., Ali, S. & Kumar, M. (2019) Chapter 10 - Cyanobacteria/Microalgae for Distillery Wastewater Treatment- Past, Present and the Future. In: *Microbial Wastewater Treatment* (M.P. Shah, S.Rodriguez-Couto, editors). Elsevier, pp. 195-236.

Johnston, C.T. & Tombacz, E. (2002) Surface chemistry of soil minerals. In: *Soil Mineralogy with Environmental Applications* (J.B. Dixon & D.G. Schulze, editors). Soil Science Society of America, Madison, WI, pp. 37 – 67.

Kennedy, M., Droser, M., Mayer, L., Pevear, D. & Mrofka, D. (2006) Late Precambrian Oxygenation; Inception of the Clay Mineral Factory. *Science*, New York, N.Y., 311.

Khang, V.V., Korovkin, M.V. & Ananyeva, L.G. (2016) Identification of clay minerals in reservoir rocks by FTIR spectroscopy. *IOP Conf.Ser. Earth Environ. Sci*., **43**.

Kuentz, M. & Roethlisberger, D. (2003) Rapid assessment of sedimentation stability in dispersions using near infrared transmission measurements during centrifugation and oscillatory rheology. *European Journal of Pharmaceutics and Biopharmaceutics*, **56**, 355–361.

Kumari, N. & Mohan, C. (2021) Basics of Clay Minerals and Their Characteristic Properties. In: *Clay and Clay Minerals* (M.D.N. Gustavo, editor). IntechOpen.

Laird, D.A. (1999) Layer charge influences on the hydration of expandable 2:1 phyllosolicates. *Clays and Clay Minerals*, **47**, 630–636.

Laird, D.A. (2006) Influence of layer charge on swelling of smectites. *Applied Clay Science*, **34**, 74–87.

La Quita-Mai, M. (2005) Significance of Cell Surface Charge on Microbial Susceptibility to Chitosan. Master's Thesis, University of Tennessee, 6-8.

Liu, D. (2015) Enterotoxin-Producing Staphylococcus aureus. In: *Molecular Medical Microbiology (Second Edition)* (Y.W. Tang, M. Sussman, D. Liu, I. Poxton & J. Schwartzman, editors). Academic Press, **55**, pp. 979-995.

Lünsdorf, H., Erb, R.W., Abraham, W.R. & Timmins, K.N. (2000) "Clay Hutches": A novel interaction between bacteria and clay minerals. *Environ. Microbiol*., **2**, 161–168.

Lützenkirchen, J., Preočanin, T., Kovačević, D., Tomišić, V., Lövgren, L. & Kallay, N. (2012) Potentiometric titrations as a tool for surface charge determination. *Croatica chemica acta*, **85(4)**, 391-417.

Macgregor, A. (2013) Medicinal terra sigillata: a historical, geographical and typological review. *Geological Society London Special Publications*, **375**, 113-136.

Malvern Instruments (2009) Zetasizer Nano User Manual. MAN0317.

Malvern Instruments Limited. (2015) Zeta potential - An introduction in 30 minutes. Technical note.

Mckeen, A. & Geehan, T. (1989) Drilling mud: Monitoring it and managing it. *Oilfield Review*, **1**, 7-1989.

Meunier, A. (2005) *Clays*. Spinger, pp 207-213.

Miu, F., Zhao, Q. & Lui, L. (2013) Experimental study on the electrokinetics of kaolinite particles in aqueous suspension. *Physiochem. Probl. MI*., **49**, 659-672.

Moll, W. (2001) Baseline Studies of the Clay Minerals Society Source Clays: Geological Origin. *Clays and Clay Minerals - CLAYS CLAY MINER*., **49**, 374-380.

Money, N.P. (2004) The fungal dining habit–a biomechanical perspective. *Mycologist*, **18**, 71–76.

Morais, L., Cordao-Neto, M. & Tarantino, A. (2019) Aggregation process of kaolinite clay. *E3S Web of Conferences*.

Mosher, R.A., Wolfgang, T. & Milan, B. (1986) An explanation for the plateau phenomenon in isoelectric focusing. *Journal of Chromatography*, **351**, 31-38.

Mullet, M., Fievet, P., Reggiani, J.C. & Pagetti, J. (1997) Surface electrochemical properties of mixed oxide ceramic membranes: Zeta-potential and surface charge density. *Journal of Membrane Science*, **123**, 255-265.

Murray, H. H. (2007) Occurrences, processing and application of kaolins, bentonite, palygorskite sepiolite, and common clays. *Applied Clay Mineralogy*, **55**, 644–645.

Mustafa, S., Dilara, B., Nargis, K., Naeem, A. & Shahida, P. (2002) Surface properties of the mixed oxides of iron and silica. *Colloids and Surfaces A: Physicochemical and Engineering Aspects*, **205**, 273-282.

Ndlovu, B., Farrokhpay, S., Forbes, E. & Bradshaw, D. (2014) Characterisation of kaolinite colloidal and flow behaviour using its crystallinity measurements. *Powder Technology*.

Noh, J.S. & Schwarz, J.A. (1989) Estimation of the point of zero charge of simple oxides by mass titration. *Journal of Colloid and Interface Science*, **130**, 157-164.

O'Brien, R.W., Cannon, D.W. & Rowlands, W.N. (1995) Electroacoustic determination of particle size and zeta potential. *J. Colloid Interface Sci*., **173**, 406-418.

O'Day, P., Parks, G. & Brown, G. (1994) Molecular Structure and Binding Sites of Cobalt(II) Surface Complexes on Kaolinite from X-ray Absorption Spectroscopy. *Clays and Clay Minerals - CLAYS CLAY MINER*., **42**, 337-355.

Paluszkiewicz, C., Holtzer, M., Bobrowski, A. (2008) FTIR analysis of bentonite in moulding sands. *Journal of Molecular Structure*, **880(1–3)**, 109–114.

Park, S.J. & Seo, M.K. (2011) Intermolecular Force. Interface *Science and Technology*, Elsevier, **18**, 1-57.

Parks, G.A. & Bruyn, P.L.D. (1962) Zero point of charge of oxides. *Journal of Physical Chemistry*, **66**, 967-974.

Pecini, E. & Avena, M. (2013) Measuring the Isoelectric Point of the Edges of Clay Mineral Particles: The Case of Montmorillonite. *Langmuir : the ACS journal of surfaces and colloids*, **29**.

Phipps, J. (2014) Engineering minerals for performance application: An industrial perspective. *Clay Minerals*, **49(1)**, 1-16.

Photos-Jones, E., Edwards, C., Haner, F., Lawton, L., Kean, C., Leonard, A. & Perdikatsis, V. (2017) Archaeological medicinal earths as antibacterial agents: the case of the Basel Lemnian sphragides. *Geological society: special publications. Geology and medicine: historical connections*, **452**, 141-153.

Photos-Jones,E., Knapp, C.W., Venieri, D., Christidis, G.E., Elgy, C., Valsami-Jones, E., Gounaki, I. & Andriopoulou, N.C. (2018) Greco-Roman mineral (litho)therapeutics

and their relationship to their microbiome: The case of the red pigment miltos. *Journal of Archaeological Science: Reports*, **22**, 179-192.

Pironon, J., Pelletier, M., de Donato, P. & Mosser-Ruck, R. (2003) Characterization of smectite and illite by FTIR spectroscopy of interlayer $NH4^+$ cations. *Clay Minerals, Mineralogical Society*, **38 (2)**, 201-211.

Preocanin, T., Abdelmonem, A. & Lutzenkirchen, G. M. (2016) Charging Behavior of Clays and Clay Minerals in Aqueous Electrolyte Solutions — Experimental Methods for Measuring the Charge and Interpreting the Results. In: *Clays, Clay Minerals and Ceramic Materials Based on Clay Minerals* (G.Morari Do Nascimento, editor). IntechOpen.

Preocanin, T. & Kallay, N. (1998) Application of Mass Titration to Determination of Surface Charge of Metal Oxides. *Croatica chemica acta*, **71(4)**, 1117-1125.

Pruett, R.J. (2016) Kaolin deposits and their uses: Northern Brazil and Georgia, USA. *Applied Clay Science*, **131**, 3-13.

Ramos-Tejada, M.M., de Vicente, J., Ontiveros, A. & Duran, J.D.G. (2001) Effect of humic acid adsorption on the rheological properties of sodium montmorillonite suspensions. *J. Rheol*., **45**, 1159–1172.

Ross, C.S. & Hendricks, S.B. (1945) Minerals of the Montmorillonite Group. *United States Geological Survey Professional*, **Paper No. 205-B**, 79.

Ross, C.S. & Shannon, E.V. (1926) The minerals of bentonite and related clays and their physical properties. *American Ceramic Society Journal*, **9(2)**, 77-96.

Schofield, R. K. & Samson, H. R. (1954) Flocculation of kaolinite due to the attraction of opposite charged crystal faces. *Disc. Faraday Soc*., **18**, 138.

Secor, R.B. & Radke, C.J. (1985) Spillover of the diffuse double layer on montmorillonite particles. *J. Colloids Interface Sci*., **103**, 237–244.

Sposito, G. (1984) The Surface Chemistry of Soils. *Oxford Univ. Press*, New York.

Sposito, G. (1992) Characterization of particle surface charge. In: *Environmental Particles* (J. Buffle & H.P. van Leeuwen, editors), Environmental Analytical and Physical Series, **1**, Lewis, London.

Stumm, W. (1992) *Chemistry of the Solid-Water Interface*. J. Wiley & Sons, Inc., New York.

Stumm, W. & Morgan, J.J. (1981) *Aquatic Chemistry*. Wiley-Interscience, New York.

Tawfik, M., Ahmed, N. & Ward, A. (2018) Characterization of kaolin-filled polymer composites. *Society of Plastics Engineers.* 10.2417/spepro.004978.

Tironi, A., Trezza, M.A., Irassar, E. & Scian, A.N. (2012) Thermal Treatment of Kaolin: Effect on the Pozzolanic Activity. *Procedia Materials Science*, **1**, 343–350.

Tombácz, E., Ábrahám, I., Gilde, M. & Szántó, F. (1990) The pH-dependent colloidal stability of aqueous montmorillonite suspensions. *Colloids Surf.*, **49**, 71-78.

Tombácz, E. & Szekeres, M. (2004*)* Colloidal behavior of aqueous montmorillonite suspensions: the specific role of pH in the presence of indifferent electrolytes. *Applied Clay Science*, **27(1–2)**, 75-94.

Tournassat, C., Bourg, I. C., Steefel, C. I. & Bergaya, F. (2015) *Surface Properties of Clay Minerals*. Developments in Clay Science, Elsevier, pp. 5-31.

Van Olphen, H. (1963) *An Introduction to Clay Colloid Chemistry*. Interscience, New York.

Venieri, D., Gounaki, I., Christidis, G.E., Knapp, C., Bouras-Vallianatos, P. & Photos-Jones, E. (2020) Minerals Bridging the Gaps: Bole and Terra Sigillata as Artefacts, as Simples and as Antibacterial Clays. *Minerals*, **10(348)**.

Wang, Q., Garrity, G.M., Tiedje, J.M. & Cole, J.R. (2007) Naive bayesian classifier for rapid assignment of rRNA sequences into the new bacterial taxonomy. *Appl. Environ. Microbiol*., **73(16)**, 5261–5267.

Wanner, H., Albinsson, Y., Karnland, O., Wieland, E., Wersin, P. & Charlet, L. (1994) The acid/base chemistry of montmorillonite. *Radiochim. Acta*, **66/67**, 157–162.

Warshaw, C.M. & Roy, R. (1961) Classification and a scheme for the identification of layer silicates. *Geological Society of American Bulletin*, **72**, 1455-1492.

Watkins, K.E. & Unnikrishnan, M. (2020) Evasion of host defenses by intracellular Staphylococcus aureus. In: *Advances in Applied Microbiology* (G.M. Gadd & S. Sariaslani, editors). Academic Press, **112**, pp. 105-141.

Weaver, C.E. & Pollard, L.D. (1973) *The Chemistry of Clay Minerals*. Elsevier, Amsterdam, The Netherlands, pp. 55–77.

Weiss, A. (1969) Organic derivatives of clay minerals, zeolites and related minerals. In: *Organic Geochemistry* (G. Eglinton & M.T.J. Murphy, editors). Springer, Berlin, Heidelberg, pp. 737–781.

Wilkinson, N., Metaxas, A., Quinney, C., Wickramaratne, S., Reineke, T. & Dutcher, C. (2017) pH Dependence of Bentonite Aggregate Size and Morphology on Polymer-Clay

Flocculation. *Colloids and Surfaces A: Physicochemical and Engineering Aspects*, **537**, 281-286.

Zhou, Z. & Gunter, W. D. (1992) The Nature of the Surface Charge of Kaolinite. *Clays Clay Minerals*, **40**, 365-368.

Zviagina, B.B., Drits, V.A. & Dorzhieva, O.V. (2020) Distinguishing Features and Identification Criteria for K-Dioctahedral 1*M* Micas (Illite-Aluminoceladonite and Illite-Glauconite-Celadonite Series) from Middle-Infrared Spectroscopy Data. *Minerals*, **10(2)**,153.

Żymankowska-Kumon, S., Holtzer, M. & Grzegorz, G. (2011) Thermal analysis of foundry bentonites. *Archives of Foundry Engineering*, **11**. 209-213.

Appendix 1: AutoQuan® software spectra

- **SWy-2**

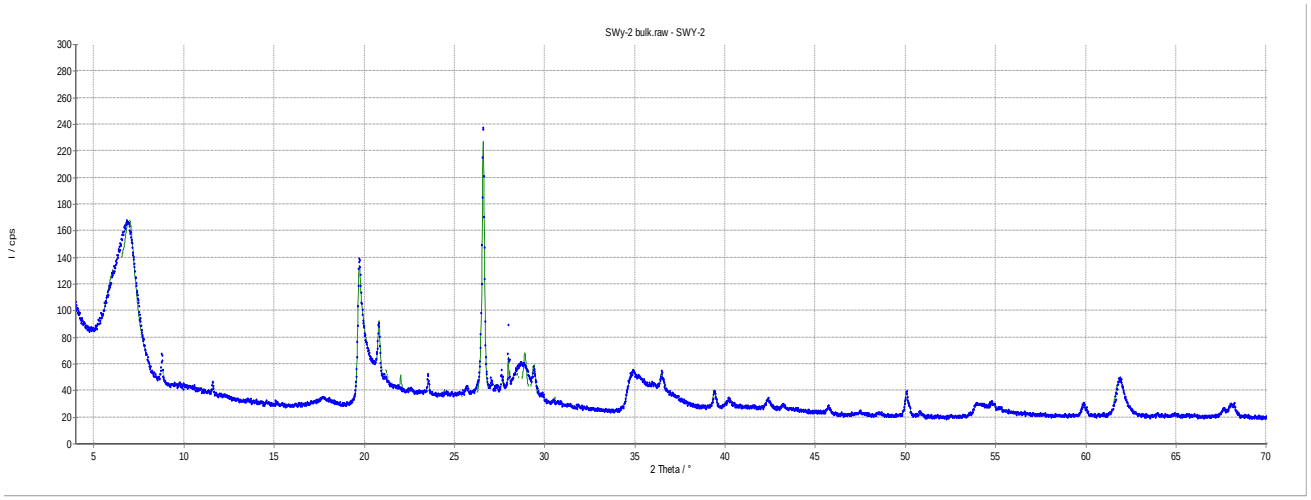

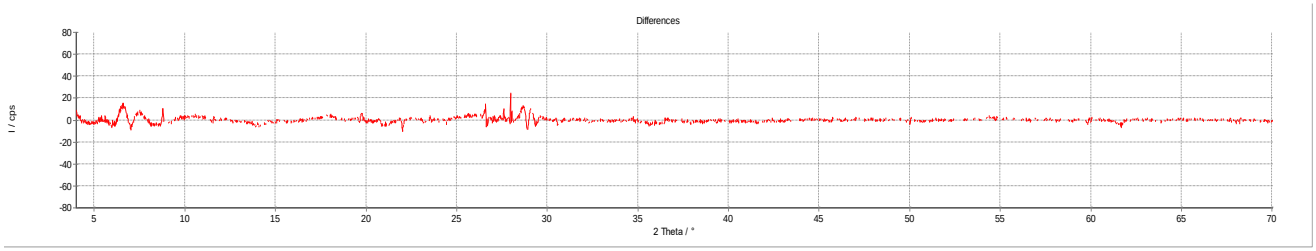

Figure A 1.1: Quantitative analysis of SWy-2 sample and correlation chart

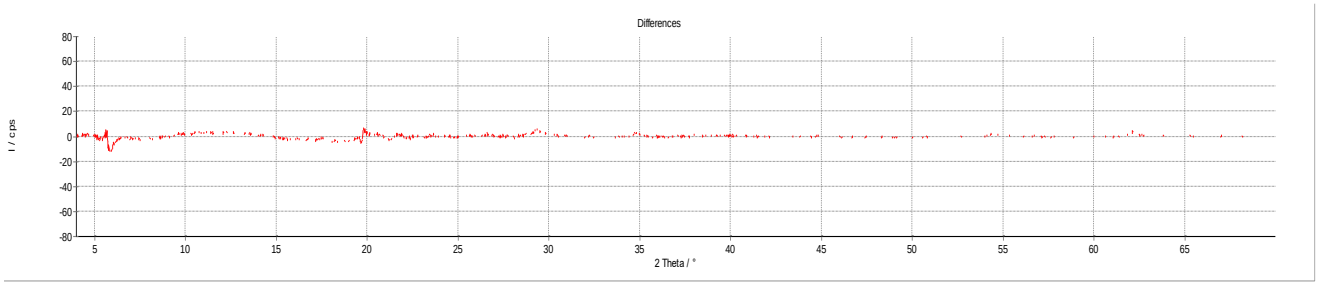

Figure A 1.2: Quantitative analysis of B3 sample and correlation chart

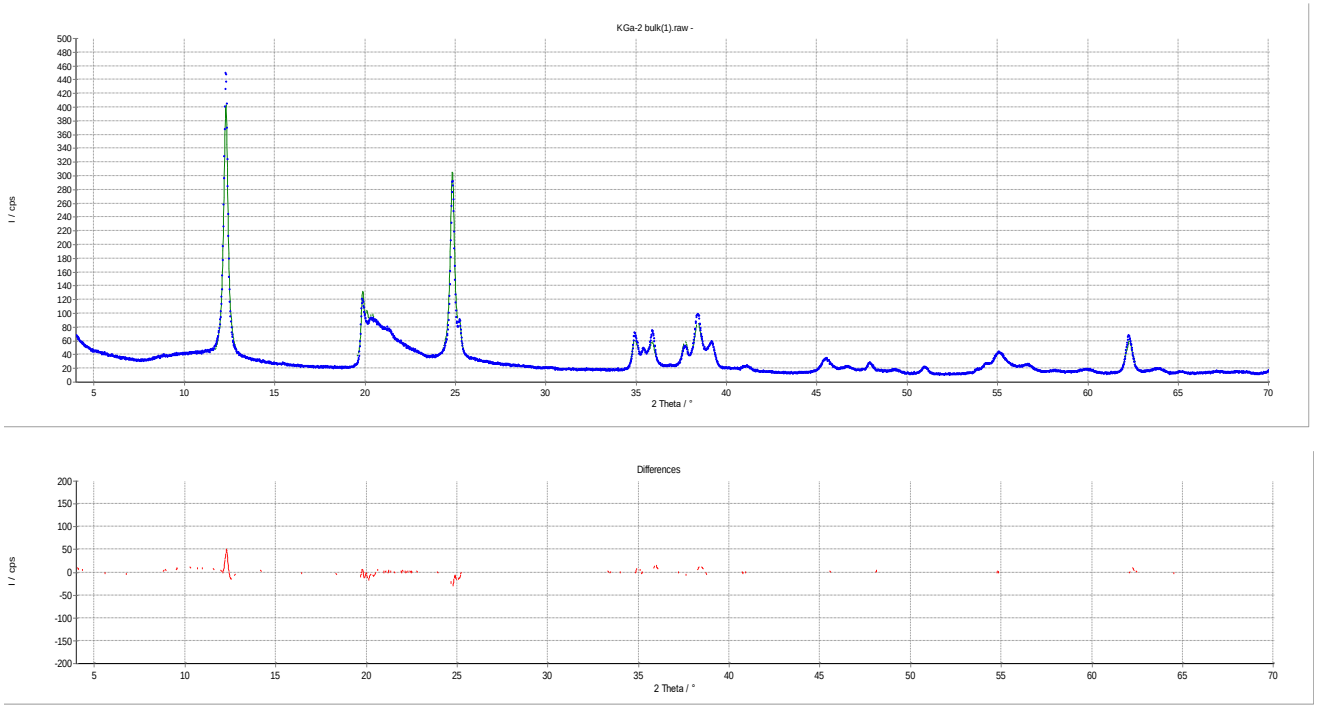

Figure A 1.3: Quantitative analysis of KGa-2 sample and correlation chart

Appendix 2: Titration data

1		B3	2		3	
V (mL)	**pH**		**V (mL)**	**pH**	**V (mL)**	**pH**
0	9,17		0	9,19	0	9,13
0,05	8,09		0,05	8,13	0,05	8,03
0,1	7,37		0,1	7,41	0,1	7,02
0,105	6,96		0,105	7,02	0,105	6,93
0,11	6,89		0,11	6,86	0,11	6,88
0,115	6,77		0,115	6,8	0,115	6,83
0,12	6,68		0,12	6,74	0,12	6,76
0,125	6,6		0,125	6,67	0,125	6,7
0,13	6,54		0,13	6,61	0,13	6,65
0,135	6,49		0,135	6,55	0,135	6,58
0,14	6,44		0,14	6,5	0,14	6,54
0,145	6,42		0,145	6,45	0,145	6,5
0,15	6,42		0,15	6,43	0,15	6,46
0,155	6,39		0,155	6,41	0,155	6,44
0,16	6,37		0,16	6,4	0,16	6,42
0,165	6,33		0,165	6,4	0,165	6,4
0,17	6,28		0,17	6,38	0,17	6,39

0,175	6,24	0,175	6,32	0,175	6,39
0,18	6,21	0,18	6,28	0,18	6,37
0,185	6,17	0,185	6,23	0,185	6,32
0,19	6,14	0,19	6,17	0,19	6,29
0,195	6,12	0,195	6,12	0,195	6,24
0,2	6,1	0,2	6,08	0,2	6,19
0,205	6,08	0,205	6,04	0,205	6,15
0,21	6,06	0,21	6,01	0,21	6,11
0,215	6,03	0,215	5,97	0,215	6,08
0,22	6	0,22	5,94	0,22	6,03
0,225	5,98	0,225	5,91	0,225	6
0,23	5,95	0,23	5,87	0,23	5,97
0,235	5,92	0,235	5,82	0,235	5,94
0,24	5,9	0,24	5,78	0,24	5,9
0,245	5,88	0,245	5,75	0,245	5,87
0,25	5,86	0,25	5,73	0,25	5,85
0,26	5,79	0,26	5,64	0,26	5,72
0,27	5,72	0,27	5,53	0,27	5,61
0,28	5,64	0,28	5,45	0,28	5,52
0,29	5,58	0,29	5,39	0,29	5,42
0,3	5,54	0,3	5,35	0,3	5,38
0,31	5,5	0,31	5,31	0,31	5,35
0,32	5,46	0,32	5,28	0,32	5,31
0,35	5,24	0,35	5,17	0,35	5,2
0,38	5,11	0,38	5,04	0,38	5,12
0,41	5,01	0,41	4,97	0,41	5,03
0,44	4,92	0,44	4,91	0,44	4,95
0,47	4,84	0,47	4,86	0,47	4,89
0,5	4,79	0,5	4,81	0,5	4,84
1	4,42	1	4,5	1	4,59
1,5	4,23	1,5	4,17	1,5	4,3
2	4,08	2	4,02	2	4,19
2,5	3,96	2,5	3,9	2,5	4,04
3	3,88	3	3,82	3	3,92
3,5	3,79	3,5	3,75	3,5	3,81
4	3,74	4	3,7	4	3,76
5	3,44	5	3,41	5	3,5
6	3,24	6	3,15	6	3,23
7	3,05	7	3,03	7	3,11
8	2,99	8	2,95	8	3,04
9	2,93	9	2,87	9	2,97
10	2,84	10	2,79	10	2,89
11	2,75	11	2,7	11	2,81
12	2,68	12	2,64	12	2,74

1	Swy2	2		3	
V (mL)	**pH**	**V(mL)**	**pH**	**V(mL)**	**pH**
0	8,72	0	8,76	0	8,68
0,05	8,59	0,05	8,59	0,05	8,55
0,1	8,42	0,1	8,44	0,1	8,41
0,15	8,28	0,15	8,32	0,15	8,28
0,2	7,95	0,2	8,03	0,2	8,09
0,25	7,78	0,25	7,85	0,25	7,94
0,3	7,54	0,3	7,62	0,3	7,67
0,35	7,42	0,35	7,51	0,35	7,53
0,355	7,34	0,355	7,4	0,355	7,45
0,36	7,25	0,36	7,29	0,36	7,36
0,365	7,18	0,365	7,2	0,365	7,25
0,37	7,11	0,37	7,13	0,37	7,19
0,375	7,05	0,375	7,07	0,375	7,1
0,38	6,99	0,38	6,97	0,38	6,95
0,385	6,93	0,385	6,9	0,385	6,87
0,39	6,88	0,39	6,83	0,39	6,82
0,395	6,83	0,395	6,78	0,395	6,79
0,4	6,79	0,4	6,74	0,4	6,76
0,405	6,75	0,405	6,71	0,405	6,73
0,41	6,72	0,41	6,71	0,41	6,7
0,415	6,72	0,415	6,71	0,415	6,7
0,42	6,71	0,42	6,69	0,42	6,7
0,425	6,7	0,425	6,66	0,425	6,68
0,43	6,67	0,43	6,63	0,43	6,67
0,435	6,64	0,435	6,6	0,435	6,63
0,44	6,61	0,44	6,57	0,44	6,6
0,445	6,58	0,445	6,55	0,445	6,58
0,45	6,56	0,45	6,53	0,45	6,56
0,455	6,52	0,455	6,5	0,455	6,53
0,46	6,48	0,46	6,46	0,46	6,5
0,465	6,46	0,465	6,43	0,465	6,48
0,47	6,44	0,47	6,41	0,47	6,47
0,475	6,41	0,475	6,38	0,475	6,45
0,48	6,38	0,48	6,35	0,48	6,42
0,485	6,34	0,485	6,31	0,485	6,39
0,49	6,32	0,49	6,28	0,49	6,36
0,495	6,29	0,495	6,26	0,495	6,33
0,5	6,26	0,5	6,25	0,5	6,31
0,52	6,02	0,52	6,07	0,52	6,14
0,54	5,87	0,54	5,98	0,54	6
0,56	5,74	0,56	5,9	0,56	5,89

0,58	5,63	0,58	5,8	0,58	5,78
0,6	5,5	0,6	5,61	0,6	5,68
0,65	5,18	0,65	5,27	0,65	5,35
0,7	4,94	0,7	5,03	0,7	5,12
0,75	4,79	0,75	4,85	0,75	4,94
0,8	4,63	0,8	4,72	0,8	4,79
0,85	4,54	0,85	4,61	0,85	4,69
0,9	4,47	0,9	4,53	0,9	4,6
0,95	4,39	0,95	4,43	0,95	4,51
1	4,3	1	4,35	1	4,4
2	3,82	2	3,94	2	3,9
3	3,75	3	3,81	3	3,78
4	3,62	4	3,69	4	3,66
5	3,49	5	3,58	5	3,6
6	3,32	6	3,5	6	3,53
7	3,24	7	3,42	7	3,46
8	3,17	8	3,34	8	3,39
9	3,11	9	3,25	9	3,3
10	3,06	10	3,17	10	3,22
11	3,02	11	3,1	11	3,14

1		**KGa-2**	**2**		**3**
V (mL)	**pH**		**V (mL)**	**pH**	**V (mL)**	**pH**
0	8,85		0	8,9	0	8,94
0,1	7,37		0,1	7,5	0,1	7,41
0,15	6,81		0,15	6,92	0,15	6,78
0,2	6,04		0,2	6,07	0,2	5,99
0,25	5,78		0,25	5,85	0,25	5,72
0,3	5,54		0,3	5,59	0,3	5,46
0,35	5,33		0,35	5,37	0,35	5,28
0,4	5,18		0,4	5,22	0,4	5,16
0,45	5,05		0,45	5,09	0,45	5,07
0,5	4,92		0,5	4,95	0,5	4,97
0,55	4,81		0,55	4,84	0,55	4,86
0,6	4,72		0,6	4,76	0,6	4,79
0,65	4,63		0,65	4,68	0,65	4,71
0,7	4,55		0,7	4,6	0,7	4,64

0,75	4,48	0,75	4,53	0,75	4,58
0,8	4,4	0,8	4,48	0,8	4,5
0,85	4,32	0,85	4,42	0,85	4,44
0,9	4,25	0,9	4,37	0,9	4,29
0,95	4,16	0,95	4,3	0,95	4,22
1	4,08	1	4,21	1	4,17
1,05	4,01	1,05	4,15	1,05	4,1
1,1	3,93	1,1	4,06	1,1	4,02
1,15	3,87	1,15	4	1,15	3,94
1,2	3,8	1,2	3,92	1,2	3,87
1,25	3,73	1,25	3,84	1,25	3,81
1,3	3,66	1,3	3,78	1,3	3,73
1,35	3,61	1,35	3,7	1,35	3,66
1,4	3,55	1,4	3,63	1,4	3,6
1,45	3,5	1,45	3,56	1,45	3,54
1,5	3,44	1,5	3,51	1,5	3,47
2	3,4	2	3,46	2	3,42
2,5	3,37	2,5	3,4	2,5	3,38
3	3,33	3	3,35	3	3,32
3,5	3,29	3,5	3,29	3,5	3,26
4	3,26	4	3,24	4	3,22
4,5	3,23	4,5	3,18	4,5	3,17
5	3,2	5	3,12	5	3,14
5,1	3,18	5,1	3,07	5,1	3,11
5,2	3,16	5,2	3,03	5,2	3,08
5,3	3,12	5,3	2,99	5,3	3,04
5,4	3,07	5,4	2,96	5,4	3
5,5	3,01	5,5	2,93	5,5	2,96
5,6	2,96	5,6	2,9	5,6	2,91
5,7	2,93	5,7	2,87	5,7	2,87
5,8	2,9	5,8	2,85	5,8	2,84

5,9	2,88	5,9	2,82	5,9	2,82
6	2,86	6	2,81	6	2,81
6,1	2,85	6,1	2,81	6,1	2,79
6,2	2,84	6,2	2,81	6,2	2,79
6,3	2,84	6,3	2,79	6,3	2,79
6,4	2,84	6,4	2,78	6,4	2,76
6,5	2,82	6,5	2,76	6,5	2,74
6,6	2,8	6,6	2,74	6,6	2,72
6,7	2,79	6,7	2,72	6,7	2,7
6,8	2,78	6,8	2,7	6,8	2,67
6,9	2,77	6,9	2,68	6,9	2,64
7	2,76	7	2,67	7	2,61
7,5	2,74	7,5	2,65	7,5	2,58
8	2,73	8	2,63	8	2,56
8,5	2,71	8,5	2,61	8,5	2,54
9	2,69	9	2,6	9	2,52
10	2,68	10	2,59	10	2,5
11	2,67	11	2,58	11	2,47
12	2,66	12	2,56	12	2,4
13	2,62	13	2,54	13	2,33
14	2,59	14	2,53	14	2,28
15	2,57	15	2,52	15	2,23
16	2,51	16	2,4	16	2,19
17	2,44	17	2,33	17	2,15

Appendix 3: Particle surface size data

➢ B3 sample

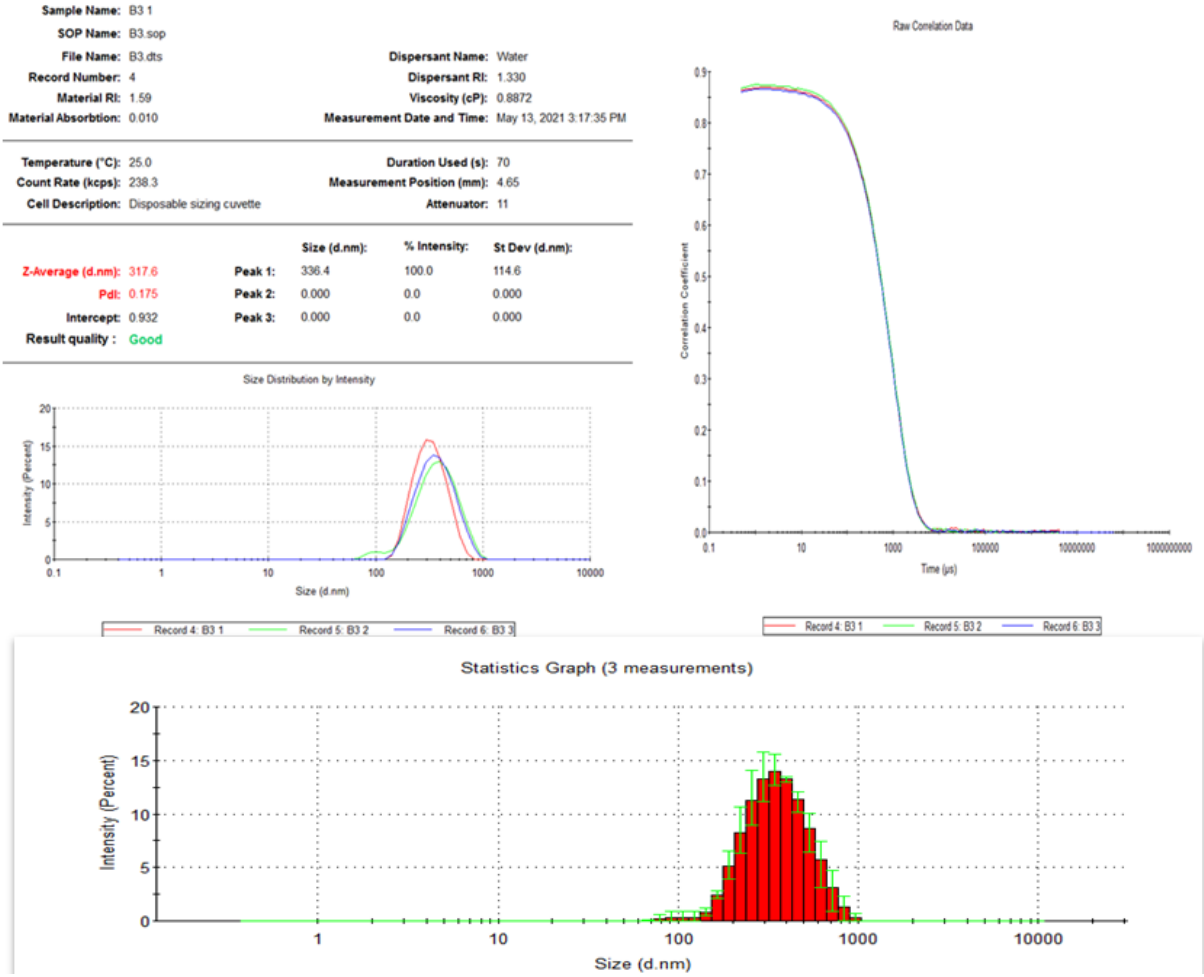

Figure A 3.1: Particle size data of B3 sample

➢ SWy-2 sample

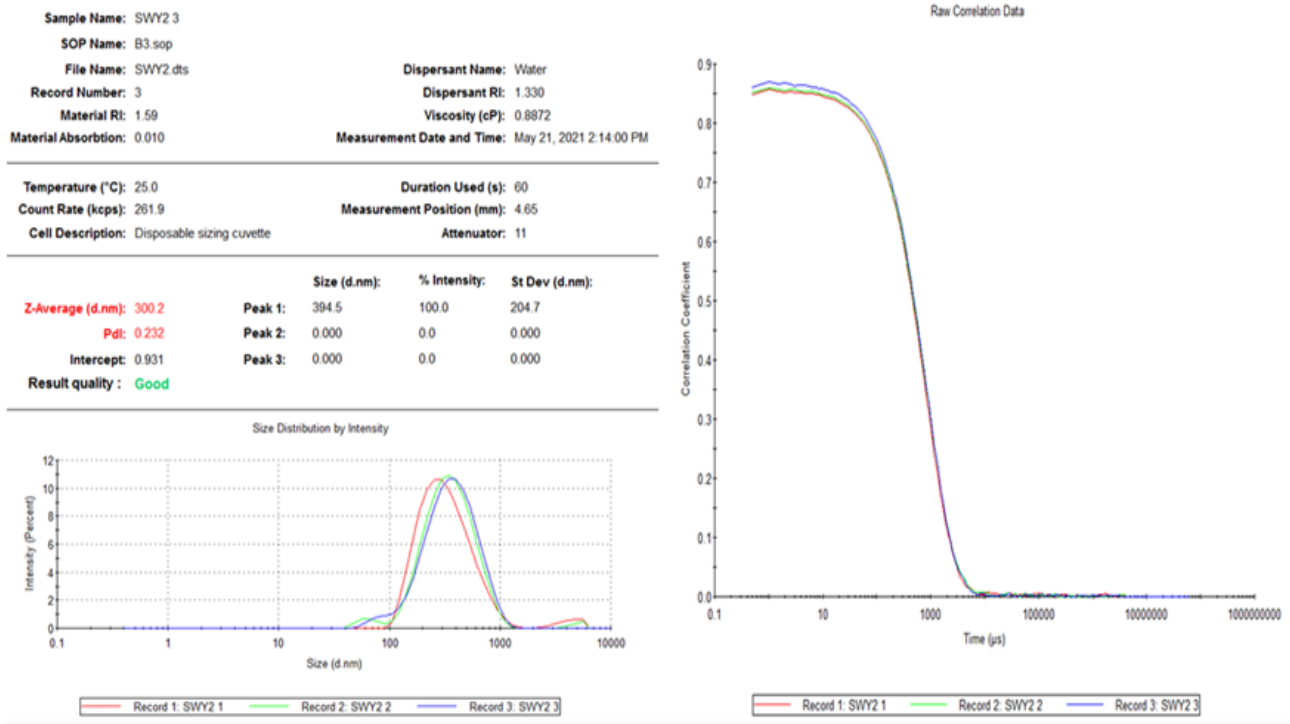

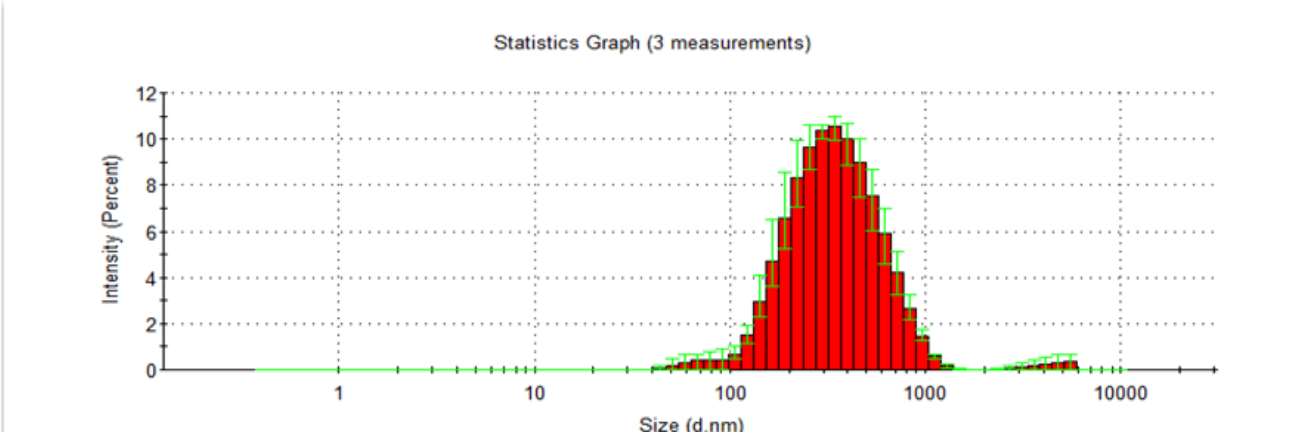

Figure A 3.2: Particle size data of SWy-2 sample

➢ KGa-2 sample

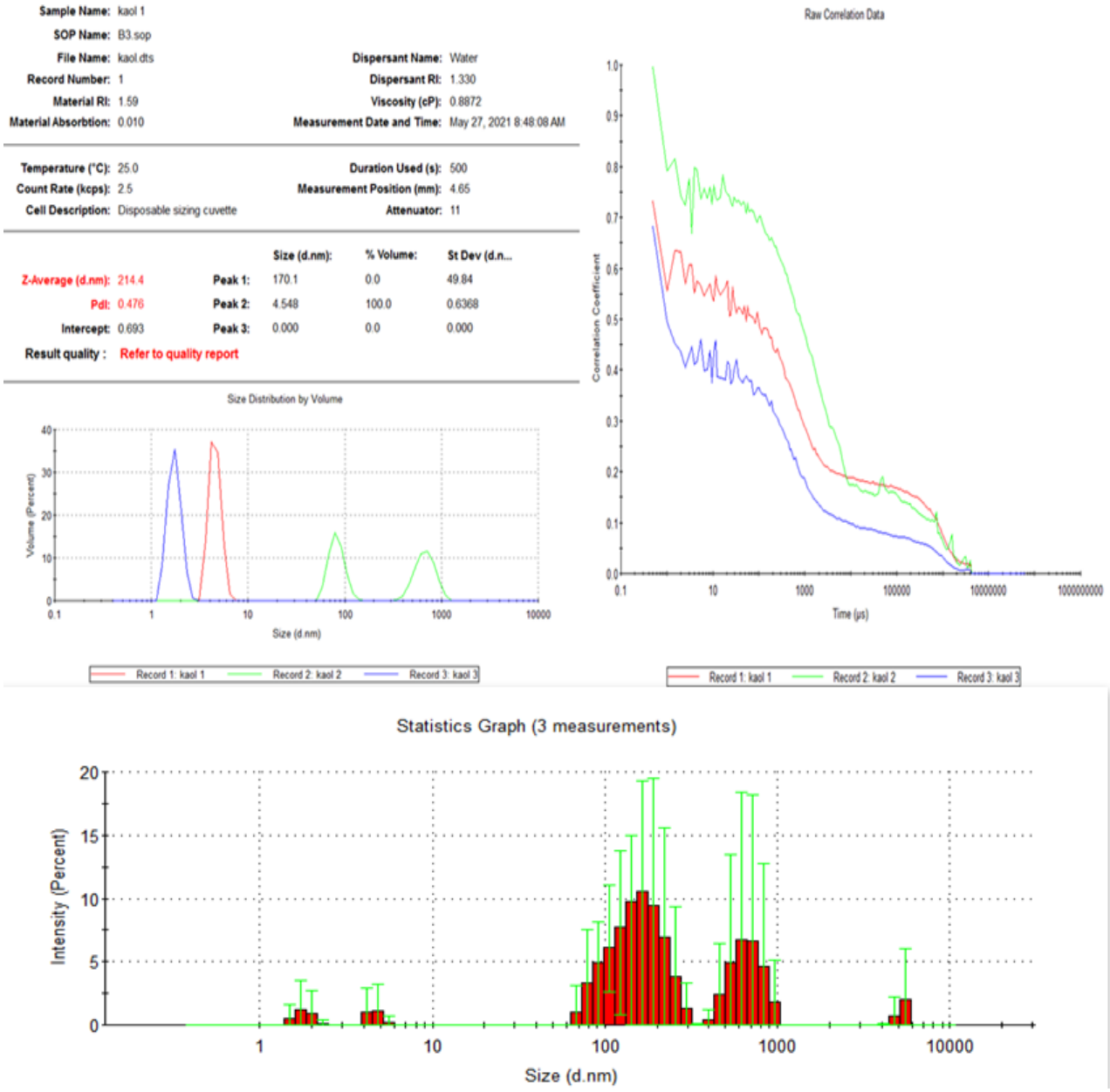

Figure A 3.3: Particle size data of KGa-2 sample

Appendix 4: Zeta potential and electrokinetic mobility data

Figure A 4.1: Electrokinetic data of B3 (IEP)

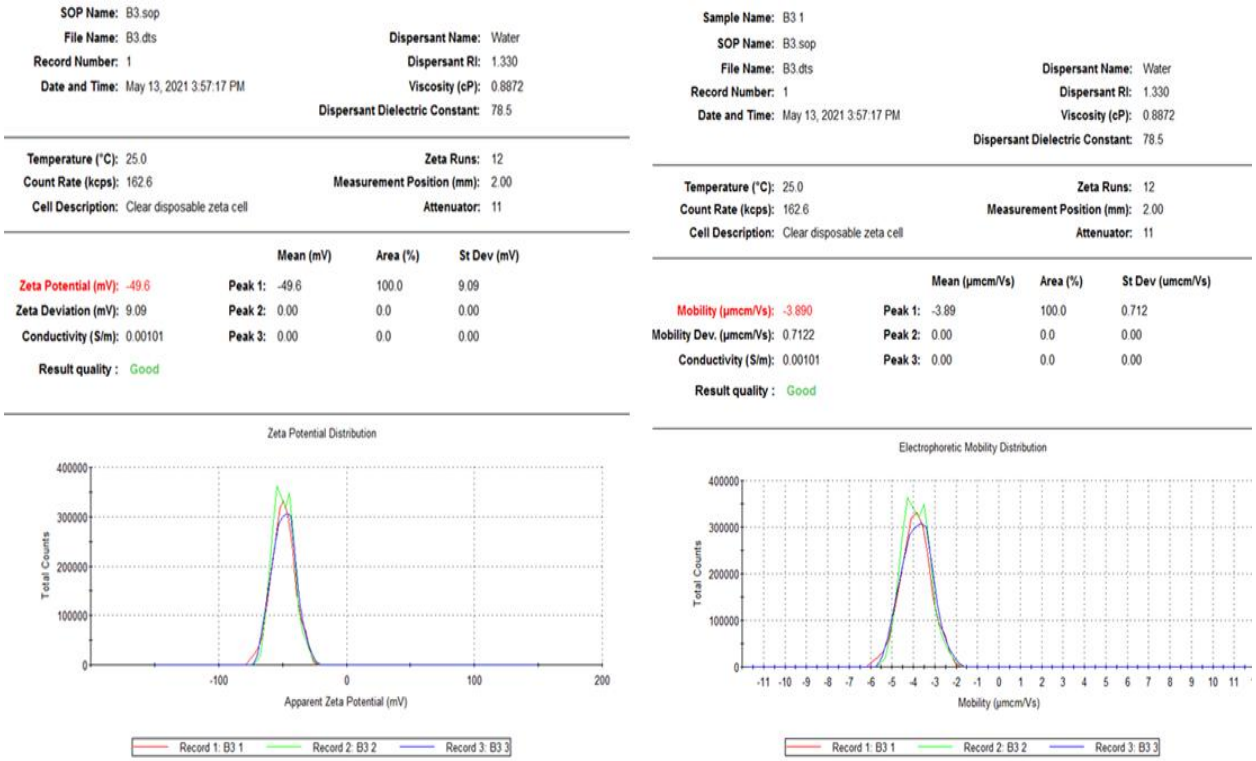

Figure A 4.2: Electrokinetic data of B3 (Buffer)

Figure A 4.3: Electrokinetic data of B3 (IEP+0.5)

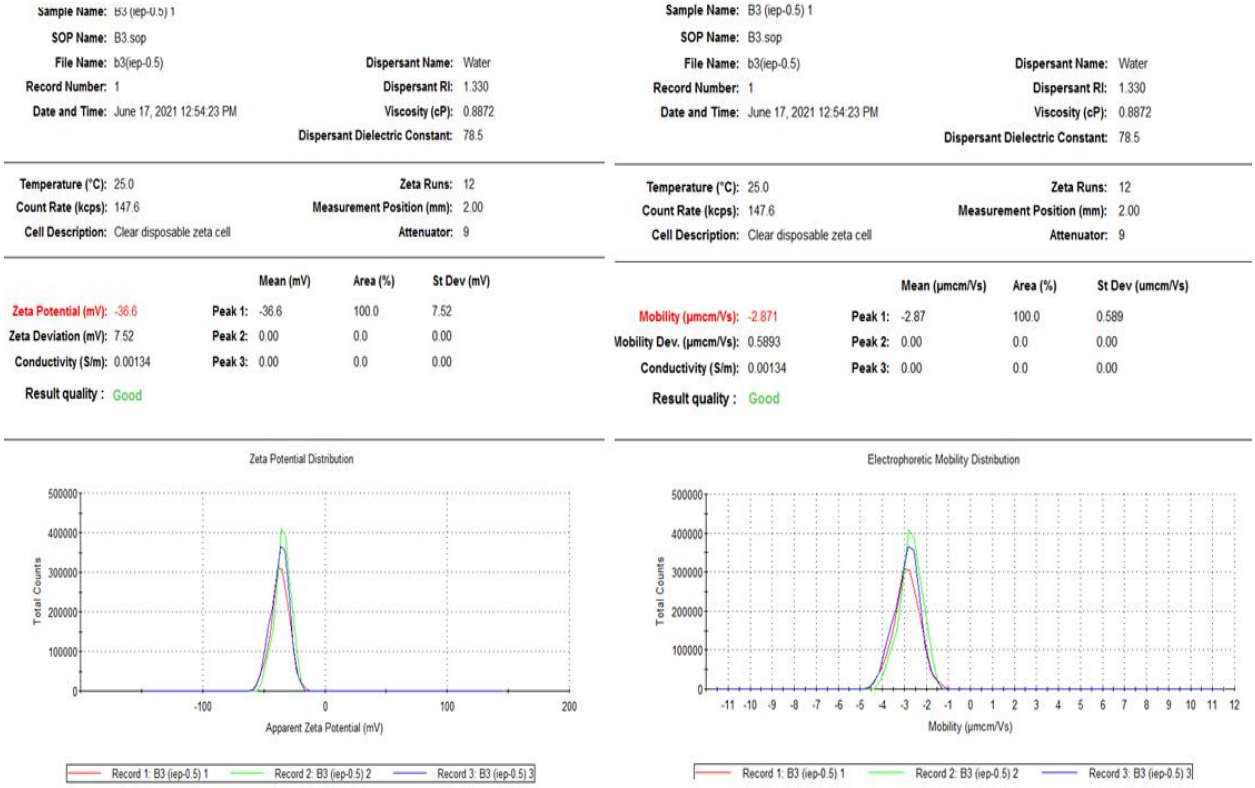

Figure A 4.4: Electrokinetic data of B3 (IEP-0.5)

Figure A 4.5: Electrokinetic data of SWy-2 (IEP)

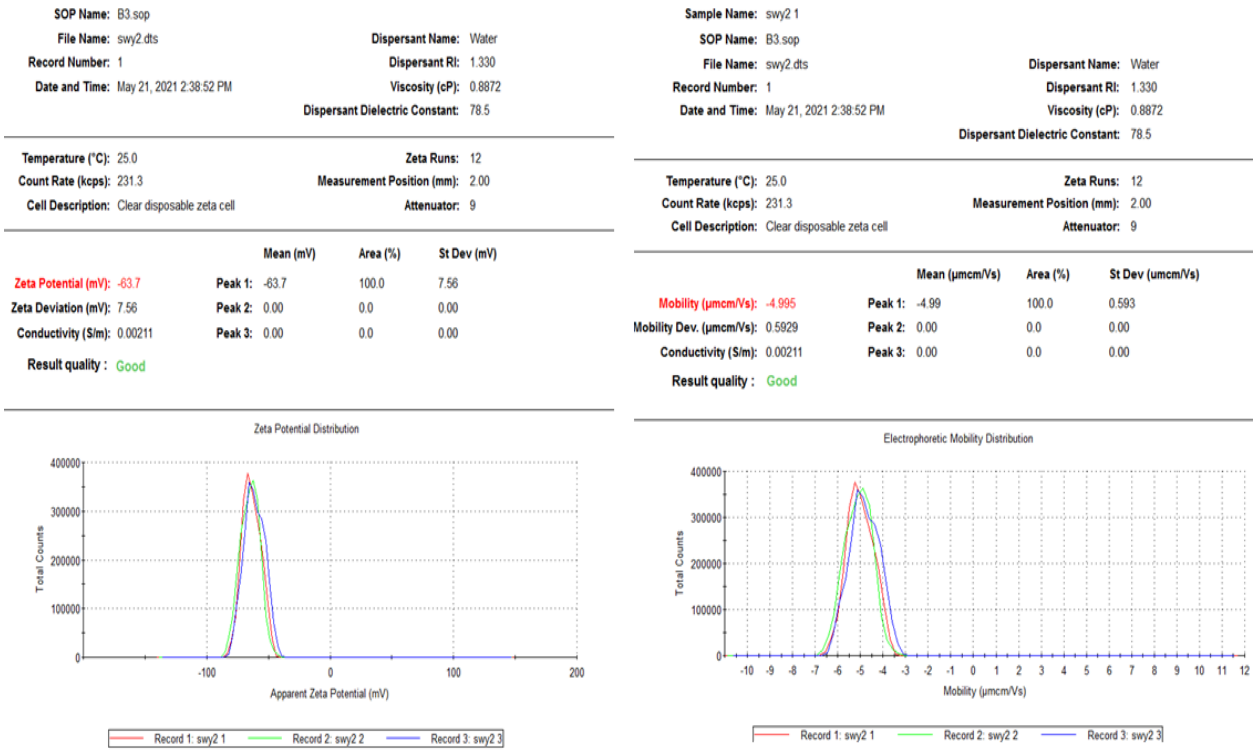

Figure A 4.6: Electrokinetic data of SWy-2 (Buffer)

Figure A 4.7: Electrokinetic data of SWy-2 (IEP+0.5)

Figure A 4.8: Electrokinetic data of SWy-2 (IEP-0.5)

Figure A 4.9: Electrokinetic data of KGa-2 (IEP)

Figure A 4.10: Electrokinetic data of KGa-2 (Buffer)

Figure A 4.11: Electrokinetic data of KGa-2 (IEP+0.5)

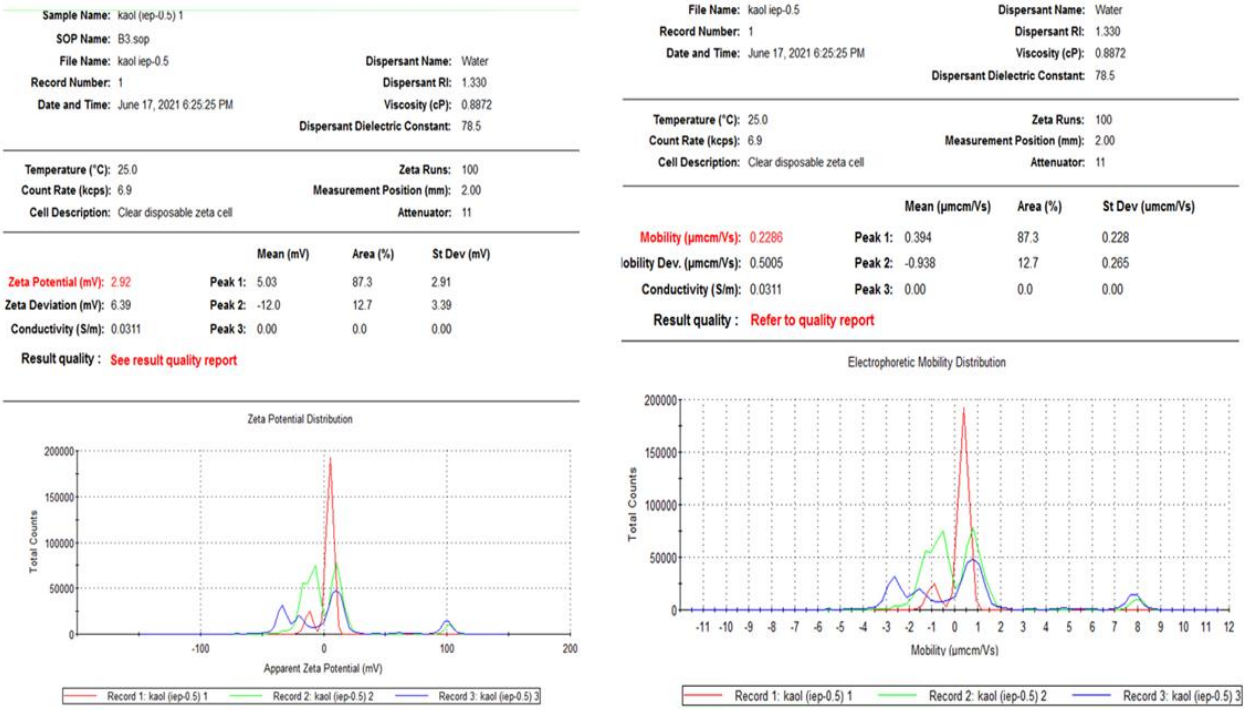

Figure A 4.12: Electrokinetic data of KGa-2 (IEP-0.5)